Doctoral Dissertation

Elucidation of the mechanism of autophagy-mediated RNA degradation by metabolome analysis

メタボローム解析を用いたオートファジーによる RNA 分解機構の解明

Hanghang Huang

December 2015

Graduate School of Engineering
Osaka University

Contents

Contents 1
Chapter 1 General Introduction 5
1.1 Autophagy 5
1.2 Autophagy in yeast 7
1.3 Metabolomics 10
1.4 Metabolomics in this study 11
1.5 Objective of this study 13
1.6 Research outline 13
Chapter 2 Metabolic profiling of *Saccharomyces cerevisiae* under starvation conditions .. 15
2.1 Introduction 15
2.2 Materials and methods 17
2.2.1 Materials and reagents 17
2.2.2 Strains and media 18
2.2.3 Yeast culture 18
2.2.4 Metabolite extraction 19
2.2.5 Metabolome analysis 20
2.3 Results 20
2.3.1 Metabolic profiling of *Saccharomyces cerevisiae* under nitrogen starvation 20
2.3.2 Transient increase in intracellular nucleoside levels were observed under different autophagy-triggering conditions 25
2.4 Discussion 27
Chapter 3 Mechanism of bulk RNA degradation via autophagy under nitrogen starvation in yeast 29
3.1 Introduction 29
3.2 Materials and methods 33
3.2.1 Materials and reagents 33
3.2.2 Yeast strains and media 34
3.2.3 Yeast culture and metabolite extraction 35
3.2.4 Metabolome analysis 35
3.2.5 Absolute quantitation 36
3.2.6 Western blotting 37

3.2.7 Fluorescence microscopy 38
3.2.8 Alkaline phosphatase (ALP) assays 38
3.2.9 Total RNA extraction, northern blot, and quantitative RT-PCR (qPCR) 39
3.3 Results 41
3.3.1 Non-selective autophagy plays the main role in autophagy-mediated RNA degradation under nitrogen starvation 41
3.3.2 Role of Pho8, a vacuolar nucleotidase 43
3.3.3 Rny1 is the nuclease responsible for RNA degradation in the vacuole 47
3.3.4 RNY1 deletion causes accumulation of RNA in the vacuole 50
3.3.5 Role of ribophagy in starvation-induced RNA degradation 53
3.3.6 Further breakdown of nucleosides in the cytoplasm 56
3.3.7 Nucleosides are transported from the vacuole into the cytoplasm partially mediated by Fun26 62
3.3.8 Excretion of bases from cells during autophagy 63
3.3.9 Starvation-induced RNA degradation is conserved in the fission yeast 69
3.4 Discussion 70
Chapter 4 Conclusions 75
4.1 Summary 75
4.2 Future perspectives 76
Acknowledgment 78
References 80
List of Publications 92
Appendix 93
I. Optimization of experimental conditions and methods 93
II. Growth curves 95
III. Principal Component Analysis (PCA) 96
IV. MRM transition information 97
V. Supplementary data for Fig. 2-4 103
VI. Supplementary data for Fig. 2-7 104
VII. Supplementary data for Fig. 3-2A 105
VIII. Supplementary data for Fig. 3-4 106
IX. Supplementary data for section 3.3.8 107
X. Changes in intracellular ribose levels in WT and *atg2*Δ under nitrogen starvation .. 108

Chapter 1 General Introduction

1.1 Autophagy

Autophagy is a membrane-dynamic self-degradation system well conserved among eukaryotes, during which cytoplasmic components are delivered to the lysosome/vacuole for degradation (Klionsky, 2007; Ohsumi, 2014). Recent studies on autophagy have revealed its multiple roles in physiology and pathophysiology, including starvation adaptation (Brauer et al., 2006), cellular protein and organelle clearance (Mitra, 2009), anti-aging (Cuervo *et al*., 2005), anti-microorganism (Randow, 2011), cell death (Debnath *et al*., 2005), tumor suppression (Levine, 2006), and antigen presentation (Münz, 2006). It has also drawn intensive attention in clinical medicine due to its possible relation to many diseases such as cancers and neurodegeneration (Liang *et al*., 1999; Mathew *et al*., 2009; Hara *et al*., 2006). Among its versatile roles, starvation adaptation, which is mainly to ensure nutrient supply, is considered to be the most important and basic function. It is reported that the breakdown of cellular components and the following recycling of its products are essential to ensure cellular survival during starvation by maintaining minimal essential cellular activities and cell homeostasis (Lin *et al*., 2012). In consistence with this, researchers found that autophagy-defective mutants of yeast *Saccharomyces cerevisiae* exhibited reduced viability under nitrogen starvation (Tsukada *et al*., 1993); autophagy-defective neonates of mice showed decreased amino acid concentrations in plasma and tissues and exhibited symptoms of energy depletion, during the early neonatal starvation period, which eventually died within 12 hours of delivery, around half the survival time of normal neonates (Kuma *et al*., 2004; Komatsu *et al*., 2005).

So far, three different forms of autophagy known as macroautophagy (Mehrpour *et al*., 2010), microautophagy (Kunz *et al*., 2003) and chaperone-mediated autophagy (Dice *et al*., 2007) have been described. Macroautophagy is one of the major degradative pathways in eukaryotic cells and is the only one that is capable of degrading entire organelles. This process is highly conserved among eukaryotes and has been characterized from yeast to human being (Klionsky *et al*., 2007). During macroautophagy, a double-layered membrane originates from a site known as the phagophore assembly site (PAS) to engulf cargoes,

cytoplasmic constituents, forming a double-membrane vesicle termed autophagosome, which is immediately delivered to the vacuole. The outer layer then fuses with the lysosomal/vacuolar membrane and the inner membrane structure, which is called an autophagic body, is released into the lysosomal/vacuolar lumen and degraded by the lysosomal/vacuolar enzymes (**Fig. 1-1**). On the other hand, microautophagy involves the engulfment of cytoplasmic contents by direct invagination of the lysosome/vacuole. Chaperone-mediated autophagy (CMA) refers to a less common form of autophagy, which is hitherto only found in mammals. It mediates the degradation of some subsets of cytosolic proteins (and sometimes proteins from other compartments after they enter the cytosol) in lysosomes, selectively targeted by a cytosolic chaperone protein (Kaushik *et al*., 2011).

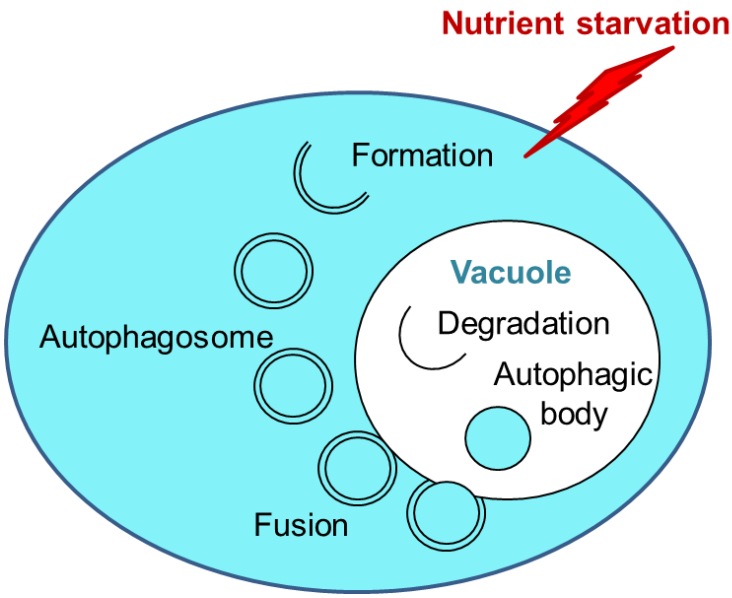

Fig. 1-1. Process of macroautophagy in yeast

During the past few decades, various research methods for autophagy study have been developed in response to the distinct needs of different research objectives and approaching directions. The predominant monitoring methods employed by researchers to date can be generally summarized into three types: microscopy, biochemical methods, and detection of protein modifications using SDS-PAGE and western blotting (**Table 1-1**) (Klionsky *et al*., 2007). Microscopy is primarily to monitor autophagic membrane dynamics, while biochemical methods and detection of protein modifications are mostly to evaluate autophagic

activity by assaying either the activity of a certain enzyme or the processing of a specific protein. Autophagy is the process of decomposing macromolecules into small metabolites, the release of which inevitably causes metabolic fluctuations at some level. Nevertheless, none of the conventional methods described in **Table 1-1** provides any information on cellular metabolome. Therefore, new approaches from metabolome level are expected to provide new information on autophagy, which thereby leads to novel insights into this complex mechanism.

Table 1-1. Conventional methods for monitoring autophagy (Klionsky *et al.*, 2007)

Assay type	**Available assay**
microscopy	Acridine orange (F), Autophagic body (E, F, L) and autophagosome (E, F) formation and accumulation, GFP-Atg8 localization (E, F), GFP-LC3 (F), LysoTracker Red (F), MDC (F), Precursor Ape1 localization (F), Sequestration of cytosolic markers (F), TAKA assay (F)
biochemical method	Ams1 activity, Ape1 activity, Atg1 kinase activity, Peroxisomal enzyme inactiviation, Pho8Δ60 activity, Protein degradation, Sequestration of cytosolic markers
protein modification	Active site CtoS[a], Ape1 processing, Ape1 synthesis, Atg8-GFP processing, Atg8-PE formation and membrane association, Atg8 synthesis, Atg12-Atg5 conjugation, Atg13 phosphorylation, Fox3 degradation, GFP-Atg8 and GFP-LC3 processing, LC3-Ⅰ conversion, LC3 C-terminal processing, LC3-Ⅱ turnover, Pex14 processing, Protease protection

E, electron microscopy; F, fluorescence microscopy; L, light microscopy. GFP, green fluorescent protein; MDC, monodansylcadaverine; TAKA, transport of Atg9 after knocking-out Atg1; Ams1, α-mannosidase; Ape1, aminopeptidase Ⅰ. [a]Mutation of cysteine to serine

1.2 Autophagy in yeast

Although autophagy was first discovered in mammalian cells in the late 1950s and morphologically confirmed in the 1960s, it was not until decades later that the major breakthrough was made in unraveling the molecular mechanism of this process (Clark, 1957; Ashford *et al.*, 1962). A milestone of the study on the molecular basis of autophagy is its discovery in yeast and the identification of its contributing genes by Ohsumi and his colleagues (Takeshige *et al.*, 1992; Tsukada M *et al.*, 1993). Autophagy in yeast was first described in 1992, following which, a large quantity of autophagy-related genes (ATGs) that are involved in this process, were identified successively through genetic screening for autophagy-defective mutants (Takeshige *et al.*, 1992; Tsukada M *et al.*, 1993). There are several different types of autophagy, including the starvation-induced non-selective macroautophagy and selective autophagy such as mitophagy, a mitochondrion-selective degradation pathway upon starvation (Lemasters *et al.*, 2005), cytoplasm to vacuole targeting (Cvt) pathway, a constitutive and selective delivery of the hydrolase aminopeptidase I (Ape1),

α-mannosidase (Ams1) and possibly aspartyl aminopeptidase (Yhr113w/Ape4) (Harding *et al.*, 1995; Scott *et al.*, 1997), pexophagy, a peroxisome-selective degradation pathway (Till *et al.*, 2012), and the piecemeal microautophagy of the nucleus (PMN) pathway, a selective degradation system for nuclear contents (Roberts *et al.*, 2003) (**Fig. 1-2**). Up to now, 40 ATGs have been identified in yeast (Ohsumi, 2014; Mochida *et al.*, 2015), of which, 19 Atg proteins, Atg1-Atg10, Atg12-Atg14, Atg16-Atg18, Atg29, Atg31, and Atg38 have been identified as components essential for autophagosome formation, which can be divided into five functional groups, namely Atg1 kinase and its regulators, ubiquitin-like Atg8 conjugation system, ubiquitin-like Atg12 conjugation system, phosphatidylinositol (PtdIns)-3-kinase complex I, and Atg2-Atg18 complex and Atg9 (**Table 1-2**). Besides, 17 (Atg1-Atg10, Atg12-Atg16, Atg18, and Atg22) are essential for all types of autophagy, 4 (Atg17, Atg29, Atg31, and Atg38) are specifically indispensable to starvation-induced non-selective autophagy and the rest are essential for one or more specific selective types of autophagy but dispensable to non-selective autophagy (**Fig. 1-2**). The 17 common essential ATG genes mainly contribute in two ways: 15 are involved in membrane dynamics and the other 2 are related to degradation of autophagic body. Similar molecular mechanisms are shared among selective macroautophagy pathways (**Fig. 1-3**). They require a receptor that interacts with its specific cargo, and a scaffold protein (Atg11) at the PAS, which mediates recruitment of Atg8, a component that is essential for phagophore expansion by conjugating to the membrane lipid phosphatidylethanolamine (PE). Besides ATGs, some genes originally known for other functions such as *UBP3/BRE5* encoding the ubiquitin protease complex Ubp3-Bre5, and *NVJ1/VAC8* encoding the nucleus-vacuole (NV) junction proteins Nvj1 (an outer nuclear membrane protein) and Vac8 (a vacuolar membrane protein), were also found to have important roles during specific types of selective autophagy (Kraft *et al.*, 2008; Dawaliby *et al.*, 2010). These autophagy-contributing genes provide powerful tools for studying the molecular mechanisms of these unique pathways such as the signaling process and the formation of autophagosomes.

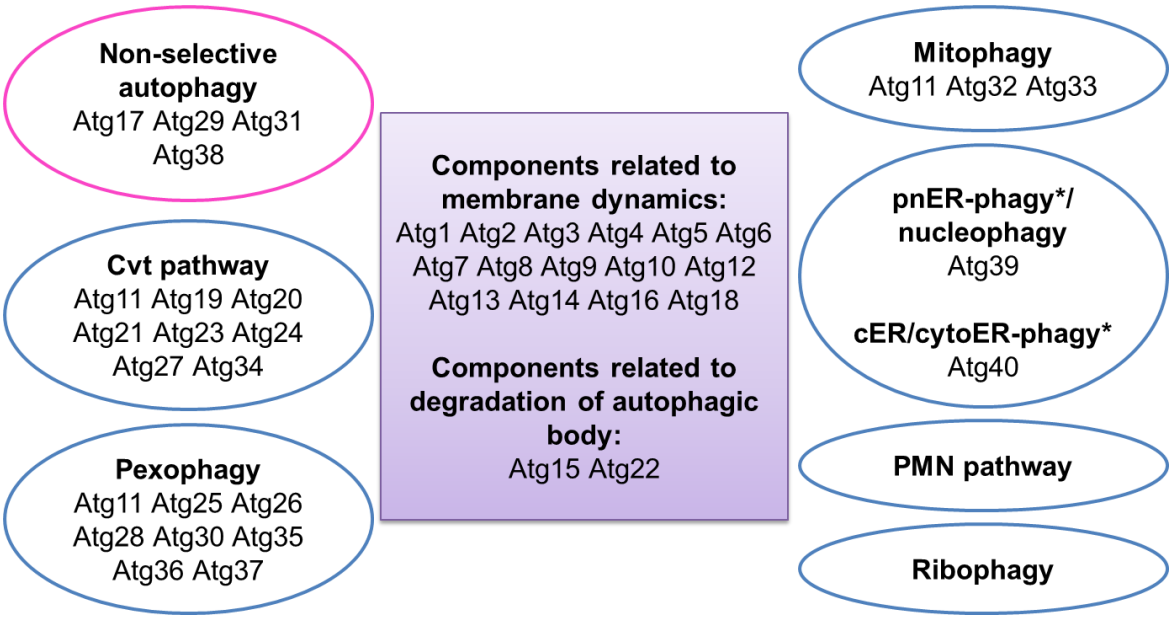

Fig. 1-2. Various types of autophagy and *au*t*o*pha*g*y-related (Atg) proteins

(pink) non-selective autophagy; (blue) selective autophagy

*pnER: perinuclear ER, cER/cytoER: cortical ER/cytoplasmic ER

Table 1-2. Functional groups and their members for autophagosome formation

	Functional groups	Components
1	Atg1 kinase and its regulators	Atg1, Atg13, Atg17, Atg29, Atg31
2	Ubiquitin-like Atg8 conjugation system	Atg8, Atg4, Atg7, Atg3
3	Ubiquitin-like Atg12 conjugation system	Atg12, Atg7, Atg10, Atg5, Atg16
4	PtdIns-3-kinase complex I	Vps34, Vps15, Atg14, Atg6, Atg38
5	Atg2-Atg18 complex and Atg9	Atg2, Atg18, Atg9

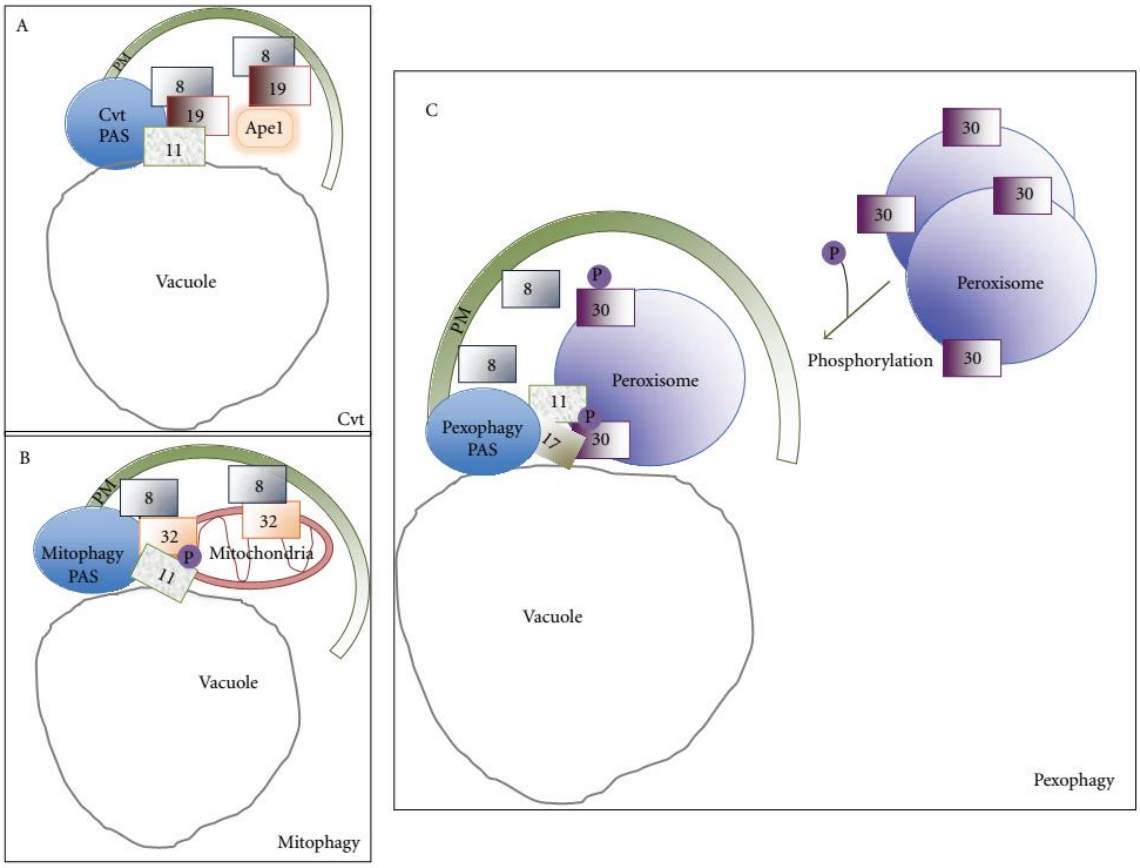

Fig. 1-3. Mechanism of selective types of macroautophagy in *Pichia pastoris*. (A) In the Cvt pathway, Atg19 and Atg34 are the receptors for its two cargo proteins Ape1 and Ams1, respectively. (B) Atg32 is a mitochondrial outer membrane protein, which is responsible for the initiation of the mitophagy-specific phagophore membrane expansion from the PAS. (C) In pexophagy, Atg30 (Atg36 in *S. cerevisiae*), which is localized at the peroxisome membrane, functions as the receptor via the interaction with two peroxisomal membrane proteins, Pex3 and Pex14. (cited from Till *et al*., 2012)

1.3 Metabolomics

Metabolomics is the scientific study of metabolites, the intermediates and products of metabolism. It is the interdisciplinary research field combining biology, analytical chemistry, and bioinformatics, which concerns cutting-edge technologies. Metabolomics has been proved effective in various fields from medicine (drug discovery, drug development, clinical diagnostics (Kim *et al*., 2007; Kleemann *et al*., 2007)), agriculture (genetics and breeding, genetically modified food (Schauer, 2006)), food (quality control (Jumhawan *et al*., 2013)) to bioindustry (strain improvement, bioproduction pathway design). Metabolome represents the

complete set of metabolites in a cell, tissue, or organism, and metabolomics concerns the comprehensive determination of metabolite levels in the metabolome, which gives the information of a large quantity of metabolites of a particular moment, as well as their changes over time in response to environmental stimuli. Metabolites are the direct participants of metabolic pathways and also the end products of gene expression flow. They reflect the downstream effects of gene and protein regulation, from which, important information of cellular processes can be obtained. Thus, by the comprehensive analysis of metabolome, metabolomics best represents the overall cellular functional state. Besides, as entire genome information is not necessary in metabolomics, it also facilitates studies with genetically uncharacterized organisms, because unlike genes or proteins, metabolites are universal. Typically, the different types of metabolomics analyses can be separated into two major approaches: targeted and non-targeted analyses. In targeted analysis (e.g. metabolic profiling), the targets are pre-decided and depending on different analytical platforms. The information of the target compounds are either extracted from the metabolomics data after a scanning measurement or designed to be acquired from the measurement in the first place, either way, normally by referring to a reference library. The limited size of most current reference libraries thus becomes the major drawback of this approach that hinders the use of the remaining information of a sample. In contrast, during a non-targeted approach (e.g. metabolic fingerprinting), the compounds are not necessarily identified and the information of both identified compounds and unknown compounds is considered for further analysis. Metabolic profiling is the quantitative or qualitative determination of a set of related compounds involved in specific metabolic pathways, which can give an instantaneous snapshot of the physiological state of the analyzed subject (Fiehn, 2002). With its high sensitivity and quantitativity, metabolome analysis is capable of capturing slight changes in metabolite levels, making itself one of the most powerful tools to monitor cellular states and processes.

1.4 Metabolomics in this study

Autophagy is closely related to the metabolome. It involves the degradation of large quantities of autophagic cargoes including different organelles and macromolecules like proteins. Although the transporting pathways and mechanisms are various, one thing in

common is that the degradation intermediates and products of these organelles and macromolecules would no doubt bring a strong impact on the metabolome. Thus, by evaluating the metabolite levels as well as the changes over time during the process of autophagy, new insights and understanding of its mechanism and physiological role can be anticipated. However, until recently, there had been no reported approach from the viewpoint of overall autophagy-induced metabolic changes for autophagy study. In this study, I employed techniques of metabolomics for the investigation of autophagy process. It was considered that by monitoring the time-resolved changes induced by autophagy, vital information that is difficult or even impossible to gain by the traditional methods could be obtained.

During the course of the study, interesting changes in RNA-related metabolites were observed, which strongly suggested the degradation of RNA via autophagy. Although autophagy has been the research interests of numerous researchers for decades, there is still a lack of understanding of autophagy-mediated RNA degradation. In fact, almost nothing with regard to the molecular details has been clarified so far. Therefore, I applied metabolomics to the investigation of autophagy-mediated RNA degradation for an understanding of its mechanism and significance (see Chapter 3).

Ion-pairing liquid chromatography-electrospray ionization mass spectrometry (IP-LC-ESI-MS) has been proved to be effective in separating and analyzing high polar metabolites including nucleotides (Hashim *et al.*, 2014; Walseth *et al.*, 1980). However, it exhibits very poor sensitivities towards most nucleosides such as adenosine and cytidine, and bases such as adenine and cytosine. Pentafluorophenylpropyl (PFPP) stationary phase has shown unique retention of small, polar analytes including most nucleosides, bases and amino acids (Igarashi *et al.*, 2011). As a complement to each other, in this study, I optimized and combined two analytical platforms, IP-LC-ESI-MS with C18 column and LC-ESI-MS with PFPP column, to cover as many metabolites as possible, especially the related ones involved in nucleic acid metabolism.

1.5 Objective of this study

As described above, no information regarding the metabolome during autophagy had ever been reported due to the limitation of traditional approaches. To deepen our knowledge on autophagy, this study approached from a brand-new viewpoint for autophagy study. The overall objective of this study is, to gain novel insights into the mechanism of autophagy by investigating autophagy-induced metabolic changes, meanwhile demonstrating the power of metabolomics in discovering and solving physiological problems. Overall changes in the metabolome during autophagy were first investigated, which highlighted RNA-related metabolites as a potential point of interest, as described in Chapter 2. The autophagy-mediated RNA degradation mechanism was then elucidated in Chapter 3.

1.6 Research outline

Metabolomics was applied to autophagy to investigate the changes induced by autophagy at metabolome level. In Chapter 2, I performed and compared the metabolic profiling of yeast *S. cerevisiae* X2180 (wild-type) and an autophagy-defective mutant under three commonly studied autophagy-triggering conditions. The results revealed very interesting changing patterns in nucleosides, which strongly suggested RNA degradation induced by autophagy. Because of the relatively low recognition of autophagic RNA degradation, the mechanism of this process remained mostly unknown. Therefore, in Chapter 3, I focused my research on elucidating the mechanism of autophagy-induced RNA degradation. With a combination of metabolome analysis to monitor the dynamic changes of intra- and extra-cellular metabolites under starvation conditions and molecular genetic approaches tractable in yeast (in collaboration with Professor Ohsumi from Tokyo Institute of Technology), a comprehensive picture of RNA degradation via autophagy was successfully characterized. Specifically, this study identified the enzymes involved in the process and characterized the dynamic flow of RNA metabolism under starvation conditions. Chapter 3 was approached in several steps according to the different focuses of the research objective. First, the relationship between RNA degradation and various autophagic types was explored to determine the responsible type of autophagy for starvation-induced RNA degradation. Second, the functional enzyme(s) for each step of this process in *S. cerevisiae* was identified, including a ribonuclease, a nucleotidase, a nucleoside transpoter and two nucleosidases. To

acquire a more comprehensive picture of the overall process, the changes in absolute concentrations of both intra- and extra-cellular degradation products were monitored, which revealed an unexpected fact that the bases derived from the degraded RNA were excreted out of the cell after deamination. Finally, to examine the universality of autophagy-mediated RNA degradation, this phenomenon was confirmed in the fission yeast *Schizosaccharomyces pombe*, a phylogenetically distant species from the budding yeast *S. cerevisiae*. Similar RNA catabolism via autophagy was proved to be well conserved in other organisms. In Chapter 4, I summarized the important conclusions obtained in this study and presented the future perspectives.

Chapter 2 Metabolic profiling of *Saccharomyces cerevisiae* under starvation conditions

2.1 Introduction

Every cellular activity is maintained by a balance between continuous synthesis and degradation of constituents, proteins, nucleic acids, and lipids. Autophagy occurs constitutively at a low level, thereby serving as an important means for quality control by removing excessive or damaged proteins and organelles. Induction of massive autophagy is a rapid cellular stress response. As introduced in Chapter 1, autophagy directly or indirectly facilitates cell survival under starvation conditions through autophagic degradation of its own constituents. Thus, characterization of the impact this process brings to the cellular metabolome becomes the key to the further understanding of its functional mechanism and significance. Yeast *S. cerevisiae* is one of the most commonly used models for autophagy study because of its fully characterized genome and the property of easy control and manipulation. In this study, the prototrophic wild-type strain X2180 was chosen as the parent strain to minimize metabolic requirements. The autophagy-defective mutant *atg2*Δ was used as the autophagy-defective model. Atg2 is one of the core components of autophagy which are essential for the formation of autophagosomes. No autophagy activity was observed in *atg2*Δ strain under autophagy-triggering conditions (**Fig. 2-1**). Various stress factors can trigger autophagy such as nutritional limitations (carbon, nitrogen, sulfate, phosphate, nucleic acids, auxotrophic amino acids, vitamins, metals, *etc.*), pathogen infection, endoplasmic reticulum (ER) stress, pH changes, DNA damage, mechanical stress, and hypoxia. Among all different kinds of nutrient starvations, nitrogen starvation induces the most rapid and intensive autophagy response in yeast, and was thus employed as the representative autophagy-triggering conditions for the investigation of autophagy-induced metabolic changes in this study.

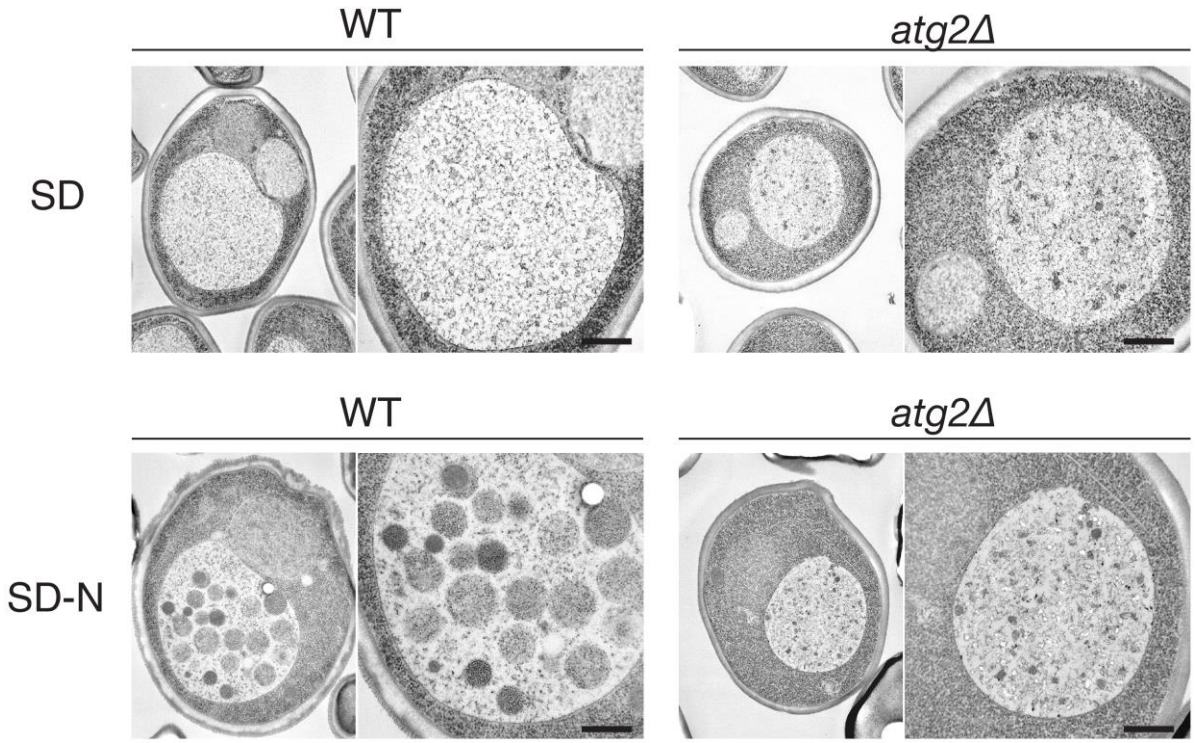

Fig. 2-1. Electron microscopic images of *pep4*Δ*prb1*Δ and *pep4*Δ*prb1*Δ*atg2*Δ cells under both growth and nitrogen starvation conditions. Cells were grown in SD to mid-log phase (OD600 = 1), and transferred to SD-N for 5 h. The cells were examined by transmission electron microscopy. Bar, 500 nm. (provided by Dr. Kawamata from Ohsumi lab)

The target of rapamycin (TOR) is a species of proteins that sense cellular nutrient state, oxygen, and energy level. They regulate a variety of important cellular processes concerning cell growth and proliferation, including ribosome biosynthesis, the initiation and elongation phases of translation, transcription of many enzymes involved in various metabolic pathways, amino acid import, and autophagy (Raught *et al.*, 2001). Under nutrient-rich conditions, the TOR protein, which is in its active state, inhibits autophagy by promoting phosphorylation of Atg13. The phosphorylated Atg13 is therefore unable to interact with Atg1 subfamily proteins to form an Atg1 kinase signaling complex, which is essential for the induction of autophagy (**Fig. 2-2;** Nakatogawa *et al*., 2009).

Rapamycin was an antifungal firstly isolated from a bacterium strain of *Streptomyces hygroscopicus* in a soil sample from Easter Island. It potently inhibits downstream signaling from the TOR protein by forming a rapamycin-FKBP12 gain-of-function complex with its

receptor, a small, ubiquitous protein termed FKBP12, but whether this complex directly interferes the kinase activity of the TOR protein is an unresolved question (**Fig. 2-2**; Raught *et al.*, 2001). Similar with nutrient depletion, inactivation of TOR by rapamycin treatment results in rapid dephosphorylation of Atg13. Dephosphorylated Atg13 associates with Atg1 subfamily proteins, and the active Atg1-Atg13 complex induces autophagy. Therefore, rapamycin induces the starvation response even under nutrient-rich conditions and is thereby commonly employed as an autophagy inducer in autophagy studies (Noda and Ohsumi, 1998).

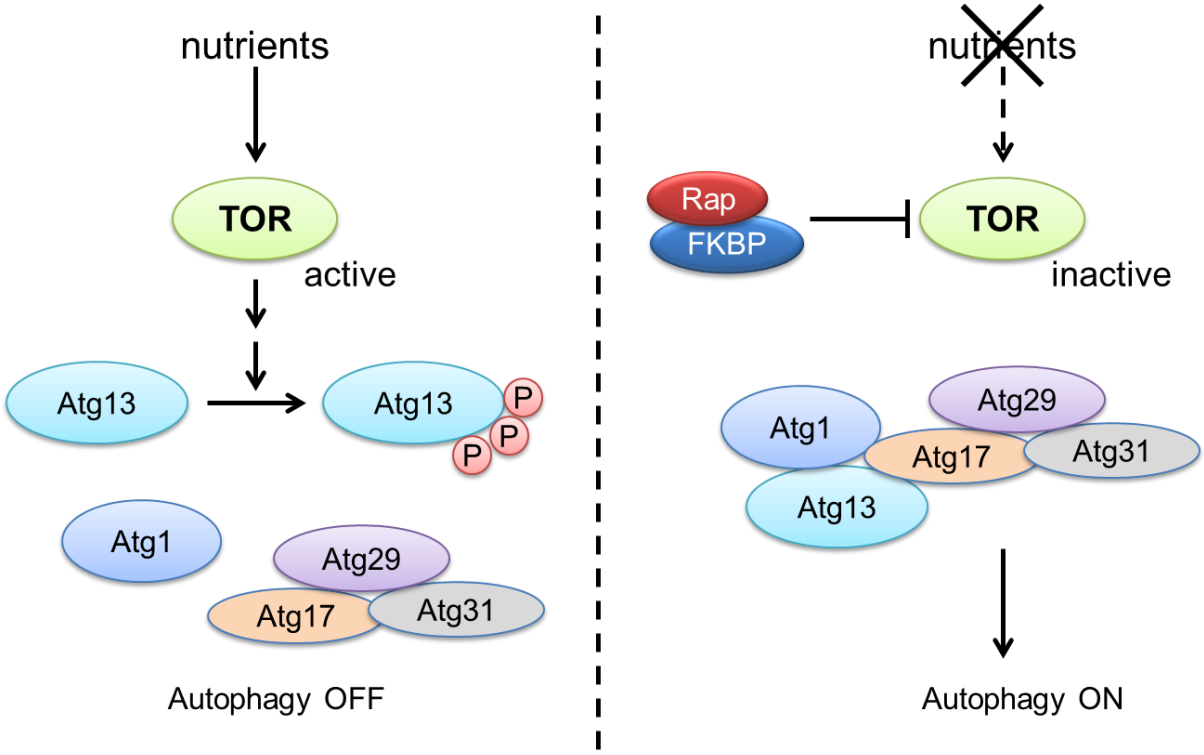

Fig. 2-2. Mechanism of TOR regulation on autophagy

2.2 Materials and methods

2.2.1 Materials and reagents

Yeast extract, peptone, and yeast nitrogen base without amino acids and ammonium sulfate were purchased from BD Difco (NJ, USA). Agarose, D-glucose, and ammonium sulfate were products of Nacalai Tesque (Kyoto, Japan). 2-(*N*-morpholino)ethanesulfonic acid (MES) and 1,4-piperazine diethanesulfonate (PIPES) were obtained from Dojindo (Kumamoto, Japan), and potassium hydroxide (KOH), potassium chloride (KCl), formic acid,

acetic acid, methanol, distilled water, and ultrapure water were all from Wako (Osaka, Japan). Tributylamine (TBA) and (+)-10-camphorsulfonic acid were purchased from Sigma-Aldrich Corp. MO, USA), and methionine sulfone was the product of Research Chemicals Ltd (Lancashire, UK). Acetonitrile and Chloroform were obtained from Kanto Chemical Co. (Inc., Tokyo, Japan) and Chameleon Reagent (Osaka, Japan), respectively.

2.2.2 Strains and media

Yeast strains used in this chapter are listed in **Table 2-1**. *atg2*Δ was provided by Ohsumi lab from Tokyo Institute of Technology (Huang *et al.*, 2014).

Table 2-1. Yeast strains used in Chapter 2

S. cerevisiae

Strain	**Genotype**	**Source**
X2180-1B	*MATα SUC2 mal mel gal2 CUP1*	Yeast Genetic Stock Center
MMY3	*X2180-1B;atg2*Δ*::kanMX6*	(Huang *et al.*, 2014)

Minimal synthetic defined (SD) medium (SD; 0.17% yeast nitrogen base without amino acids and ammonium sulfate, 0.5% ammonium sulfate, 2% glucose) was used to increase the cell density. To induce autophagy, nitrogen-deprivation medium (SD-N; 0.17% yeast nitrogen base without amino acids and ammonium sulfate, 2% glucose), carbon-deprivation medium (SD-C; 0.17% yeast nitrogen base without amino acids and ammonium sulfate, 0.5% ammonium sulfate) or rapamycin-included medium (SD+RP; 0.17% yeast nitrogen base without amino acids and ammonium sulfate, 0.5% ammonium sulfate, 2% glucose, 0.2 μM rapamycin) was used. All media used were buffered with 50 mM MES/KOH (pH 6.2).

2.2.3 Yeast culture

Frozen stocked (-80 ℃) strains were streaked onto a complete medium (YPD) agar plate (yeast extract 10 g/L, peptone 20 g/L, glucose 20 g/L, agarose 20 g/L) and grown at 30 ℃ for two days. A single colony was then inoculated to 5 mL of fresh SD medium in a 50 mL conical tube (BD Falcon™, NJ, USA) and allowed to grow at 30 ℃, 180 rpm in a rotary shaker overnight. A portion of this pre-culture broth was added to 50 mL of fresh SD medium

in a shaking flask and grown to an OD_{600} of 1.0. The 0h-point sample was collected as follows: Five OD_{600} units (OD_{600} × milliliters) of cells were poured into a filter funnel connected to a vacuum system to separate cells from culture medium. A nylon filter membrane (Millipore 25 mm diameter, 0.45 μM pore size, Millipore, MA, USA) was used to collect the cells. Four milliliters of 50 mM potassium chloride (KCl) solution precooled to 4 ℃ was immediately poured into the filter funnel to wash the cells. The filter-bound cells were then transferred into a 2 mL microcentrifuge tube (Eppendorf, Hamburg, Germany) and rapidly frozen in liquid nitrogen to halt metabolism. The time was recorded as time 0. For autophagy induction, the rest cell culture was immediately poured into a 50 mL conical tube and centrifuged at 3,000g, 30 ℃ for 3 min to deposit the cells. The supernatant was removed and an equivalent amount of washing solvent (50 mM KCl solution) was added after vortexing. Cells were centrifuged again to remove the washing solvent and shifted into a new flask containing an equivalent amount of SD-N (nitrogen starvation experiment), SD-C (carbon starvation experiment) or SD+RP (rapamycin treatment experiment) medium. Samples were then collected at the indicated time points after medium switch by fast filtration as described above. All samples were stored at -80 ℃ until extraction. OD was measured using Microplate Reader (iMark^{TM}, BIO RAD, USA) with a correction factor of 4.5.

2.2.4 Metabolite extraction

The cell samples (5 OD_{600} units) were extracted according to the Bligh-Dyer method (Blige and Dyer, 1959). Specifically, 1 mL of extraction solvent (methanol:water:chloroform at a 5:2:2 ratio, containing 0.035 μg/mL (+)-10-camphorsulfonic acid, 1 μg/mL PIPES and 0.1 mM methionine sulfone as internal standards) was added to each sample and incubated at 4 ℃ for 30 min. Then, 800 μL of the suspension was transferred to a 1.5 mL macrocentrifuge tube (Eppendorf, Hamburg, Germany) and 400 μL of distilled water was added. The sample was then vortexed and centrifuged for 3 min at 4 ℃, 16000 ×g. Eight-hundred microliters of the polar extract (supernatant) was collected, filtered (0.2 μm PTFE, Millipore), concentrated to 60 μL by centrifugal vacuum concentrator, and divided into two aliquots in two separate glass vials for LC/MS analysis.

2.2.5 Metabolome analysis

Cell extracts were analyzed by 1) PFPP stationary phase liquid chromatography (Discovery HS F5, 150 mm × 2.1 mm, particle size 3 μm, Sigma-Aldrich Corp.) coupled with ESI in both positive and negative modes to a triple-quadrupole mass spectrometer (LCMS 8030 plus; Shimadzu, Kyoto, Japan), and 2) reversed phase ion-pairing liquid chromatography with a C18 column (CERI L-column2 ODS, 150 mm × 2.1 mm, particle size 3 μm, Chemicals Evaluation and Research Institute, Kyoto, Japan) coupled with ESI in negative mode to a triple-quadrupole mass spectrometer (same with above). All compounds were verified by precursor and product masses and retention time match to authentic standards (**Table S-1 and S-2**). For 1), the mobile phases were water with 0.1% formic acid (v/v) (A) and acetonitrile with 0.1% formic acid (v/v) (B) at a flow rate of 0.2 mL/min. Concentration of B was increased from 0% to 40% and 80% from 1 to 11 min and 11 to 11.51 min, respectively, held until 12.1 min, decreased to 0% from 12.1 to 12.3 min, and then held at 0% until 15 min. The injection volume was 3 μL, and the column oven temperature was kept at 40 ℃. For 2), the mobile phases were 10 mM tributylamine and 15 mM acetic acid in water (A), and methanol (B) at a flow rate of 0.3 mL/min. Concentration of B was increased from 0% to 25% and 90% from 0.5 to 7.5 min and 7.5 to 11 min, respectively, held for 1 min, decreased to 0% until 12.1 min, and then held at 0% until 15 min. The injection volume was 3 μL, and the column oven temperature was kept at 40°C. The common MS parameters for both 1) and 2) were as follows: the probe position was +1.5 mm, the desolvation line temperature was 250 ℃, the drying gas flow was 15 L/min, and the heat block temperature was 400 ℃. The nebulizer gas flow was 3 L/min and 2 L/min for 1) and 2), respectively. Other MS parameters were determined by auto-tuning.

2.3 Results

2.3.1 Metabolic profiling of *Saccharomyces cerevisiae* under nitrogen starvation

To investigate the time-dependent changes induced by autophagy, the wild-type and autophagy-defective mutant *atg2*Δ strains were cultivated in SD medium to mid-log phase (OD_{600}=1) and transferred to SD-N medium (**Fig. 2-3**). The abrupt transition from nutrient-complete medium to nutrient-deprivation medium would effectively induce autophagy in the wild-type cells but not in the *atg2*Δ cells, as observed in **Fig.2-1**. By

comparing the metabolic differences between the two strains, effects of autophagy to cellular metabolome should be observed. The experimental conditions and methods were investigated and optimized specifically for this study including the medium pH, aeration efficiency, washing method for sampling, sampling OD, sampling method, and extraction method (a part of the data were presented in **Appendix I**). From the preliminary experimental results, the differences in most metabolites between the two strains were found to mainly appear in the first few hours after starvation (data not shown), thus, the sampling points were decided at 0, 0.5, 1, 1.5, 2, 4 h points after starvation.

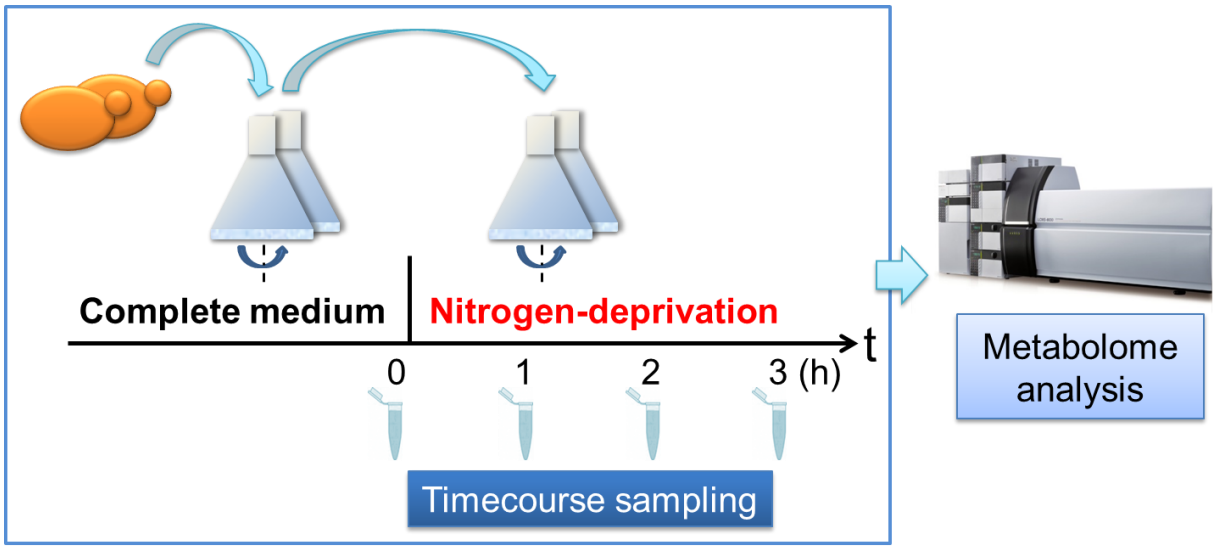

Fig. 2-3. Schematic illustration of the experimental procedure

A total of 95 metabolites were identified, covering a large portion of different metabolic pathways (**Table 2-2)**. Among the identified metabolites, 44 were determined to be significantly different between the wild-type and *atg2*Δ strains at at least one sampling point within the first 4 h after starvation at a confidence interval of 95% by student *t*-test, as shown with underlines. No significant difference was observed at 0 h-point between the two strains, indicating that there was no significant difference between the wild type and autophagy-defective mutants when there were sufficient nutrients in the environment, as also demonstrated by the same doubling time in SD medium (~2 h; see **Appendix II**).

Table 2-2. List of identified compounds

Amino acids/Peptides	Nucleotides	Sugar phosphates	Others
Alanine	3'-AMP	F1P	3PGA
Arginine	5'-AMP	G1P	1,3-BPG
Aspartate	5'-CMP	R5P	Phosphate
Asparagine	3'-GMP	Ru5P	α-Glycerophosphate
Cysteine	5'-GMP	G6P	β-Glycerophosphate
Cystine	3'-UMP	F6P	Lactate
Glutamine	5'-UMP	S7P	Nicotinate
Glutamate	5'-XMP	F1,6P	Phosphoenolpyruvate
Glycine	5'-IMP	F2,6P	2-Isopropylmalate
Histidine	cAMP	DHAP	Pantothenate
Isoleucine	ADP	PRPP	Glyoxylate
Leucine	CDP		Orotate
Lysine	GDP		Trehalose
Methionine	UDP		
Phenylalanine	ADP-Ribose		
Proline	UDP-Glucose		
Serine	ATP		
Threonine	CTP		
Tryptophan	GTP		
Tyrosine	UTP		
Valine			
Homoserine			
Glutathione			
Citric acid intermediates	**Nucleosides**	**Cofactors**	**Bases**
Pyruvate	Adenosine	NAD	Adenine
Citrate	Guanosine	NADH	Guanine
Isocitrate	Cytidine	NADP	Xanthine
2-Oxoglutarate	Uridine	FMN	Hypoxanthine
Succinate	Inosine	FAD	Uracil

Fumarate Malate Oxalacetate	Deoxyadenosine Deoxyguanosine Deoxycytidine Thymidine	Acetyl CoA	

*underlines: significantly different between the wild-type and *atg2*Δ strains (*t*-test, $p<0.05$)

Most metabolites that were determined to be significantly different between the wild-type and *atg2*Δ strains within 4 hours after starvation were mainly involved in protein metabolism, nucleic acid metabolism and pentose phosphate pathway (PPP) (**Table 2-3**). Autophagy-mediated protein degradation and amino acid salvage have long been the focus of autophagy study. As expected, amino acids were depleted in both strains soon after starvation. However, although an immediate recovery was expected in most amino acids as a direct consequence of the bulk protein degradation in the wild-type cells, only a few of them displayed slight increases at around 1~2 hours after starvation before further decreasing to almost the same levels with those in the *atg2*Δ strain (**Fig. 2-4**). The recovery of protein degradation product amino acids was barely observable under nitrogen starvation possibly due to its high recycling speed for protein synthesis.

Table 2-3. Significantly influenced metabolic modules

Pathways	**Related metabolites that exhibited significant differences between WT and *atg2*Δ**
Protein metabolism	Alanine, Arginine, Aspartate, Glutamine, Glutamate, Isoleucine, Leucine, Phenylalanine, Threonine, Tyrosine, Valine,
Nucleic acid metabolism	3'-AMP, 5'-CMP, 3'-GMP, 5'-GMP, 3'-UMP, 5'-UMP, cAMP, Adenosine, Guanosine, Cytidine, Uridine, Inosine, Deoxyadenosine, Deoxyguanosine, Deoxycytidine, Thymidine, Adenine, Guanine, Xanthine, Hypoxanthine, Uracil, PRPP
PPP	R5P, Ru5P, G6P, F6P, S7P, NADP

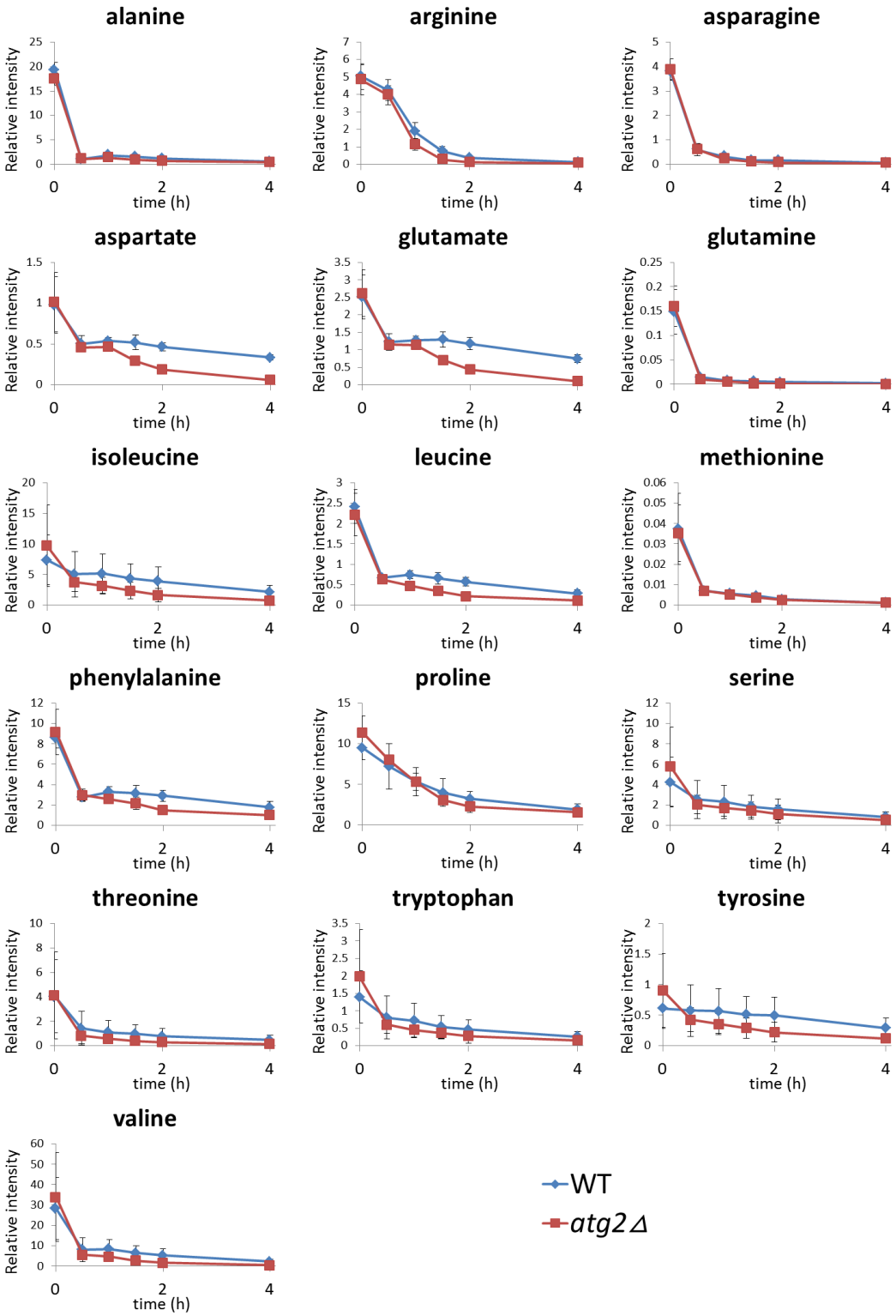

Fig. 2-4. Time-dependent changes in amino acids under nitrogen starvation. The wild-type and *atg2*Δ cells were grown in SD to mid-log phase and transferred to SD-N at time 0. All data are means of quadruplicates. The error bars represent the standard deviation.

Surprisingly, a lot more metabolites around nucleic acid metabolism than those around protein metabolism exhibited significant changes between the wild type and *atg2*Δ, especially, all nucleosides and bases were included. In contrast to the unremarkable differences in amino acids, dramatic differences were observed in the four basic RNA nucleosides, which displayed a similar pattern (**Fig. 2-5**). The wild-type cells exhibited transient increases in nucleosides between 2-fold to 30-fold relative to the basal levels after being transferred to nitrogen-deprivation medium: intracellular levels increased for up to 1 h (for adenosine, guanosine, and cytidine) or 1.5 h (for uridine), started decreasing, and subsided after 4 h of starvation. By contrast, such transient increase was not observed in the *atg2*Δ cells at any time during nitrogen starvation, suggesting the occurrence of autophagy-induced RNA degradation (**Fig. 2-5**).

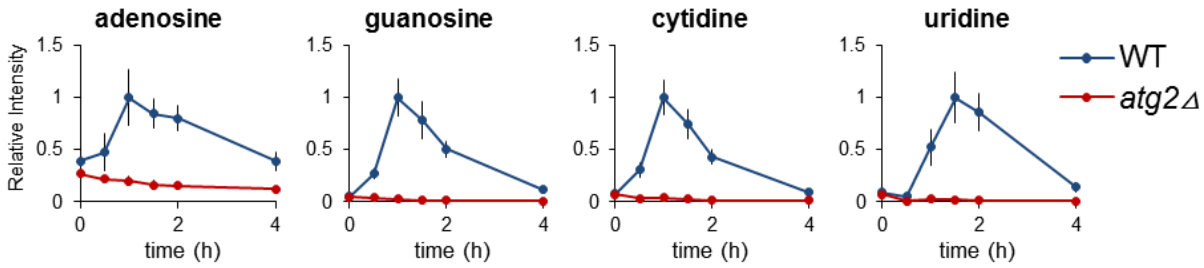

Fig. 2-5. Time-dependent changes in nucleosides under nitrogen starvation. The wild-type and *atg2*Δ cells were grown in SD to mid-log phase and transferred to SD-N at time 0. Cell extracts were analyzed by LC/MS as described in 2.2.4. Results are presented as normalized intensities on the basis of peak height of each metabolite in the wild-type cells. All data are means of quadruplicates. The error bars represent the standard deviation.

2.3.2 Transient increase in intracellular nucleoside levels were observed under different autophagy-triggering conditions

2.3.2.1 Metabolic profiling of S. cerevisiae under carbon starvation

To further investigate this phenomenon, I performed similar time-course metabolic profiling of *S. cerevisiae* under other autophagy-triggering conditions. Carbon deficiency is another commonly studied autophagy trigger. So I cultivated the wild-type and *atg2*Δ strains in SD medium and transferred them, separately, into carbon-deprivation medium under the same protocol of nitrogen starvation experiment (Section 2.2.3~2.2.5) except for the

replacement of nitrogen-deprivation medium with carbon-deprivation medium. As a result, autophagy was immediately induced upon the change of medium from SD to SD-C: nucleoside and 3'-NMP levels continued to increase in an autophagy-dependent manner for more than 4 hours after starvation (**Fig. 2-6**).

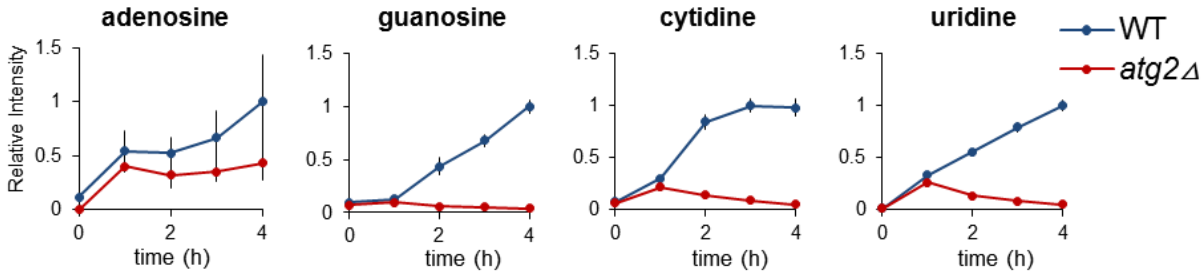

Fig. 2-6. Time-dependent changes in nucleosides under carbon starvation. The wild-type and *atg2*Δ cells were grown in SD and transferred to SD-C at time 0. Cell extracts were analyzed by LC/MS as described in 2.2.4. Results are presented as normalized intensities on the basis of peak height of each metabolite in the wild-type cells. All data are means of triplicates. The error bars represent the standard deviation.

2.3.2.2 Metabolic profiling of S. cerevisiae treated by rapamycin

In addition, I also examined the change in nucleosides in the wild-type and *atg2*Δ strains treated by rapamycin. The cells were first cultivated in SD medium until OD_{600} reached one. After the sampling for 0h-point, all the cells were collected and transferred into rapamycin-included SD medium. The other details are the same as in the nitrogen starvation and carbon starvation experiments (Section 2.2.3~2.2.5). Upon the transfer into rapamycin-included medium, nucleoside levels in the wild-type strain increased dramatically but transiently, just as observed under nitrogen starvation. Same with the other stress conditions, no such changes were observed in the *atg2*Δ strain (**Fig. 2-7**).

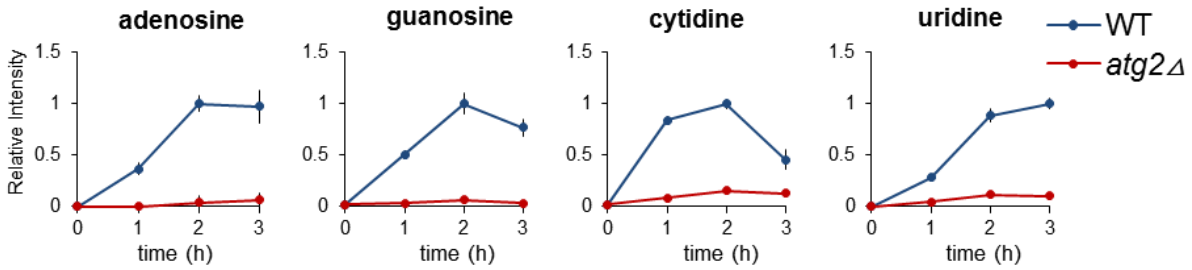

Fig. 2-7. Time-dependent changes in nucleosides after rapamycin treatment. The wild-type and *atg2*Δ cells were grown in SD and transferred to SD medium with 0.2 μM rapamycin at time 0. Cell extracts were analyzed by LC/MS as described in 2.2.4. Results are presented as normalized intensities on the basis of peak height of each metabolite in the wild-type cells. All data are means of triplicates. The error bars represent the standard deviation.

2.4 Discussion

In this chapter, I performed the metabolic profiling of *S. cerevisiae* X2180 (wild-type) and the autophagy-defective mutant *atg2*Δ under nitrogen starvation, carbon starvation and rapamycin-treatment conditions. Although the kinetics are distinctive, all autophagy-triggering conditions examined inevitably caused dramatic elevation of intracellular nucleoside levels, strongly indicating a common phenomenon that RNA is degraded by autophagy under different autophagy-triggering conditions. As autophagy is intensively induced by nitrogen starvation and lasts for at least several hours, this transient accumulation of nucleosides demonstrated that nucleosides are rapidly further metabolized during nitrogen starvation. To follow this, nitrogen starvation was selected as the representative autophagy-triggering conditions for the rest of this study (see Chapter 3).

Under nitrogen starvation, pathways around protein metabolism, nucleic acid metabolism and pentose phosphate pathway exhibited significant changes between the wild-type and *atg2*Δ strains in the first few hours after starvation. The primary functions of PPP are NADPH generation, synthesis of amino acid precursors (Glyceraldehyde 3-phosphate, Erythrose 4-phosphate and ribose 5-phosphate (R5P)), and synthesis of nucleotide precursor (R5P). It is possible that the wild type consumes more NADPH than *atg2*Δ due to its relatively more active cellular activities including protein synthesis, which becomes a driving power for PPP. Besides, a recent report suggested that the ribose moiety (ribose 1-phosphate

(R1P)/ribose) derived from the degraded RNA is rapidly converted into R5P and then enters PPP to make NADPH for antioxidant defense under carbon starvation (Xu *et al.*, 2013). If this is also true for nitrogen starvation, it might also partially contribute to the differences observed in PPP intermediates between the two strains. In this thesis, I only discussed about the metabolic changes induced by autophagy in a very short period. Indeed, preliminary experiments of longer starvation suggested other potential interesting points --- changes in metabolites involved in other parts of metabolism between the two strains such as tricarboxylic acid cycle were observed (data not shown), which is in consistence with the conclusion drawn by a previous study that autophagy defect causes mitochondria dysfunction (Suzuki *et al.*, 2011). Further investigation on long-term metabolic changes under starvation conditions might reveal new insights into autophagy.

Chapter 3 Mechanism of bulk RNA degradation via autophagy under nitrogen starvation in yeast

3.1 Introduction

Ribosomes are complex structures comprised of ribosomal RNAs and proteins at a ratio closed to 1:1. Under nutrient-rich conditions, ribosomal subunits are assembled at a remarkable rate (>2,000 ribosomal subunits/minute) in yeast cells, piling up to about 200,000 ribosomes in a single cell, accounting for almost 50% of all cellular proteins and 80% of total RNA in growing cells (Kraft *et al.*, 2008). The synthesis of ribosomes, however, is immediately stopped under nutrient-depleted conditions and superfluous ribosomes are decomposed in a sense of providing the essential nutrients as well as reducing the rate of protein synthesis to maintain a minimal requirement of basic energetic activities for cell survival. From the microscopic images of *S. cerevisiae* taken under nitrogen starvation conditions, we can see that most autophagic bodies contain the same, occasionally even higher density of ribosomes as the cytoplasm (Takeshige *et al.*, 1992, **Fig. 2-1**). Recently, a novel selective type of autophagy for ribosome degradation, ribophagy, has been reported in yeast (Kraft *et al.*, 2008). Although the mechanisms are not completely understood, it is clear that ribosomes are targets of both selective and non-selective autophagic degradation.

During ribosome degradation via autophagy, not only ribosomal proteins, but also a large number of ribosomal RNAs must be degraded in the vacuole/lysosome. Pioneer work by Mortimore showed that RNA degradation is induced in perfused rat liver due to amino acid starvation (Lardeux *et al.*, 1987; Lardeux and Mortimore, 1987; Lardeux *et al.*, 1988; Mortimore *et al.*, 1989). They published a series of related articles using ^{14}C-labelled cytidine as a marker for RNA degradation in perfused rat liver previously labelled *in vivo* with [6-^{14}C]orotic acid during 1987~1989. Nevertheless, they did not provide any direct proof of the relation between autophagy and RNA degradation, and the mechanism of the degradation process was barely described. Because autophagy has been recognized as a mechanism mainly to salvage amino acids from proteins for the past few decades, autophagy studies were mostly focused on autophagic proteolysis. As opposed to the fact that the mechanism of

protein degradation was extensively studied, little attention has been paid to autophagic RNA degradation and the molecular details were still waiting to be uncovered.

As introduced in section 1.2, there are various types of autophagy, the major starvation-induced non-selective autophagy and other selective types with particular targets. To elucidate the degradation mechanism of RNA, I started by investigating which type of autophagy is involved in the generation of nucleosides during starvation. In order to clarify the main autophagic type that is directly related to the accumulation of nucleosides, one to two essential components for each type were selected and the metabolic profiles of their knockout mutants under nitrogen starvation were compared with that of the wild type to evaluate the contribution of each independent type to starvation-induced RNA degradation (**Table 3-1**). Atg17 is a member of the Atg1 kinase signaling complex, which localizes other proteins to the PAS (Kabeya *et al*., 2005). Atg11 functions as a scaffold protein at the PAS for selective types of autophagy by interacting with Atg8 (Yorimitsu *et al*., 2005; Farré *et al*., 2013). Atg32 is a mitochondrial outer membrane protein. It initiates the mitophagy-specific phagophore membrane expansion during mitophagy (Okamoto *et al.*, 2009; Kanki *et al.*, 2009). Nvj1 is an outer nuclear membrane protein, which associates with a vacuolar membrane protein Vac8 to form the nucleus-vacuole (NV) junctions during PMN pathway (Dawaliby *et al.*, 2010). Atg19 is known as the receptor for the cargo proteins of Cvt pathway, Ape1 (Scott *et al.*, 2001).

Ubp3 and Bre5, a ubiquitin deconjugation enzyme and its cofactor, are needed for ribosome-specific pathway, ribophagy, which degrades ribosomes preferentially to other cytosolic components during nitrogen starvation (Kraft *et al.*, 2008). Interestingly, they were found to mediate preferential degradation of only ribosomal 60S proteins, but not 40S proteins. Ubp3 is an *ub*iquitin-specific *p*rotease. Although the mechanism is not fully understood, it is possible that ribosomes are originally in an ubiquitinated state before the recognition of autophagic membranes and in order to trigger the engulfment or to complete the autophagosome after the engulfment, the ubiquitin needs to be removed by Ubp3. Thus, Ubp3 might acts as a regulator of selective engulfment of ribosomes, possibly by working on

a “ribosome receptor” to selectively target ribosomes, which is so far not identified yet (Kraft *et al.*, 2008).

In addition, common essential components involved in different parts of autophagy process were also discussed. Atg2, which was used as the negative control for this whole study, is the most downstream ATG protein in the PAS organization process. It localizes Atg18 to autophagic membranes, forming an Atg2-Atg18 complex, whose recruitment to the PAS requires an interaction between phosphatidylinositol 3-phosphate and Atg18 (Obara *et al.*, 2008). Atg7 participates in two important conjugation processes which result in the covalent modification of Atg8 with PE and the covalent attachment of Atg12 to Atg5, respectively. These two conjugation systems are essential for the membrane initiation and elongation of autophagosome (Mizushima *et al.*, 1998). *PEP4* and *PRB1* encode proteinase A and proteinase B, respectively, both of which are located in the vacuole. Proteinase A and proteinase B are the major vacuolar proteases, activating themselves and other hydrolases such as carboxypeptidase Y and their deletions cause accumulation of autophagic bodies in the vacuole under starvation because the autophagic bodies, which are delivered to the vacuole, cannot be broken down (Takeshige *et al.*, 1992).

Table 3-1. Targeted components for different types of autophagy

Selectivity	Type	Essential components	
Non-selective	Non-selective autophagy	Atg17	Atg2, Atg7 Pep4, Prb1
Selective	Mitophagy	Atg11, Atg32	
	Pexophagy	Atg11	
	PMN pathway	Nvj1	
	Cvt pathway	Atg11, Atg19	
	Ribophagy	Ubp3, Bre5	

The canonical RNA degradation process is shown in **Fig. 3-1**. First, a long RNA single strand is hydrolyzed by ribonucleases (RNases) into nucleoside monophosphates. Based on

the type of the ribonuclease, either 5’-nucleoside monophosphates (5’-NMP) or 3’-nucleoside monophosphates (3’-NMP) are produced. The phosphate group is then taken by a nucleotidase, leaving the nucleoside which is further converted into a base and a ribose (pyrimidine nucleoside) or a ribose-1-phosphate (purine nucleoside). Bases and their derivatives are listed in **Table 3-2**.

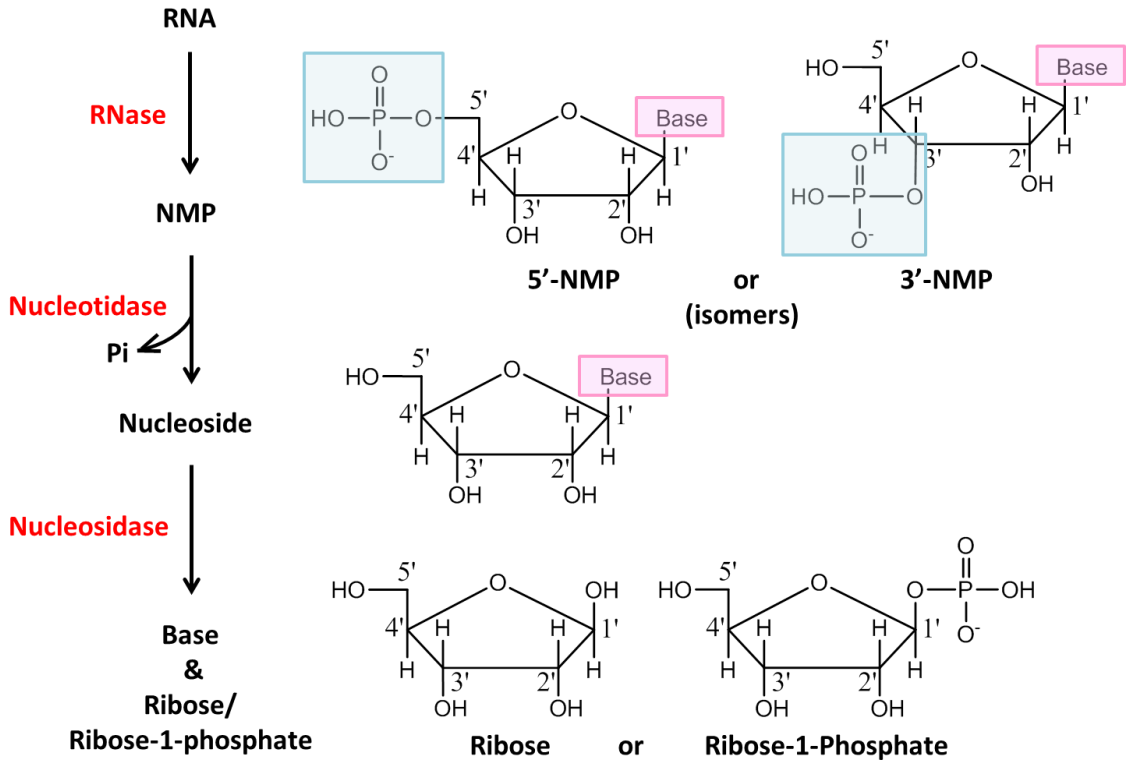

Fig. 3-1. Canonical RNA degradation process

Table 3-2. Bases and their derivatives

Type	Purine				Pyrimidine	
NMP	3’/5’-AMP	3’/5’-GMP	3’/5’-IMP	3’/5’-XMP	3’/5’-CMP	3’/5’-UMP
Nucleoside	Adenosine	Guanosine	Inosine	Xanthosine	Cytidine	Uridine
Base	Adenine	Guanine	Hypoxanthine	Xanthine	Cytosine	Uracil

RNases play important roles in many aspects of RNA metabolism. Multiple types of RNase have been identified and classified according to their structural and biochemical

properties. Broadly, RNases can be divided into endoribonucleases and exoribonucleases. Classical biochemical studies revealed the existence of alkaline RNases, such as the RNase T1 and RNase A families, and acid RNases, comprising the RNase T2 family (Irie, 1999). RNase T2 is an endonuclease with weak base specificity that is found in all organisms. In yeast, Rny1 is the sole T2 family RNase identified to date, but its biological role in the vacuole has not yet been fully understood (MacIntosh *et al.*, 2001).

In this chapter, metabolome analysis (e.g. metabolic profiling), combined with molecular biological techniques, was employed to characterize RNA degradation process under nitrogen starvation. Changes in the metabolome profiles of *S. cerevisiae* cells subjected to abrupt transition from complete minimal medium to nitrogen-deprivation medium were analyzed by Liquid Chromatography - Mass Spectrometry (LC/MS). In addition, since autophagy is known to be highly conserved among eukaryotes, it is interesting to examine whether the mechanism of autophagy-induced RNA degradation is preserved among different organisms. Therefore, to demonstrate this mechanism as a universal strategy for cells to adjust to starvation conditions, I further examined its universality by conducting time-course metabolome analysis of the fission yeast, *Schizosaccharomyces pombe*, under nitrogen starvation. (The content of this chapter was conducted in collaboration with Professor Ohsumi from Tokyo Institute of Technology.)

3.2 Materials and methods

3.2.1 Materials and reagents

Same as in section 2.2.1.

Important standards including adenine, cytosine, guanine, uracil, adenosine, guanosine, uridine, cytidine 5'-monophosphate, guanosine 5'-monophosphate, xanthosine 5'-monophosphate, uridine 5'-monophosphate, thymidine 5'-monophosphate, cytidine 5'-diphosphate, guanosine 5'-diphosphate, uridine 5'-diphosphate, adenosine 5'-triphosphate, cytidine 5'-triphosphate, guanosine 5'-triphosphate, and uridine 5'-triphosphate were purchased from Wako (Osaka, Japan). Cytidine and uridine 3'-monophosphate were obtained from Kohjin co. ltd. (Tokyo, Japan) and Carbosynth (Compton, UK), respectively. Others including xanthine, hypoxanthine, adenosine 3'-monophosphate, adenosine

5’-monophosphate, adenosine 5’-diphosphate, guanosine 3’-monophosphate, thymidine 3’-monophosphate, adenosine 5’-diphosphate ribose, and uridine 5’-diphosphate glucose were all from Sigma-aldrich corp. (Mo, USA).

3.2.2 Yeast strains and media

Yeast strains used in this chapter are listed in **Table 3-3**. All mutant strains were provided by Ohsumi-lab from Tokyo Institute of Technology

Table 3-3. Yeast strains used in this chapter

S. cerevisiae

Strain	**Genotype**	**Source**
X2180-1B	*MATα SUC2 mal mel gal2 CUP1*	Yeast Genetic Stock Center
MMY3	*X2180-1B;atg2Δ::kanMX6*	(Huang *et al.*, 2014)
JOY27	*X2180-1B;atg7Δ::kanMX4*	(Onodera and Ohsumi, 2005)
MMY7	*X2180-1B;atg11Δ::kanMX6*	(Huang *et al.*, 2014)
MMY9	*X2180-1B;atg17Δ::kanMX6*	(Huang *et al.*, 2014)
MMY10	*X2180-1B;atg19Δ::kanMX6*	(Huang *et al.*, 2014)
MMY198	*X2180-1B;atg32Δ::kanMX6*	(Huang *et al.*, 2014)
MMY279	*X2180-1B;nvj1Δ::kanMX6*	(Huang *et al.*, 2014)
TMK971	*X2180-1B;pep4Δ::kanMX6 prb1Δ::hphNT1*	(Huang *et al.*, 2014)
MMY156	*X2180-1B;pep4Δ::zeo prb1Δ::hphNT1, atg2Δ::kanMX6*	(Huang *et al.*, 2014)
MMY361	*X2180-1B;phm8Δ::kanMX6*	(Huang *et al.*, 2014)
TMK974	*X2180-1B; pho8Δ::kanMX6*	(Huang *et al.*, 2014)
MMY204	*X2180-1B;rny1Δ::natNT2*	(Huang *et al.*, 2014)
MMY375	*X2180-1B;rny1Δ::natNT2, atg2Δ::kanMX6*	(Huang *et al.*, 2014)
MMY337	*X2180-1B;RNY1-GFP::kanMX6*	(Huang *et al.*, 2014)
MMY356	*X2180-1B;RNY1-GFP::kanMX6 atg2Δ::hghNT1*	(Huang *et al.*, 2014)
TMK826	*X2180-1B;PHO8-GFP::kanMX6*	(Huang *et al.*, 2014)
MMY647	*X2180-1B;PNP1-GFP::kanMX6*	(Huang *et al.*, 2014)
MMY649	*X2180-1B;URH1-GFP::kanMX6*	(Huang *et al.*, 2014)
TMK852	*X2180-1B;PHO8-GFP::kanMX6 atg2Δ::hghNT1*	(Huang *et al.*, 2014)

MMY334	*X2180-1B;ubp3Δ::kanMX6*	(Huang *et al.*, 2014)
MMY339	*X2180-1B;bre5Δ::kanMX6*	(Huang *et al.*, 2014)
MMY722	*X2180-1B;ubp3Δ::kanMX6, rny1Δ::hyhNT1*	(Huang *et al.*, 2014)
MMY720	*X2180-1B;bre5Δ::kanMX6, rny1Δ::hyhNT1*	(Huang *et al.*, 2014)
MMY13	*X2180-1B;pep4Δ::kanMX6*	(Huang *et al.*, 2014)
MMY254	*X2180-1B;urh1Δ::kanMX6*	(Huang *et al.*, 2014)
MMY256	*X2180-1B;pnp1Δ::kanMX6*	(Huang *et al.*, 2014)
MMY20	*X2180-1B; pho8::GPD^{p}-pho8Δ60::natNT2*	(Huang *et al.*, 2014)
MMY24	*X2180-1B;pho8::GPD^{p}-pho8Δ60::natNT2 atg2Δ::kanMX6*	(Huang *et al.*, 2014)
MMY384	*X2180-1B;pho8::GPD^{p}-pho8Δ60::natNT2 rny1Δ::kanMX6*	(Huang *et al.*, 2014)
MMY108	*X2180-1B; atg8Δ::GFP-ATG8::hphNT1 atg11Δ::kanMX6*	(Huang *et al.*, 2014)
MMY465	*X2180-1B; atg8Δ::GFP-ATG8::hphNT1 atg11Δ::natNT2 rny1Δ::kanMX6*	(Huang *et al.*, 2014)
MMY467	*X2180-1B; atg8Δ::GFP-ATG8::hphNT1 atg11Δ::natNT2 pho8Δ::kanMX6*	(Huang *et al.*, 2014)
MMY30	*X2180-1B; pho8::GPD^{p}-pho8Δ60::natNT2 atg11Δ::kanMX6*	(Huang *et al.*, 2014)
MMY34	*X2180-1B; pho8::GPD^{p}-pho8Δ60::natNT2 atg17Δ::kanMX6*	(Huang *et al.*, 2014)
MMY36	*X2180-1B; pho8::GPD^{p}-pho8Δ60::natNT2 atg19Δ::kanMX6*	(Huang *et al.*, 2014)

Schizosaccharomyces pombe

Strain	***Genotype***	**Source**
JY1	*h^{-}*	(Kohda *et al.*, 2007)
JV905	*h^{-} ura4.d18 atg1::ura4^{+}*	(Kohda *et al.*, 2007)

3.2.3 Yeast culture and metabolite extraction

Cells were cultivated as described in section 2.2.3. To obtain culture fluid, 200 µL of the cell culture was filtered (0.2 µm PTFE, Millipore) and stored at -80 ℃ until the analysis. Cell samples were extracted as described in section 2.2.4. Medium samples were directly analyzed by LC/MS.

3.2.4 Metabolome analysis

Metabolites were analyzed as described in section 2.2.5.

3.2.5 Absolute quantitation

Absolute intracellular metabolite concentrations in the wild-type strain at 1 h were determined by the standard addition method. A standard mixture was made by mixing all kinds of 3'/5'-mononucleotides, nucleosides, and bases. Sixty microliters of a 2-fold dilution series of the standard mixture ranging from 5 nM to 5 μM (4.88 nM, 9.77 nM, 19.5 nM, 39.1 nM, 78.1 nM, 156 nM, 313 nM, 625 nM, 1.25 μM, 2.5 μM, 5 μM) were added to 12 identical samples (with one leaving blank) of the wild-type strain at 1 h respectively before extraction and extracted as described above. The metabolite concentrations of the spiked samples were obtained from the calibration curves derived from the spiked samples. The absolute intracellular concentrations were then calculated from the cell number determined by hemocytometery (1 OD_{600} unit corresponds to 2.7×10^7 cells/mL) and a cell volume of 42 fL (42×10^{-15} L) (Tyson *et al.*, 1979). Metabolite concentrations in other samples were calculated based on fold change in peak areas relative to the wild-type strain at 1 h. For medium samples, the external standard method was applied, and all concentrations were obtained directly from the calibration curves derived from a 2-fold dilution series of the same standard mixture ranging from 5 nM to 20 μM (4.88 nM, 9.77 nM, 19.5 nM, 39.1 nM, 78.1 nM, 156 nM, 313 nM, 625 nM, 1.25 μM, 2.5 μM, 5 μM, 10 μM, 20 μM).

Flowchart of the calculation procedure for metabolite quantitation

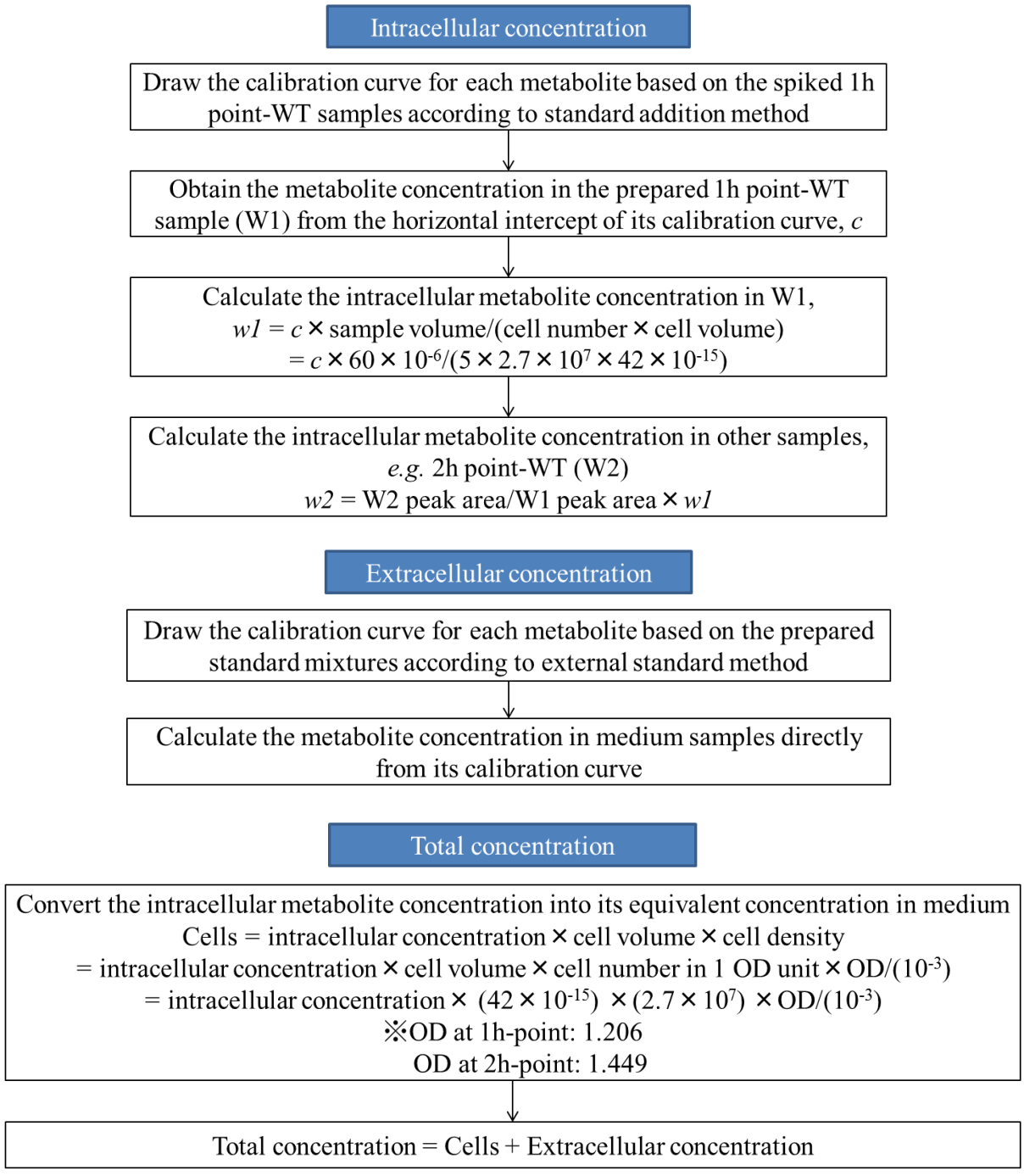

3.2.6 Western blotting

Immunoblot analyses were performed as described previously (Kushnirov, 2000). Samples corresponding to 0.5-1 OD_{600} units of cells were separated by SDS-PAGE followed by western blotting. Antibodies against GFP (1:1000, Roche), ALP (1:100, Life

Technologies-Novex), Pep4, and Prb1 were used as primary antibodies. Chemiluminescence was induced by Femtoglow HRP Substrate (Michigan Diagnostics), and images were acquired by LAS-4000 imaging. The images were processed using the Multi Gauge software (Fujifilm Life Sciences).

3.2.7 Fluorescence microscopy

Intracellular localization of proteins was examined using an inverted fluorescence microscope as described previously (Suzuki *et al.*, 2010). Images were acquired on an inverted fluorescence microscope (IX71; Olympus) equipped with a 150× total internal reflection fluorescence objective (UAPON 150×~ OTIRF, NA 1.45; Olympus) and a CCD camera (ImagEM C9100-13; Hamamatsu Photonics). Images were captured using image acquisition system, analysis software (AQUACOSMOS (Hamamatsu Photonics) or MetaMorph 7.0r4 (Molecular Devices)), and processed in Adobe Photoshop. For RNA staining, cells grown in SD or SD-N medium for 2 h were incubated with GR Green (BIO-CRAFT) for 30 min at room temperature, washed three times with PBS, and visualized by fluorescence microscopy with GFP filter. Vacuoles were labeled with FM4-64 (Molecular Probes) as described previously (Vida and Emr, 1995).

3.2.8 Alkaline phosphatase (ALP) assays

ALP assay is a method to monitor the nonspecific macroautophagy activity based on Pho8Δ60 (Noda *et al.*, 1995). Pho8Δ60 is a truncated form of the vacuolar alkaline phosphatase Pho8, which can only be delivered to the vacuole by autophagy mechanism. On delivery, the zymogen is activated upon the removal of the C-terminal propeptide and can thereby be measured enzymatically. Thus, evaluating the activity of pho8 can be seen as an indirect measurement of autophagic activity.

ALP assays were performed as described previously (Noda *et al.*, 1995). Yeast lysate was prepared by disrupting the cells with glass beads in ice-cold reaction buffer (50 mM Tris-HCl pH 9.0, 5 mM $MgCl_2$, 1 mM phenylmethylsulfonyl fluoride (PMSF), and 1 μg/ml pepstatinA (Sigma)) and the cell debris was removed by centrifugation at 10,000 g for 5 min. Alkaline phosphatase in the lysate was assayed with para-Nitrophenyl Phosphate (p-NPP)

(Wako) as a substrate by the method of Torriani (Torriani, 1960) in the presence of 1 mM PMSF and 1 μg/ml pepstatin A. One micromole of p-nitro-phenol gives 11.7 units of ΔA_{420}.

3.2.9 Total RNA extraction, northern blot, and quantitative RT-PCR (qPCR)

Total yeast RNA was extracted by hot phenol methods as described before (Kohrer and Domdey, 1991). Frozen yeast cell pellets (seven OD_{600} units of cells) were resuspended in 440 μl of AE buffer (50 mM Sodium acetate, 10 mM EDTA (pH 5.0)) containing 1% SDS and 1.5 g of Zirconia silica beads were added to facilitate cell lysis. Immediately, 500 μl of hot phenol/AE was added and the cells were lysed using a FastPrep 24 machine (MP Biomedicals) with a setting of 30 s at 5.5 m/s for four times. The RNAs were then recovered from the aqueous phase by precipitation with methanol.

For northern blotting, 5 μg of the extracted RNAs were separated on a denaturing formaldehyde agarose gel (1% Agarose, 1x MOPS) or on a 10% polyacrylamide gel containing Urea (SequaGel UreaGel System, National Diagnostics) and transferred to Nylon membrane (Hybond N+, GE). Oligo DNA used for the DNA probe was radiolabeled with T4 polynucleotide kinase (Takara Bio Inc.) and [α-^{32}P] ATP. The other DNA probes were synthesized with a Random Primer DNA Labeling Kit Ver.2 (Takara Bio Inc.) and [α-^{32}P] dCTP using PCR products corresponding to the coding region of the gene of interest. All probes were hybridized using PerfecthybPlus (Sigma) according to the recommendations of the manufacturer. Images were acquired by PhosphorImager (FLA-7000 image analyzer, Fujifilm Life Sciences) and quantified using Multi Gauge software (Fujifilm Life Sciences). Oligonucleotides for northern blotting are listed in **Table 3-4**.

For qPCR, total RNAs were cleaned up using the RNeasy mini kit (Qiagen). To eliminate genomic DNA, on-column DNase I digestion (Amplification Grade, Invitrogen) was performed according to the RNeasy kit instruction. cDNA was prepared using a SuperScript III First-Strand Synthesis System for RT-PCR kit (Invitrogen) with random hexamers according to the manufacturer's instructions. One microgram of total RNA was reverse-transcribed into cDNA. Abundance of each RNA (rRNA, tRNA, snRNA, snoRNA, and mRNA) was determined by a StepOnePlus™ realtime PCR system (Life technologies)

using Power SYBR Green PCR Master Mix (Life technologies). Gene-specific primers for each gene are described in **Table 3-4**. The PCR efficiency of the primer pairs was evaluated by the dilution series method using cDNA as the template. The cycling parameters were: 95℃ for 10 min, followed by 40 cycles of amplification at 95℃ for 15 sec and 60℃ for 1 min. Melting-curve data of PCR products was then collected to verify the presence of a single amplification product. Relative expression levels were determined by the $2^{-\Delta\Delta Ct}$ method, as the PCR efficiencies of all gene-specific primers were within a permissive range as described in the manufactured manual. The RNA levels were normalized by U4 (snRNA) or SnR189 (snoRNA) abundance, and the fold change between growth and nitrogen-starvation conditions was calculated.

Table 3-4. Oligonucleotides and probes for northern blotting and qPCR

(A) Single stranded probe for Northern blot	**sequence (5'-3')**		**Reference**
25S RNA	ACCCACGTCCAACTGCTGT		(Pestov and Shcherbik, 2012)
18S RNA	AGAATTTCACCTCTGACAATTG		(Pestov and Shcherbik, 2012)
$tRNA^{leu}$	TGCCGCCTTAGACCACTCGGCCAACCCTCC		(Huang *et al.*, 2014)
$tRNA^{Phe}$	CTGGCGCTCTCCCAACTGAGCTAAATCCGC		(Huang *et al.*, 2014)
$tRNA^{Val}$	AGATGCCATAACCGACTAGACCACGAAACC		(Huang *et al.*, 2014)
$tRNA^{Arg}$	TCAGACGCGTTGCCATTACGCCACGCGAGC		(Huang *et al.*, 2014)
SnRNA(U4)	CACCGAATTGACCATGAGGAGACGGTCTGG		(Huang *et al.*, 2014)
SnoRNA(SnR13)	TTCCACACCGTTACTGATTT		(Huang *et al.*, 2014)
SnoRNA(SnR50)	CTTTGTTTGATTCAATCACGAAAAATCTGCTGC		(Huang *et al.*, 2014)
(B) Oligonucleotides for Northern blot	**Forward primer (5'-3')**	**Reverse primer (5'-3')**	**Reference**
HSP26	CCGCTCGAGCGTTGGAC TTTTTTTAATATAA	CGGGATCCGTTACCCCA CGATTCTTGAGAA	(Onodera and Ohsumi, 2005)

(C) Oligonucleotides for qRT-PCR	**Forward primer (5'-3')**	**Reverse primer (5'-3')**	**Reference**
$tRNA^{Arg}$	GCTCCTCTAGTGCAATGG	TCGAACCCGGATCACAG	(Huang *et al.*, 2014)
RDN18	AACTCACCAGGTCCAGACACA ATAAGG	AAGGTCTCGTTCGTTATCGCA ATTAAGC	(Huang *et al.*, 2014)
RDN25	CCTGATGTCTTCGGATGGATTT	TCCTCTGGCTTCACCCTATT	(Huang *et al.*, 2014)
SnR189	CCAAGGACCGGTATTATTGTAG G	GTACTTATTCTCGAACTCGGT TGTA	(Huang *et al.*, 2014)
U4	TCCTTATGCACGGGAAATACG	TGAGGAGACGGTCTGGTTTA	(Huang *et al.*, 2014)
U6	GTAACCCTTCGTGGACATTTG	AAACGGTTCATCCTTATGCAG	(Huang *et al.*, 2014)

U14	GGTGATGAAAGACTGGTTCCT	GTCTCTAAAGAAGAGCGGTCAC	(Huang *et al.*, 2014)
TAF10	ATATTCCAGGATCAGGTCTTCCGTAGC	GTAGTCTTCTCATTCTGTTGATGTTGTTGTTG	(Teste *et al.*, 2009)
ATG8	CCTGAGAAGGCCATCTTCATTT	CCGTCCTTATCCTTGTGTTCTT	(Huang *et al.*, 2014)

3.3 Results

3.3.1 Non-selective autophagy plays the main role in autophagy-mediated RNA degradation under nitrogen starvation

Similar with *atg2*Δ, mutants lacking *ATG7* or *ATG17*, both of which are essential for starvation-induced autophagy, exhibited no accumulation of nucleosides at all (**Fig. 3-2A**). By contrast, deletion of *ATG19, ATG32* or *NVJ1*, which are necessary for the Cvt pathway, mitophagy and the PMN pathway, respectively, did not affect the transient increases in nucleoside levels (**Fig. 3-2A**). Atg11 was originally identified as an essential component for the Cvt pathway. However, recent studies suggested that although not essential, Atg11 also functions together with the core autophagy components during starvation-induced autophagy (Mao *et al.*, 2013). In agreement with this, *atg11*Δ cells exhibited a moderate increase in nucleoside levels as compared with the wild-type cells (**Fig. 3-2A**). To evaluate the autophagic activities in these mutants, ALP assay was performed. In accordance with the metabolome data, autophagic activity of *atg11*Δ cells was partially defective (**Fig. 3-2B**), which is considered to be the primary cause that led to the reduced level of nucleoside increase. To further confirm that the accumulated nucleosides were derived from the degradation of autophagic bodies relying on vacuolar proteases, a double-deletion strain of vacuolar protease Pep4 and Prb1, *pep4*Δ*prb1*Δ, was constructed. As expected, in *pep4*Δ*prb1*Δ cells, the increase in nucleoside levels was completely abolished (**Fig. 3-2A**), demonstrating that disruption of autophagic bodies is required for the generation of nucleosides. These data indicate that non-selective autophagy contributes substantially to the increase in nucleoside levels during starvation, whereas selective autophagy plays a less significant role. Ribophagy is discussed separately in section 3.3.5.

A.

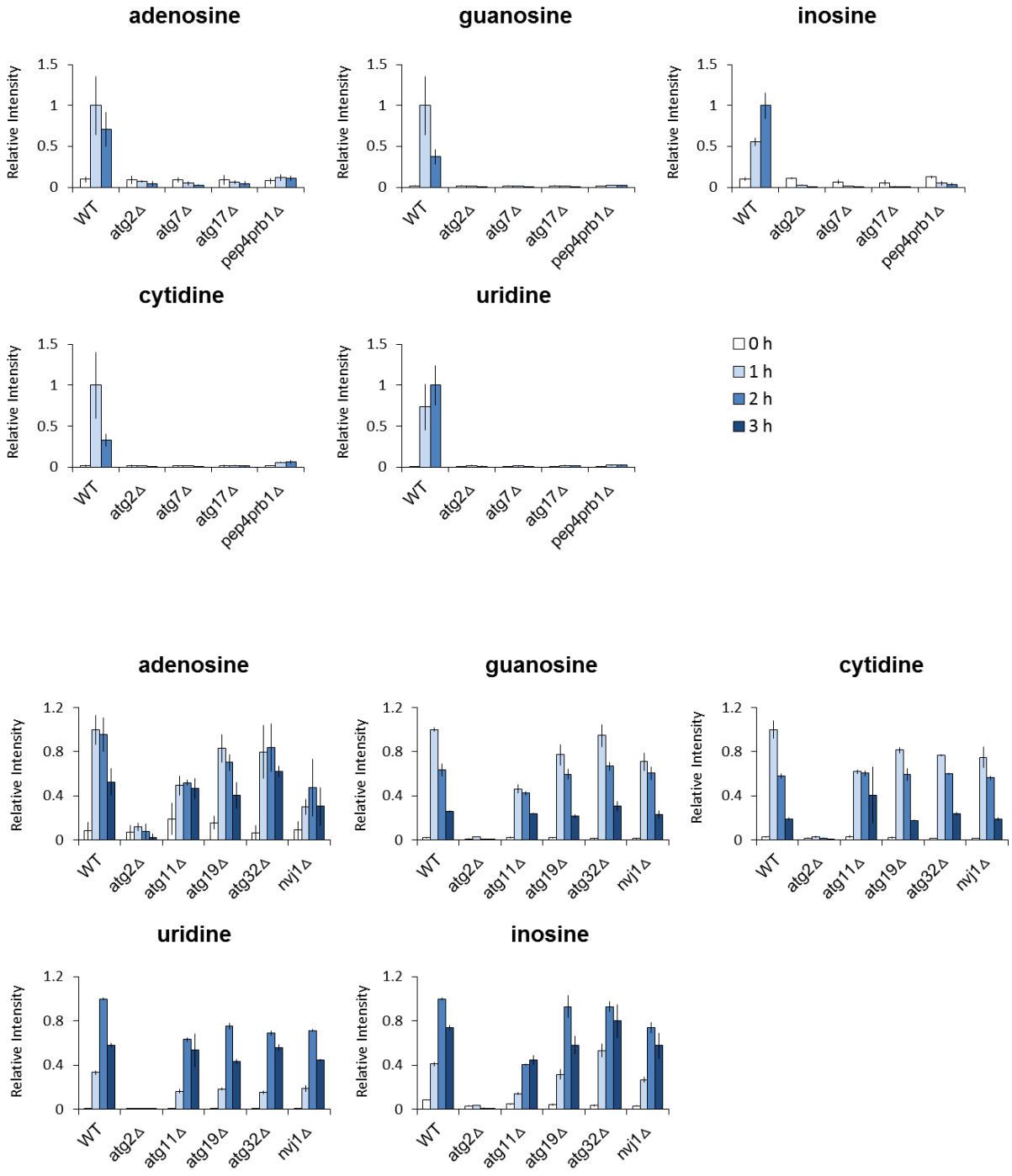
adenosine
guanosine
inosine
cytidine
uridine
Relative Intensity
0 h
1 h
2 h
3 h
WT
atg2Δ
atg7Δ
atg17Δ
pep4prb1Δ
atg11Δ
atg19Δ
atg32Δ
nvj1Δ

B.

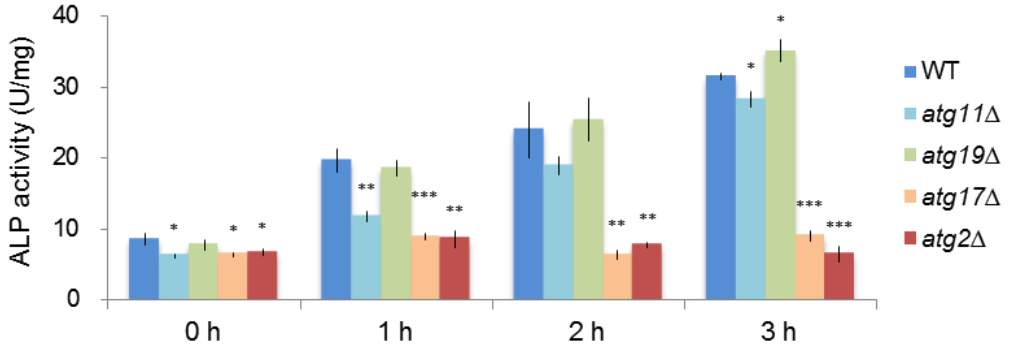

Fig. 3-2. Contribution of different autophagy forms to starvation-induced RNA degradation. (A) Time-dependent changes in nucleoside levels under nitrogen starvation. The wild-type, *atg2*Δ, *atg7*Δ, *atg11*Δ, *atg17*Δ, *atg19*Δ, *atg32*Δ, *nvj1*Δ, and *pep4*Δ*prb1*Δ cells were grown in SD to mid-log phase and transferred to SD-N at time 0. Samples were analyzed by LC/MS as described in 2.2.4. Results are presented as normalized intensities on the basis of peak height of each metabolite in the wild-type cells. (B) ALP assay (Pho8Δ60). Cells expressing Pho8Δ60 were grown in SD to mid-log phase and transferred to SD-N at time 0. Cell lysates were prepared at the indicated time point and subjected to the ALP assay. All data are means of triplicate samples. The error bars represent the standard deviation. Asterisk, P<0.05; double asterisk, P<0.005; triple asterisk, P<0.0005 (paired *t*-test, two-tailed)

3.3.2 Role of Pho8, a vacuolar nucleotidase

It is reasonable to consider that these nucleosides originated from the degradation of cytoplasmic RNAs in the vacuole, and that each nucleoside was primarily derived from its corresponding nucleotide. Electron microscopic observation of cells under nutrient starvation presented morphological evidence showing that cytoplasmic ribosomes are sequestered to autophagosomes and delivered to the vacuole for degradation (Takeshige *et al.*, 1992; **Fig. 2-1**). Given that ribosomes are highly abundant supramolecular structures composed of proteins and ribosomal RNAs (rRNA) at a nearly 1:1 weight ratio (Warner, 1999), it is likely that the nucleosides detected under starvation were mostly derived from rRNAs.

I first investigated how nucleosides were generated from nucleotides. Recently, Phm8 was identified as a nucleotidase responsible for RNA degradation under starvation in yeast

(Xu *et al.*, 2013). If Phm8 functions in starvation-induced RNA degradation process by dephosphorylating nucleotides, *phm8*Δ cells should produce reduced levels of nucleosides, and consequently accumulate higher levels of nucleotides. Contrary to this expectation, the *phm8*Δ cells accumulated similar levels of both nucleosides and nucleotides (3'-NMPs; see below) to those observed in the wild-type cells, indicating that Phm8 is not requisite for RNA degradation under nitrogen starvation (**Fig. 3-3**).

A

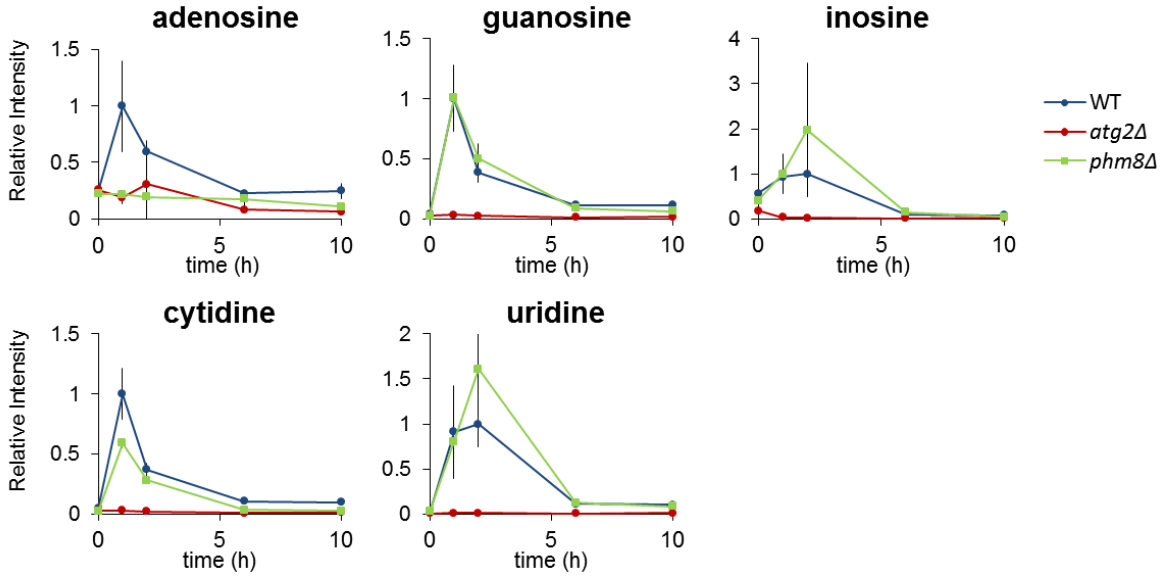

B

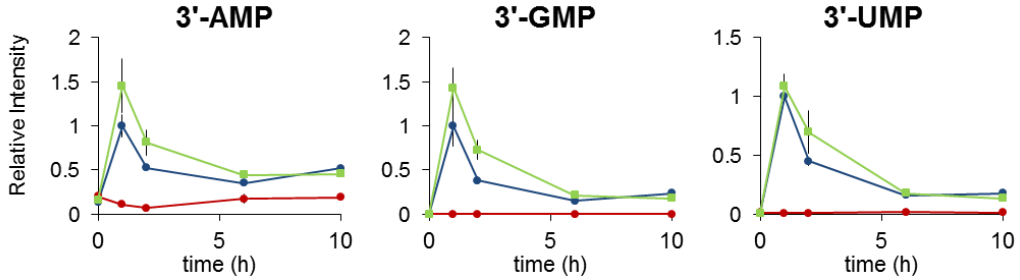

Fig. 3-3. Time-dependent changes in intracellular nucleoside and nucleotide levels under nitrogen starvation. The wild-type, *atg2*Δ and *phm8*Δ cells were grown in SD and transferred to SD-N at time 0. Samples were analyzed by LC/MS as described in 2.2.5. The results are presented as normalized intensities on the basis of peak height of each metabolite in the wild-type cells. All data are means of triplicate samples. The error bars represent the standard deviation. (A) Nucleosides. (B) 3'-NMPs.

As a matter of this result, instead, I selected the vacuolar nonspecific phosphatase, Pho8, as a candidate phosphatase/nucleotidase (Kaneko *et al.*, 1982; Klionsky and Emr, 1989). In the *pho8*Δ cells, the increase of nucleosides was dramatically diminished during nitrogen starvation (**Fig. 3-4A**).

5'-NMP levels (5'-AMP, 5'-GMP, 5'-CMP, and 5'-UMP) were slightly higher in *pho8*Δ cells than in the wild-type, *atg2*Δ and *rny1*Δ (see section 3.3.3) cells, which exhibited similar levels (**Fig. 3-4B**). Given that the cytosol contains considerably high levels of 5'-nucleotides and other related compounds such as NAD and UDP-glucose, it is possible that these compounds are non-selectively enwrapped into autophagosomes and delivered to the vacuole, where they might be retained due to the absence of Pho8. However, it was obvious that Pho8 was not the only phosphatase capable of dephosphorylating 5'-NMPs. 5'-IMP and 5'-XMP were dephosphorylated rapidly even in the *pho8*Δ cells, demonstrating the existence of other efficient 5'-NMP nucleotidases. Anyway, the accumulation of 5'-NMPs in the *pho8*Δ cells was not as remarkable as I had expected. Thus, it seems likely that the nucleosides detected here were not mainly derived from 5'-NMPs.

I therefore changed my focus to 3'-NMPs. 3'-NMPs are relatively minor metabolites in growing cells, which are barely detectable by LC/MS using the protocol of this study. Although due to the lack of a high-quality authenticated standard, 3'-CMP could not be measured by the LC/MS system, the available data were sufficient for comprehending the changing patterns. Just like nucleosides, 3'-NMPs (3'-AMP, 3'-GMP, 3'-UMP) exhibited transient increases in the wild-type and *phm8*Δ cells, but not in the *atg2*Δ cells (**Fig. 3-4C&Fig. 3-3B**). As shown in **Fig. 3-4C**, in the *pho8*Δ cells, 3'-NMPs accumulated to astonishing high levels in response to nitrogen starvation. Based on these results, it is concluded that the nucleosides were derived from 3'-NMPs, not 5'-NMPs, and Pho8 is the nucleotidase responsible for autophagy-induced RNA degradation. This conclusion is consistent with previous biochemical studies showing that Pho8 is a non-specific phosphatase with broad substrate specificity, and that Phm8 is a 5'-NMP-specific nucleotidase (Plankert *et al.*, 1991; Donella-Deana *et al.*, 1993; Xu *et al.*, 2013).

A

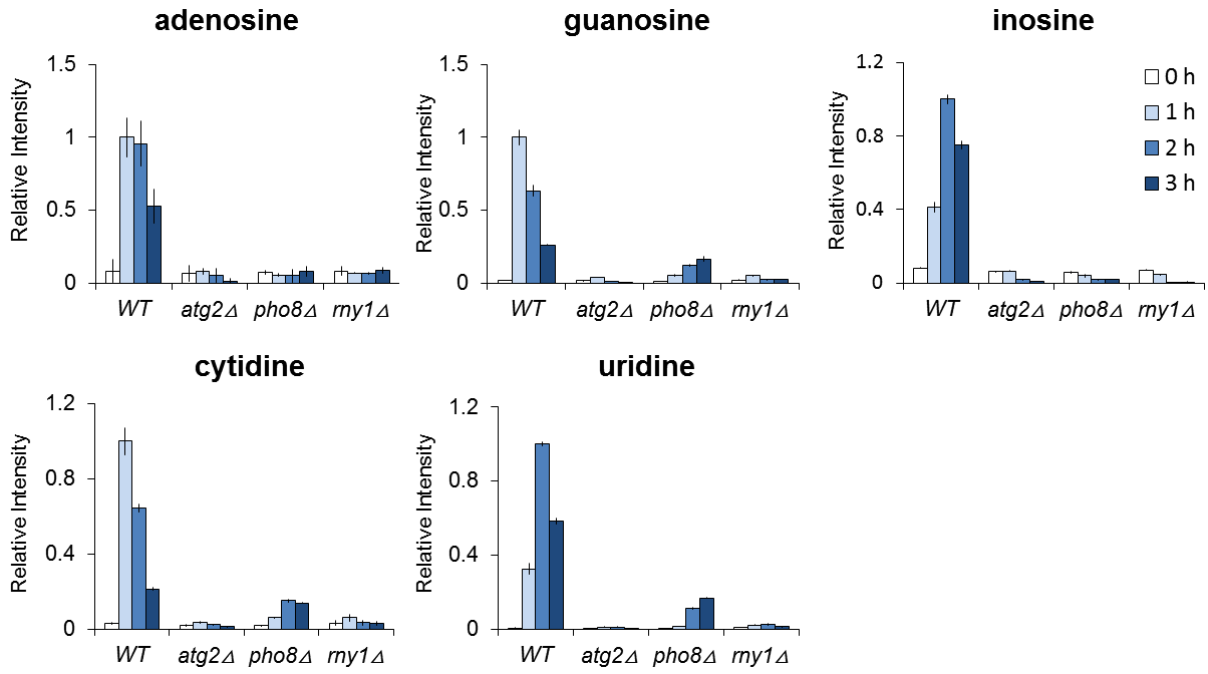
adenosine
guanosine
inosine
cytidine
uridine
Relative Intensity
0 h
1 h
2 h
3 h
WT
atg2Δ
pho8Δ
rny1Δ

B

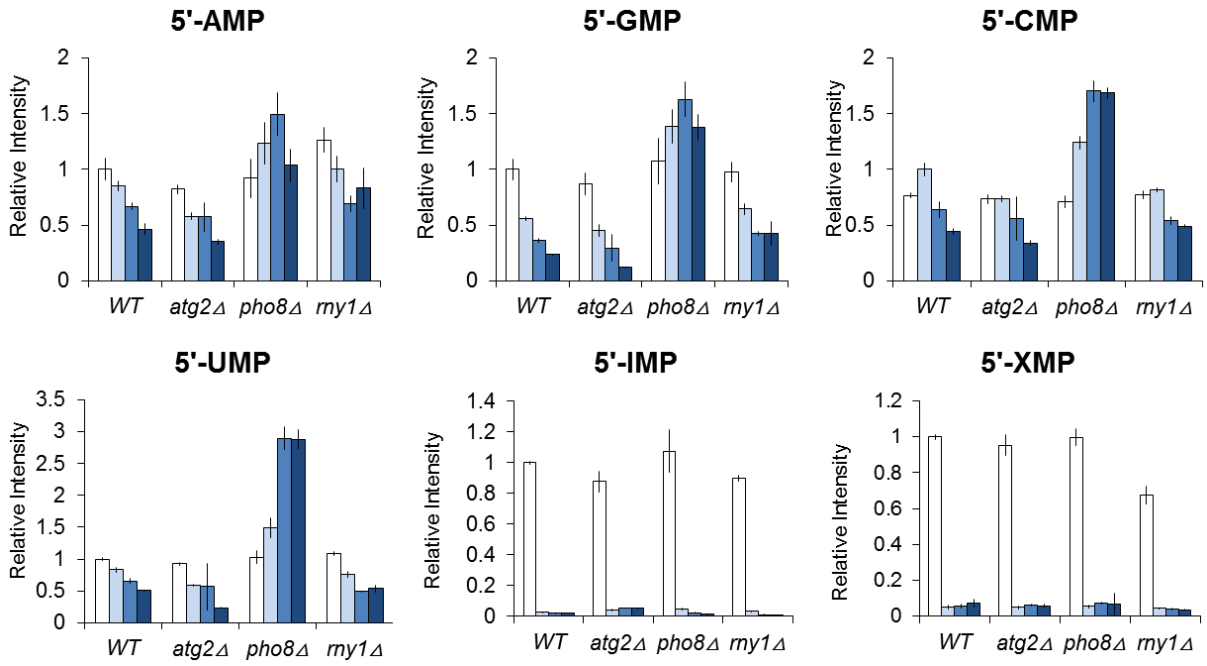
5'-AMP
5'-GMP
5'-CMP
5'-UMP
5'-IMP
5'-XMP
Relative Intensity
WT
atg2Δ
pho8Δ
rny1Δ

C

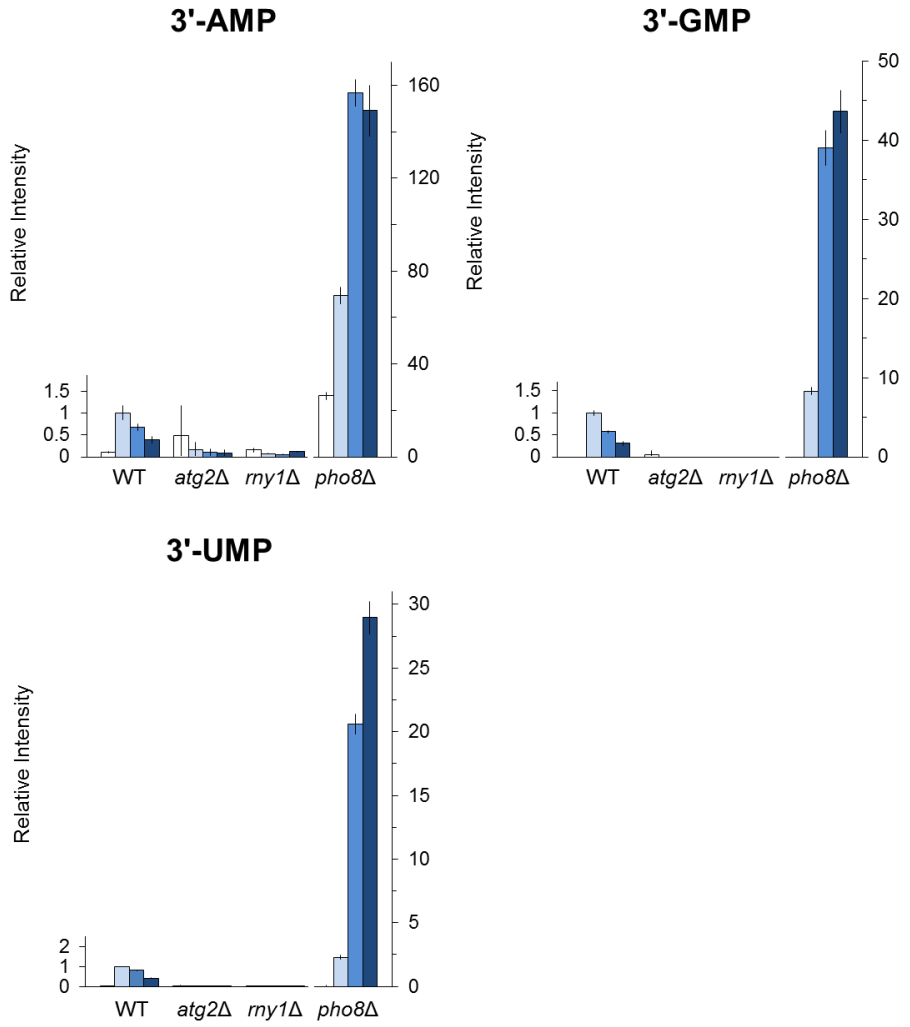

Fig. 3-4. Time-dependent changes in intracellular nucleoside and nucleotide levels under nitrogen starvation. The wild-type, *atg2*Δ, *rny1*Δ and *pho8*Δ cells were grown in SD and transferred to SD-N at time 0. Samples were analyzed by LC/MS as described in 2.2.5. The results are presented as normalized intensities on the basis of peak height of each metabolite in the wild-type cells. Note that 3'-NMPs in the *pho8*Δ were presented in a different scale. All data are means of triplicate samples. The error bars represent the standard deviation. (A) nucleosides. (B) 5'-NMPs. (C) 3'-NMPs

3.3.3 Rny1 is the nuclease responsible for RNA degradation in the vacuole

Next, I asked how 3'-NMPs were generated in the vacuole. For this, an RNase is needed. Rny1, the sole vacuolar RNase identified in *S. cerevisiae* to date, was chosen as the strongest candidate (MacIntosh *et al.*, 2001). Rny1 belongs to the T2 family of RNases, highly

conserved endoribonucleases with weak base specificity that catalyze the cleavage of single strand RNA through 2',3'-cyclic phosphate intermediates, yielding mono- or oligonucleotides with a terminal 3' phosphate group (Irie, 1999; **Fig. 3-5**). These enzymatic characteristics suggest that Rny1 acts specifically on RNA, not DNA.

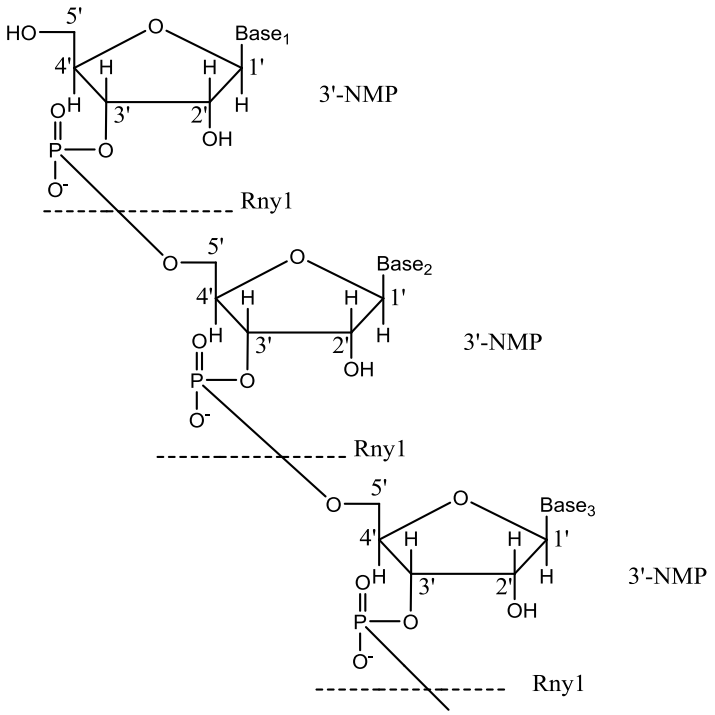

Fig. 3-5 Cleavage sites for RNase T2 family

I investigated the involvement of Rny1 in generation of 3'-NMPs during autophagy. In *rny1*Δ cells, the elevation of 3'-NMPs, and consequently that of nucleosides, were completely abolished (**Fig. 3-4A&C**). Even prolonged starvation of up to 24 h did not result in any nucleoside accumulation in the *rny1*Δ cells (**Fig. 3-6**). Therefore, it is considered that Rny1 is the essential ribonuclease for RNA degradation into mononucleotides by autophagy.

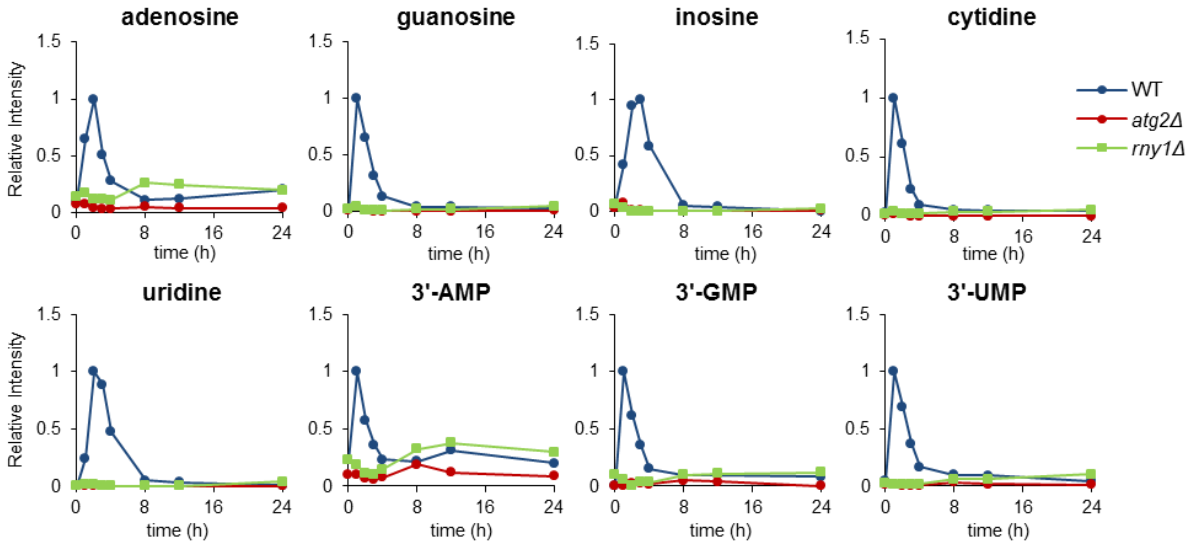

Fig. 3-6. Time-dependent changes in nucleoside and nucleotide levels under nitrogen starvation for up to 24 h. The wild-type, *atg2*Δ and *rny1*Δ cells were grown in SD and transferred to SD-N at time 0. Samples were analyzed by LC/MS as described in 2.2.5. The results are presented as normalized intensities on the basis of peak height of each metabolite in the wild-type cells.

To exclude the possibility that Rny1 and Pho8 are involved in autophagic process itself such as sensing of starvation, induction of autophagy, autophagosome formation, and protein degradation, autophagy in the *rny1*Δ and *pho8*Δ cells was examined. First, the autophagic activity in the *rny1*Δ cells was quantitatively estimated using the ALP assay (Noda *et al.*, 1995). Deletion of *RNY1* did not impair autophagic activity at all (**Fig. 3-7A**). Next, the process of autophagy was monitored by fluorescence microscopy using GFP-Atg8 as a marker. GFP-Atg8 expressed in the *rny1*Δ and *pho8*Δ cells was transported normally to the vacuoles in response to starvation (**Fig. 3-7B**). From these results, it is concluded that Rny1 and Pho8 do not affect the membrane dynamics necessary for autophagy, but instead play specific roles in RNA degradation via autophagy.

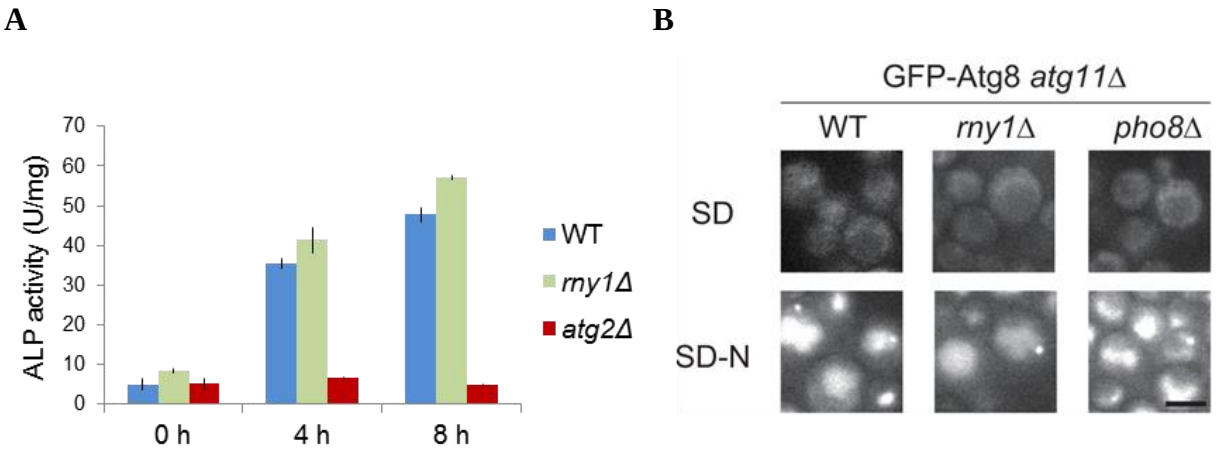

Fig. 3-7. Role of Rny1 and Pho8 during autophagy. (A) ALP assay (Pho8Δ60). The wild-type, *atg2*Δ, and *rny1*Δ cells expressing Pho8Δ60 were grown in SD to mid-log phase and transferred to SD-N at time 0. Cell lysates were prepared at the indicated time points and subjected to ALP assay. The error bars represent the standard deviation of three independent experiments. (B) GFP-Atg8 transport. To monitor starvation-induced PAS (Kawamata *et al.*, 2008), the *atg11*Δ cells were used. Cells expressing GFP-Atg8 in the *atg11*Δ, *atg11*Δ*rny1*Δ, or *atg11*Δ*pho8*Δ were grown in SD to mid-log phase and transferred to SD-N. After 2 hours of starvation, GFP-Atg8 was analyzed by fluorescence microscopy. In starvation conditions, GFP-Atg8 strongly stained vacuoles in these cells, indicating that deletion of Rny1 and Pho8 does not affect the autophagic pathway to the vacuole.

3.3.4 RNY1 deletion causes accumulation of RNA in the vacuole

Although previous studies have suggested that Rny1 and Pho8 are vacuolar enzymes, the physiological roles of these proteins in the vacuole were not yet well defined. Indeed, other physiological functions have been suggested for Rny1: under standard nutrient conditions, a fraction of Rny1 is secreted from the cell through the ER and Golgi apparatus, and has been proposed to play a role in scavenging nutrients from extracellular RNAs (MacIntosh *et al.*, 2001; Shcherbik, 2013). Thompson *et al*. suggested that Rny1 exits the vacuole to the cytosol and specifically cleaves cytosolic tRNA, as well as rRNA, in response to oxidative stress (Thompson and Parker, 2009). In the case of Pho8, although an authentic function has not been established, molecular details of its induction under phosphate starvation, delivery to the vacuole, and activation have been well studied (Kaneko *et al.*, 1985; Klionsky and Emr, 1989). Pho8 is transported to the vacuole through the ER and the Golgi apparatus. Upon reaching the vacuole, the pro-form of Pho8 is C-terminally processed to an active form by the vacuolar

protease Pep4 and Prb1. To examine the expression and cellular localization of Rny1 and Pho8 under nitrogen starvation, the wild-type and *atg2*Δ cells chromosomally expressing Rny1-GFP or Pho8-GFP via their own promoters were constructed. Rny1 and Pho8 were localized in the vacuoles, under both growth and starvation conditions, and no striking difference was observed between the wild type and *atg2*Δ (**Fig. 3-8A**). As previously suggested, a large portion of Rny1-GFP as well as Pho8-GFP were C-terminally processed and liberated from the GFP moiety in the vacuole (**Fig. 3-8B**) (Campomenosi *et al.*, 2006). By estimating the total amounts of the corresponding bands (the sum of both full-length and cleaved bands), Pho8 expression was found to be highly induced while Rny1 expression was moderately upregulated under nitrogen starvation conditions (**Fig. 3-8B**).

Microscopic monitoring of free RNA in cells was then performed using the nucleic acid-binding fluorescent dye, GelGreen (GR Green). Vacuole membranes were dyed by FM 4-64 to define the boundary of vacuoles. GelGreen is a sensitive and stable nucleic acid dye with green fluorescence while FM 4-64 selectively stains yeast vacuolar membranes with red fluorescence. Under growing conditions, the wild-type, *atg2*Δ, *rny1*Δ and *rny1*Δ*atg2*Δ cells did not show any fluorescence signals of GelGreen. By contrast, under starvation conditions, vacuoles in the wild-type cells but not the *atg2*Δ cells were faintly stained. Strikingly, the *rny1*Δ cells exhibited brightly stained vacuoles by GelGreen, indicating that in the absence of Rny1, free RNA that had not undergone further degradation was stained in the vacuole. Deletion of *ATG2* in the *rny1*Δ cells abolished starvation-induced fluorescence signals in the vacuoles, which again supports the conclusion that starvation-induced RNA degradation in the vacuole is completely autophagy-dependent. Based on these observations, it is clear that Rny1 functions as the vacuolar RNase for RNA degradation during autophagy.

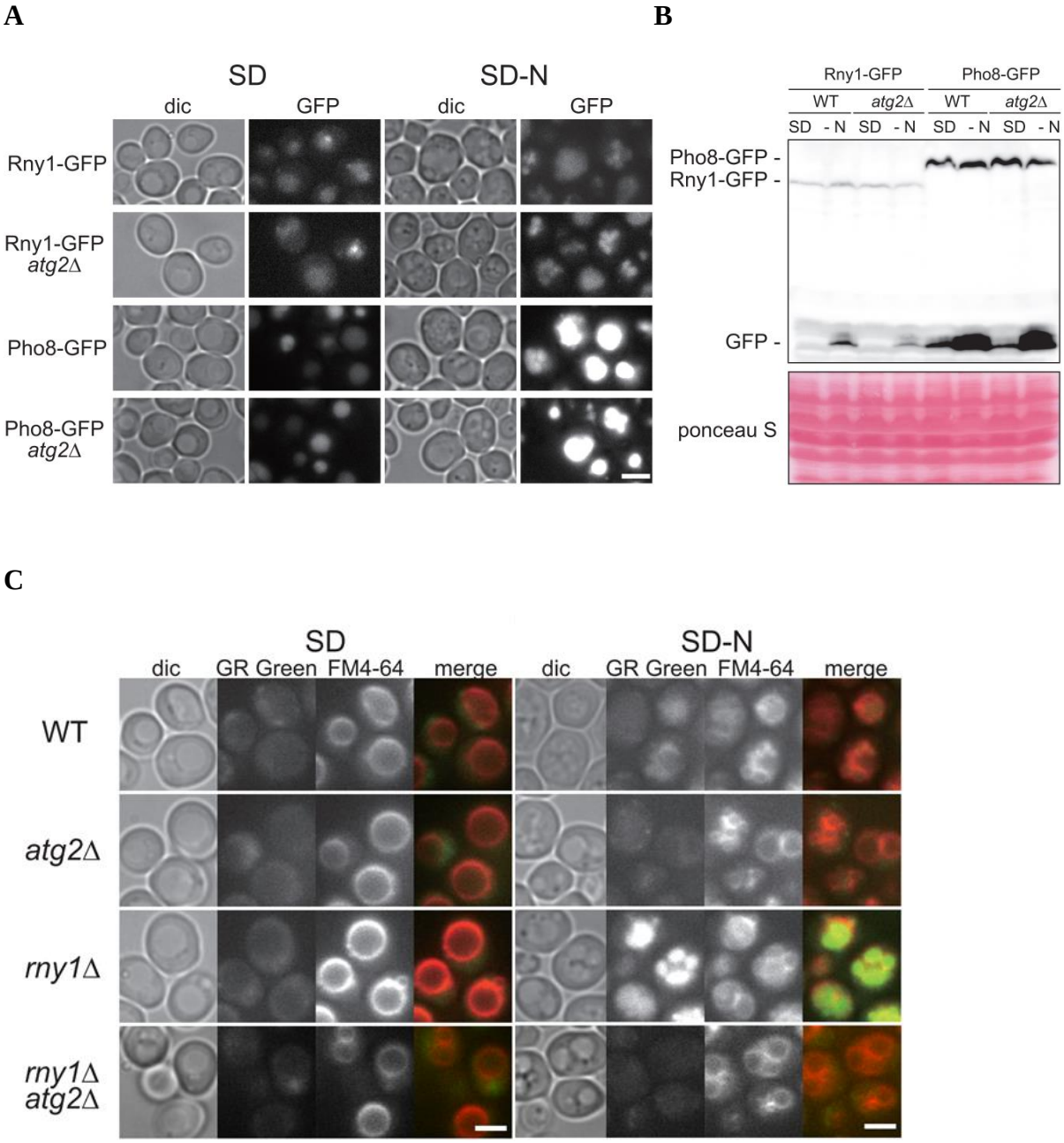

Fig. 3-8. Accumulation of RNA in the vacuole in the *rny1*Δ cells under nitrogen starvation. (A and B) Expression and localization of Rny1 and Pho8. The wild-type and *atg2*Δ cells expressing Rny1-GFP or Pho8-GFP were grown in SD to mid-log phase and transferred to SD-N. After 2 h of starvation, GFP-tagged proteins were observed by fluorescence microscopy (A) or analyzed by western-blot with anti-GFP antibody (B). (C) Detection of free RNA. The wild-type, *atg2*Δ, *rny1*Δ and *rny1*Δ*atg2*Δ cells grown in SD (left) or SD-N for 2 h (right) were stained with FM 4-64 and GelGreen and observed under a fluorescence microscope. Bar, 5 μm.

3.3.5 Role of ribophagy in starvation-induced RNA degradation

As an important pathway for ribosome degradation, I wondered whether ribophagy played a role in nucleotide metabolism under nitrogen starvation conditions. Accordingly, I performed the metabolic profiling of the *ubp3*Δ and *bre5*Δ strains and similar levels of transient accumulation of 3'-NMPs with those in the wild-type strain were observed (**Fig. 3-9A**). However, the time course of 3'-NMP generation was slightly delayed, and the conversion of 3'-NMPs to nucleosides was also slow, leading to the reductions in nucleoside increase. It is possible that these phenotypes were caused partly by some kind of defect in the formation of ribophagy-specific autophagosomes under nitrogen starvation, or simply the slow-growth phenotype of these mutants (a doubling time of ~3 h in SD medium). However, this is more likely due to the fact that Ubp3 and Bre5 are involved in the regulation of membrane trafficking processes, as reported in a previous study (Cohen *et al.*, 2003), and the absence of them led to other defects in addition to ribophagy. Specifically, Ubp3 and Bre5 form an active de-ubiquitination complex that cleaves ubiquitin from specific substrates, thus rescuing them from the degradation by proteasome. Among the many substrates, a subunit essential for the transport between the ER and the Golgi apparatus, named Sec23, is included. Vacuolar enzymes like Pep4, Prb1 and Pho8 are originally synthesized in the ER, but need to be delivered to the vacuole via the Golgi apparatus on a Sec23-dependent manner for maturation. Therefore, deletion of Ubp3 or Bre5, which might cause the proteasome degradation of Sec23, may consequently lead to partial defects in delivery and thus the following processing of vacuolar enzymes. In fact, in support of this hypothesis, western blotting using anti-Pep4, anti-Prb1, and anti-Pho8 revealed higher levels of the zymogens of Pep4, Prb1 and Pho8 (pro-Pep4, pro-Prb1 and pro-Pho8, respectively) in *ubp3*Δ and *bre5*Δ compared with the wild type under both growth and starvation conditions, demonstrating the lower efficiencies in processing these enzymes due to the partial defects in the delivery system (**Fig. 3-9B**). In addition, as a direct result, endogenous Pho8 activity was also proven to be low (**Fig. 3-9C**), which explained the lower levels of nucleoside generation in both *ubp3*Δ and *bre5*Δ cells (**Fig. 3-9A**). Microscopic monitoring of free RNA in *rny1*Δ*ubp3*Δ and *rny1*Δ*bre5*Δ using GR Green also clearly showed fluorescence signals inside the vacuoles under starvation conditions, demonstrating that RNAs are transported to the vacuole in the absence of Ubp3 and Bre5 (**Fig. 3-9D**). At present, although it is hard to estimate how many

ribosomes are delivered to the vacuole by the ribophagy pathway, it is clear that non-selective bulk autophagy is responsible for the delivery of a majority of ribosomes for autophagic degradation.

A

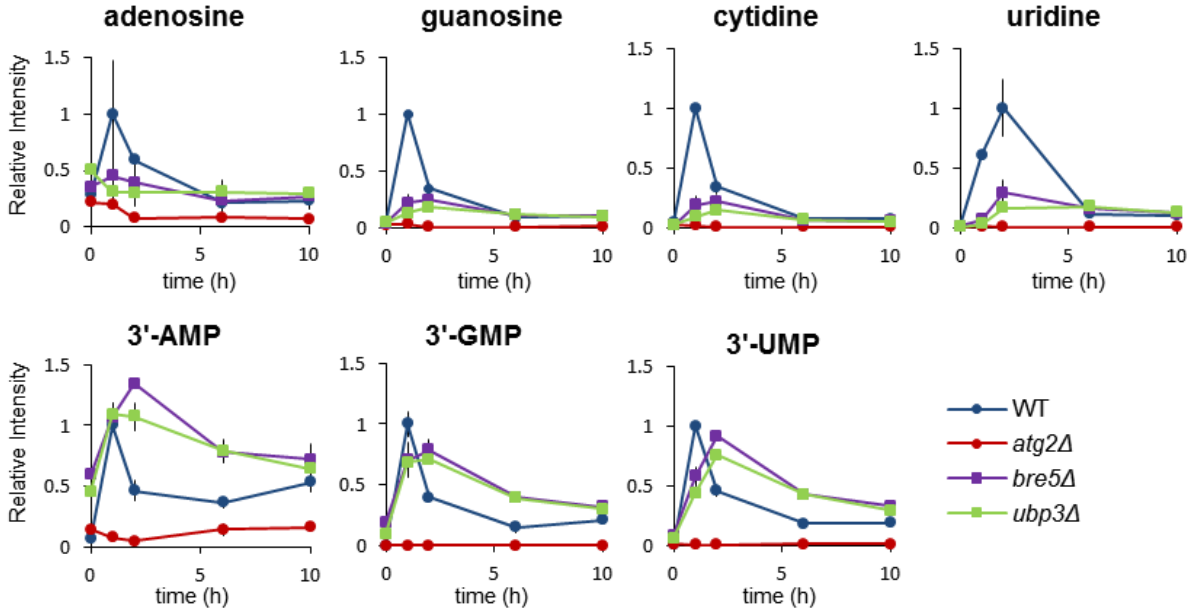

B

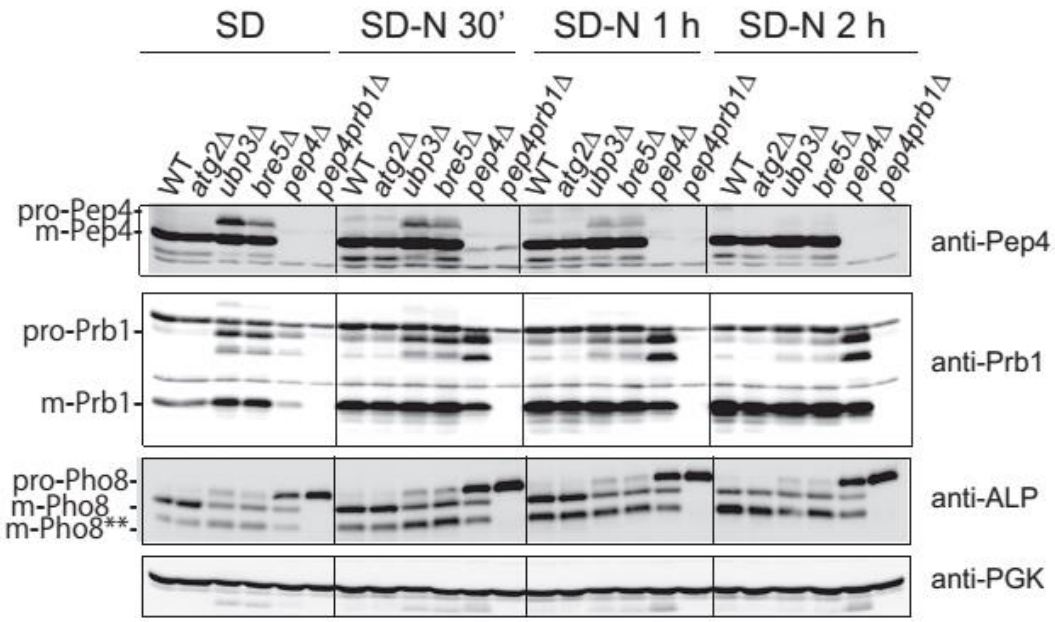

C

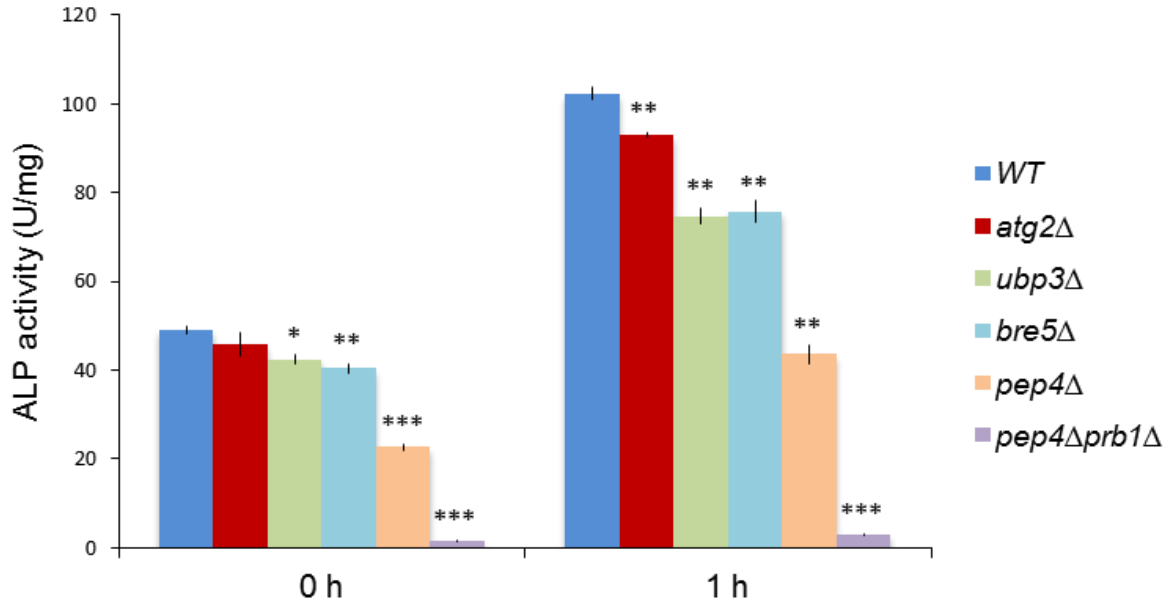

D

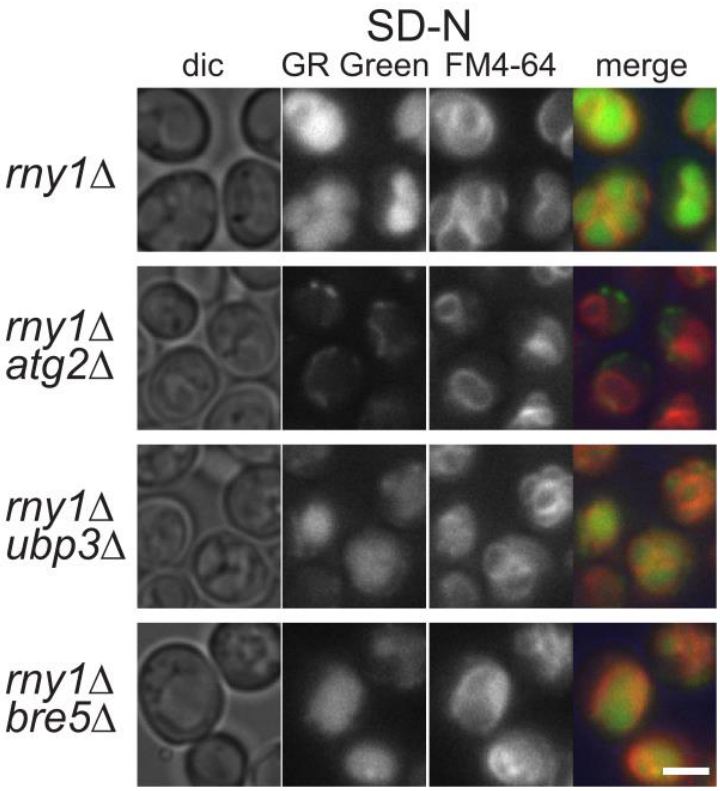

Fig. 3-9. Evaluation of ribophagy on RNA degradation under nitrogen starvation. (A) Time-dependent changes in nucleoside and nucleotide levels under nitrogen starvation. The wild-type, *atg2*Δ, *ubp3*Δ,

and *bre5*Δ cells were grown in SD to mid-log phase and transferred to SD-N at time 0. Samples were analyzed by LC/MS as described in 2.2.5. The results are presented as normalized intensities on the basis of the peak height of each metabolite in wild-type cells. All data are means of triplicates. The error bars represent the standard deviation. (B) Processing of vacuolar enzymes. The wild-type, *atg2*Δ, *ubp3*Δ, *bre5*Δ, *pep4*Δ, and *pep4*Δ*prb1*Δ cells were grown in SD to mid-log phase and transferred to SD-N. Cell lysates were prepared at the indicated time points and analyzed by western blotting using anti-Pep4, anti-Prb1, anti-ALP, and anti-PGK antibodies. m-Pho8 and m-Pho8** are membrane-bound and soluble active forms of Pho8, respectively, as demonstrated in the literature (Qiao *et al.*, 2009). (C) Enzymatic activity of endogenous Pho8. Cell lysates were prepared at the indicated time points after transferred into SD-N medium and subjected to the ALP assay. The bars represent the standard deviation of three independent experiments. Asterisk, $P<0.05$; double asterisk, $P<0.005$; triple asterisk, $P<0.0005$ (paired *t*-test, two-tailed). (D) Detection of free RNA within cells. The *rny1*Δ, *rny1*Δ*atg2*Δ, *rny1*Δ*ubp3*Δ and *rny1*Δ*bre5*Δ cells grown in SD-N for 2 h were stained with FM 4-64 and GR Green and observed under a fluorescence microscope. Bar, 5 μm.

3.3.6 Further breakdown of nucleosides in the cytoplasm

A deduced nucleotide degradation pathway was drawn based on the increasing metabolites detected in the wild-type cells relative to the *atg2*Δ cells (**Fig. 3-10**). The arrow between two metabolites represent a possible reaction on its direction. Solid arrows show the conversions with an enzyme that was either identified during this study or known previously (see below). The dashed arrows (without a question mark) are those proposed based on the results of this study but with an enzyme to be identified. The question mark indicates a putative adenosine deaminase, which has been controversial for a long time (Merkler *et al.*, 1989; Saint-Marc *et al.*, 2009).

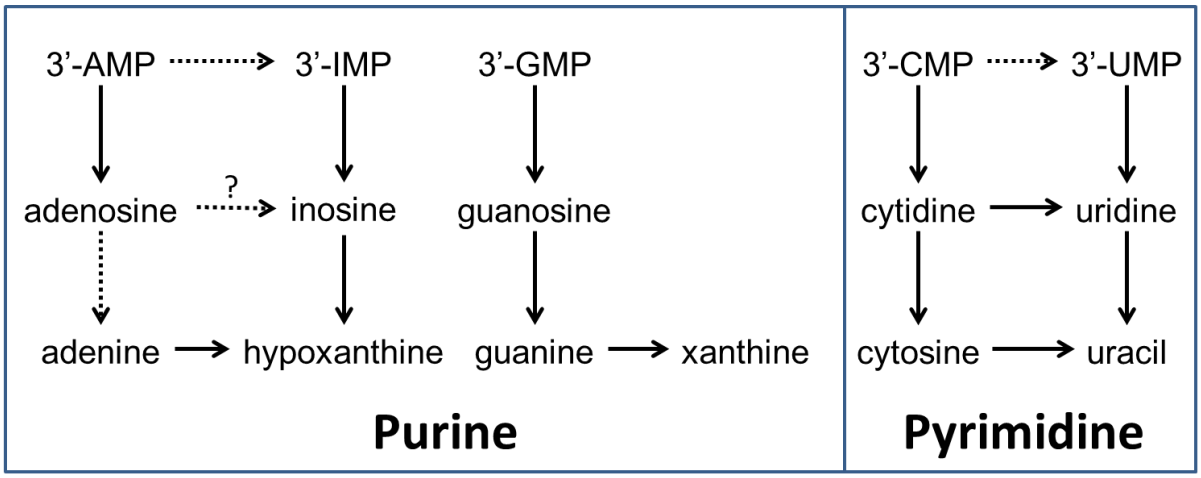

Fig. 3-10. Schematic representation of reactions of the nucleotide degradation pathway

Although autophagy continues for at least several hours under nitrogen starvation conditions (**Fig. 3-7A**), intracellular 3'-NMPs and nucleosides started to decrease soon after starvation, suggesting that these compounds are rapidly further metabolized and exist in a state of dynamic equilibrium. To obtain a comprehensive picture of autophagy-dependent RNA catabolism, I quantitated the intracellular concentrations of mononucleotides, nucleosides and bases in the wild type and *atg2*Δ under starvation with standard addition method by LC/MS (**Fig. 3-11** and **3-19A**).

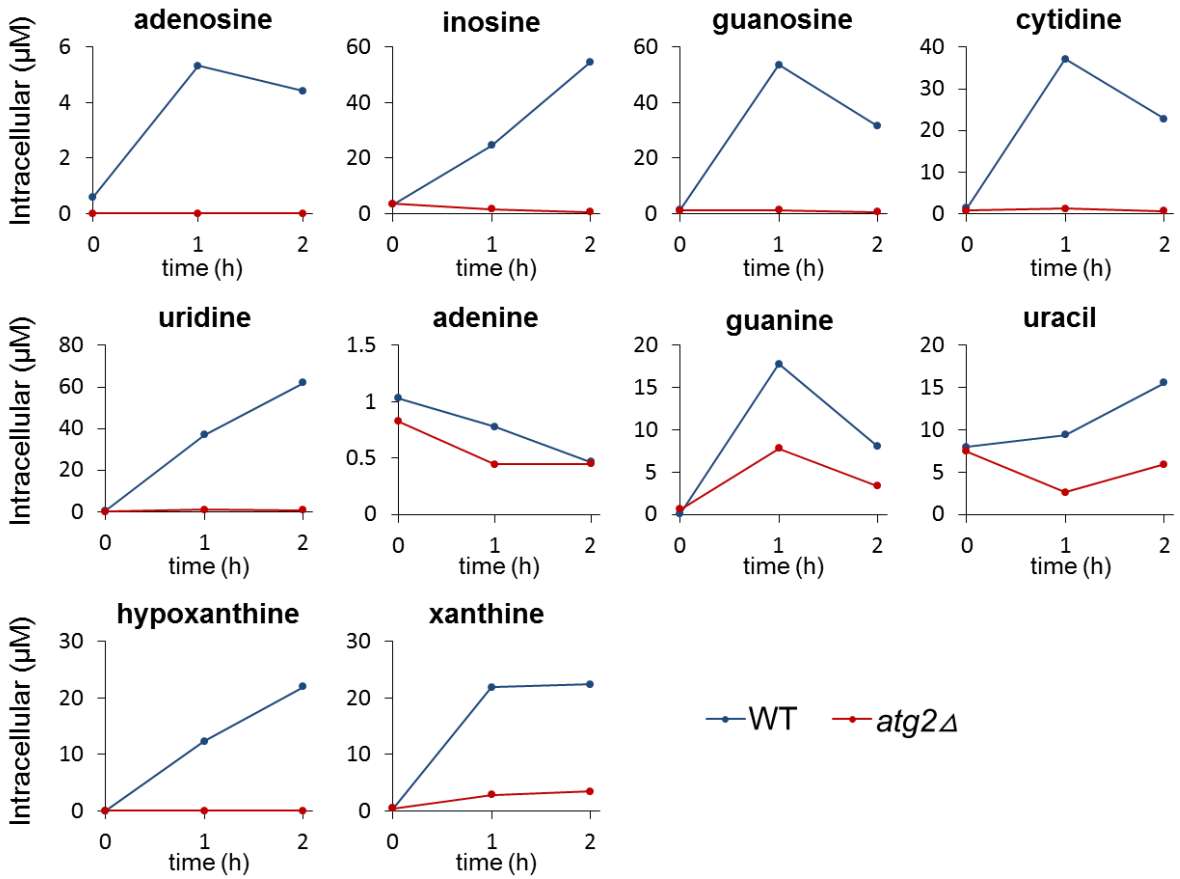

Fig. 3-11. Absolute concentrations of intracellular nucleosides and bases in WT and *atg2*Δ under nitrogen starvation

In the wild-type cells after 2 h-starvation, intracellular concentrations of nucleosides were calculated to be about 4 μM (adenosine), 30 μM (guanosine), 20 μM (cytidine), or 60 μM (inosine and uridine) and most bases at around 10 to 20 μM (**Fig. 3-11**). Autophagy-dependent generation of bases explained why nucleosides started to decrease so soon after starvation. The fact that adenosine and adenine levels were quite low as compared with other nucleosides and bases is possibly because most 3'-AMP were converted to 3'-IMP, and then to further downstream metabolites (**Fig. 3-10**), as suggested by the fact that inosine level increased to about 60 μM after 2 h of starvation in the wild-type cells (**Fig. 3-11**). Significant amounts of hypoxanthine and xanthine were also detected in an autophagy-dependent manner, strongly suggesting that enzymes normally working in the purine and pyrimidine salvage pathway function on nucleosides to produce bases under nitrogen starvation.

Pnp1 is a *p*urine *n*ucleoside *p*hosphorylase that specifically acts on guanosine and inosine (**Fig. 3-12**; Lecoq *et al.*, 2001); the enzyme responsible for the generation of adenine from adenosine has not yet been identified. Urh1 (*ur*idine *h*ydrolase) is a pyrimidine nucleoside-specific hydrolase converting cytidine and uridine into cytosine and uracil, respectively in the pyrimidine salvage pathway (**Fig. 3-12**; Kurtz *et al.*, 1999), during which, cytidine, uridine, and cytosine are all eventually turned into uracil (**Fig. 3-10**).

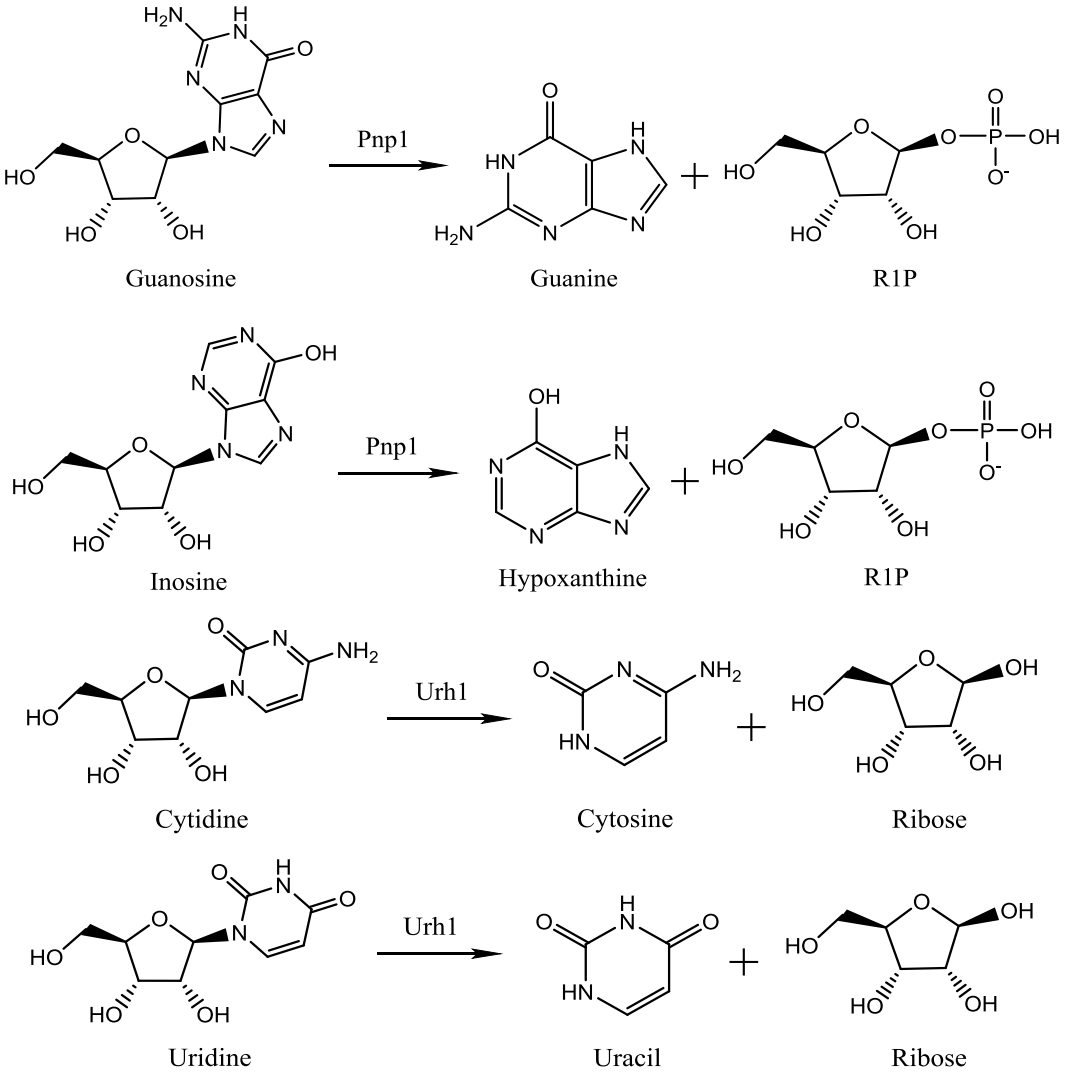

Fig. 3-12. Pnp1 and Urh1 catalyzed reactions in purine and pyrimidine salvage pathway.

I investigated the requirements for Pnp1 and Urh1 in nucleoside metabolism during nitrogen starvation. Time-course metabolic profiling of *pnp1*Δ and *urh1*Δ was carried out. In

the wild-type cells, guanosine was converted rapidly into guanine, and then to xanthine, compared with which, in the *pnp1*Δ cells, guanosine accumulated to a much higher level, whereas guanine remained very low (**Fig. 3-13A**). So, without pnp1, guanosine could not be further degraded into guanine. Given the higher accumulation of inosine in the *pnp1*Δ cells, it was assumed that similar phenomenon also occurred to inosine, although hypoxanthine was not detected during this experiment. An interesting thing is that despite the common recognition that Pnp1 does not act on adenosine, adenosine in the *pnp1*Δ cells was also found to accumulate to more than triple the amount of that in the wild-type cells. Although we cannot rule out the possibility that deletion of *PNP1* might have caused other perturbations that led to the accumulation of adenosine, it is very likely that Pnp1 also functions as adenosine phosphorylase under certain circumstances such as nitrogen starvation.

For pyrimidine nucleosides, in the *urh1*Δ cells, cytidine and uridine also exhibited slightly higher levels relative to the wild-type cells while uracil level remarkably decreased, indicating the incapability of *urh1*Δ cells to convert cytidine and uridine into cytosine (not detected) and uracil due to the absence of Urh1 (**Fig. 3-13A**). These together demonstrated Pnp1 and Urh1's function in this degradation process, which is, Pnp1 and Urh1 are the nucleosidases responsible for autophagy-mediated RNA degradation, consistent with a recent study by Xu *et al.* (Xu *et al.*, 2013).

Pnp1 and Urh1 are known as cytoplasmic enzymes. If this holds true even under starvation conditions, nucleosides must be effectively transported from the vacuole to the cytoplasm before interacting with these nucleosidases. To confirm this, the cellular localization of Pnp1 and Urh1 was monitored by chromosomally expressing Pnp1-GFP or Urh1-GFP in the wild-type cells. According to the results of microscopic observation, Pnp1 and Urh1 were indeed localized in the cytoplasm instead of the vacuole under both growth and starvation conditions, suggesting that autophagy-derived nucleosides are converted to bases in the cytoplasm (**Fig. 3-13B**).

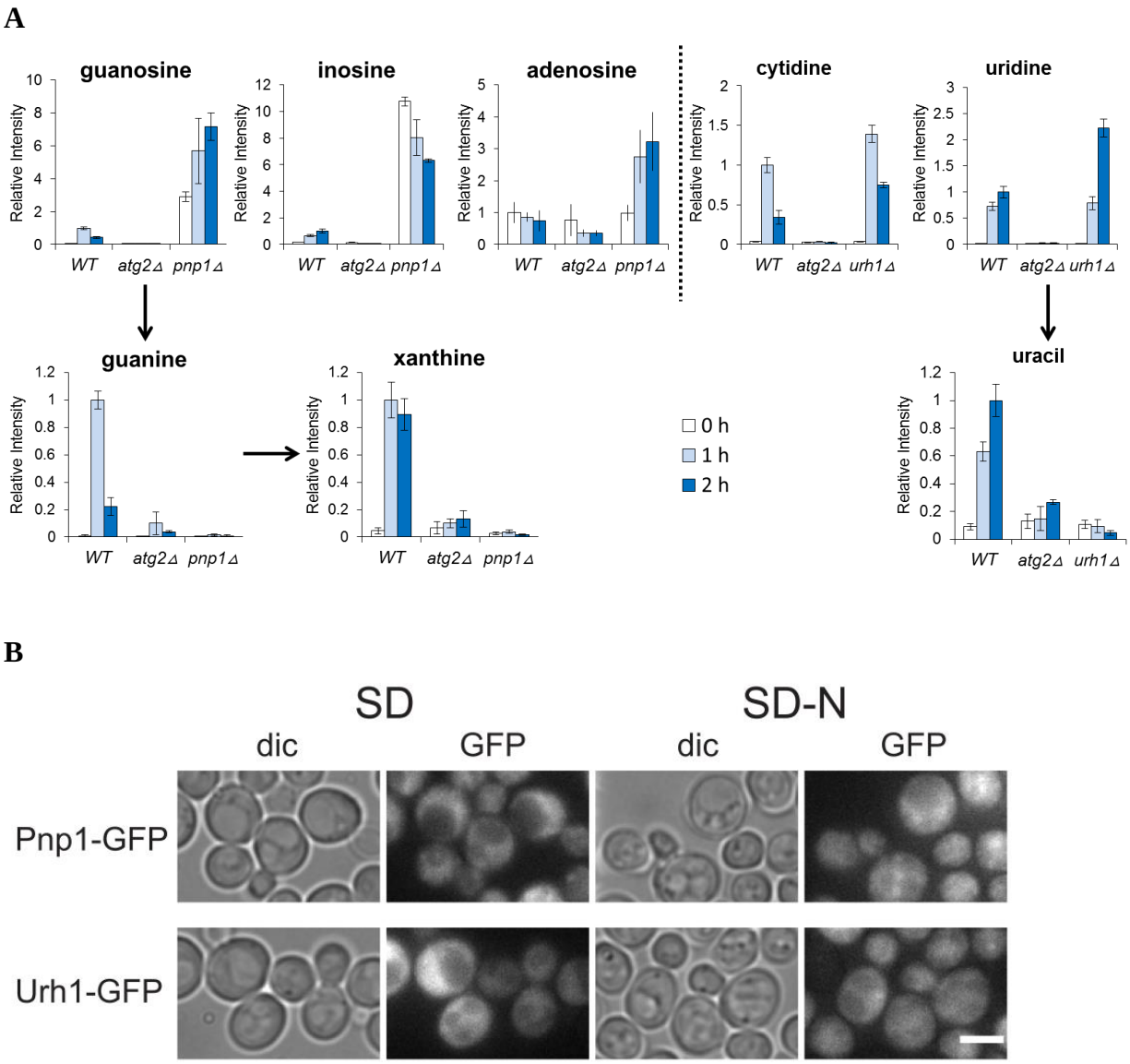

Fig. 3-13. Dynamics of intracellular nucleosides and bases in the WT, *atg2*Δ, *pnp1*Δ and *urh1*Δ cells under nitrogen starvation. (A) Time-dependent changes in nucleoside and base levels under nitrogen starvation. The wild-type, *atg2*Δ, *pnp1*Δ and *urh1*Δ cells were grown in SD to mid-log phase and transferred to SD-N at time 0. Samples were analyzed by LC/MS as described in 2.2.5. The results are presented as normalized intensities on the basis of the peak height of each metabolite in the wild-type cells. All data are means of quadruplicates. The error bars represent the standard deviation. (B) Expression and localization of Pnp1 and Urh1. Wild-type cells expressing Pnp1-GFP or Urh1-GFP were grown in SD to mid-log phase and transferred to SD-N. After 2 h of starvation, GFP-tagged proteins were analyzed by fluorescence microscopy.

3.3.7 Nucleosides are transported from the vacuole into the cytoplasm partially mediated by Fun26

As described in section 3.3.6, the nucleosides derived from the degradation need to be transported outside the vacuole to contact the two nucleosidases Pnp1 and Urh1. Fun26 is a nucleoside transporter located in intracellular membranes, which made it a good candidate for this process (Vickers *et al.*, 2000). Metabolic profiling of *fun26*Δ strain showed that the nucleosides in the *fun26*Δ cells increased to higher levels to those in the wild-type cells while the bases increased less significantly (**Fig. 3-14**). Therefore, it was inferred that due to the deletion of *FUN26*, the nucleosides could not access Pnp1 and Urh1 as efficiently as in the wild-type cells, which is to say, the nucleosides need to be transported outside the vacuole by Fun26. Nevertheless, it is believed that Fun26 is not the only functional nucleoside transporter since Fun26 deficiency did not cause complete abolishment of further breakdown of nucleosides. Bases in the *fun26*Δ cells, especially xanthine, displayed slightly higher levels to those in the *atg2*Δ cells, indicating that a part of nucleosides were successfully transported from the vacuole into the cytoplasm independent of Fun26, which demonstrated the possibility of other transporters acting in concert with Fun26. Compared with the other three nucleosides, the *fun26*Δ cells accumulated a much higher level of adenosine relative to the wild type. It is likely that Fun26 may have some level of specificity for nucleosides.

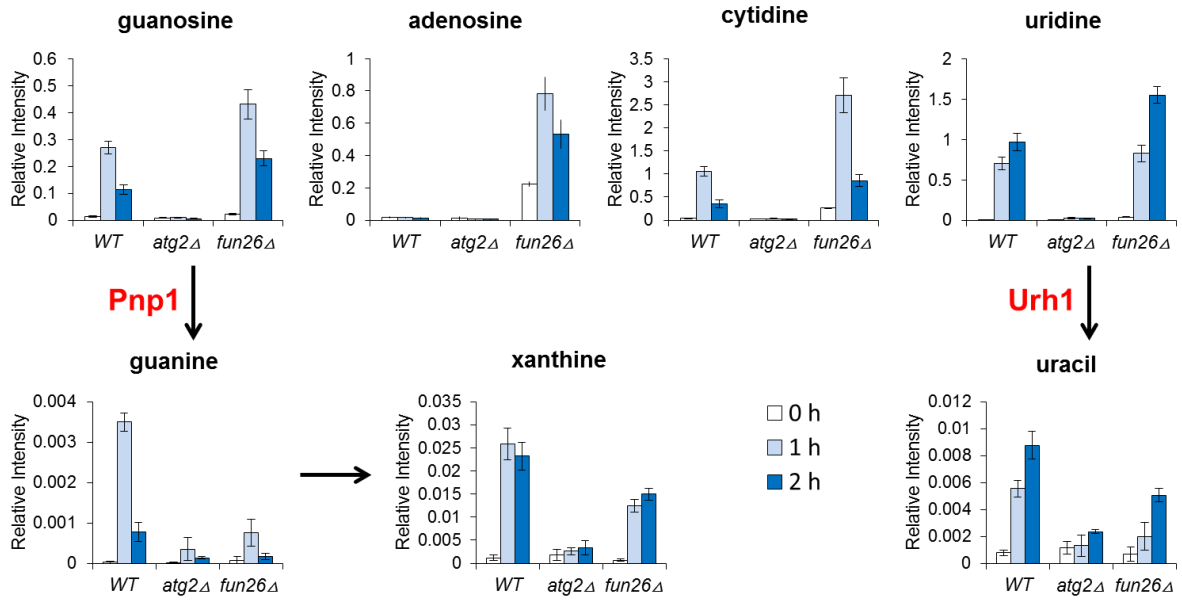

Fig. 3-14. Time-dependent changes in nucleoside and base levels under nitrogen starvation. The wild-type, *atg2*Δ and *fun26*Δ cells were grown in SD to mid-log phase and transferred to SD-N at time 0. Samples were analyzed by LC/MS as described in 2.2.5. All data are means of quadruplicates. The error bars represent the standard deviation.

3.3.8 Excretion of bases from cells during autophagy

Although nitrogen is extremely precious under nitrogen starvation, further degradation of purines and pyrimidines is unlikely in *S. cerevisiae*, because both xanthine oxidase (catalyzing the oxidation of hypoxanthine to xanthine and xanthine to uric acid) and the enzymes required for degradation of pyrimidine including uracil reductase (catalyzing the reduction of uracil to dihydrouracil) are absent in this organism. Nevertheless, like nucleosides, intracellular bases also increased transiently during autophagy. To investigate their destination, I measured the extracellular nucleotides, nucleosides and bases for the wild type and *atg2*Δ under nitrogen starvation. As a result, xanthine, uracil, and four nucleosides (inosine, guanosine, cytidine, and uridine) were found to be excreted from the wild-type cells, but not the *atg2*Δ cells, indicating that these excreted metabolites originated from autophagic degradation of RNA (**Fig. 3-15**, **3-19B and Appendix IX**). The amounts of these metabolites in the medium continued to rise for at least 10 h after starvation, which demonstrated their production by autophagy was ongoing during this whole period (**Appendix IX**). Notably, the

concentrations of xanthine and uracil secreted into the medium became very high, reaching micromolar level by 6 h (**Fig. 3-15**).

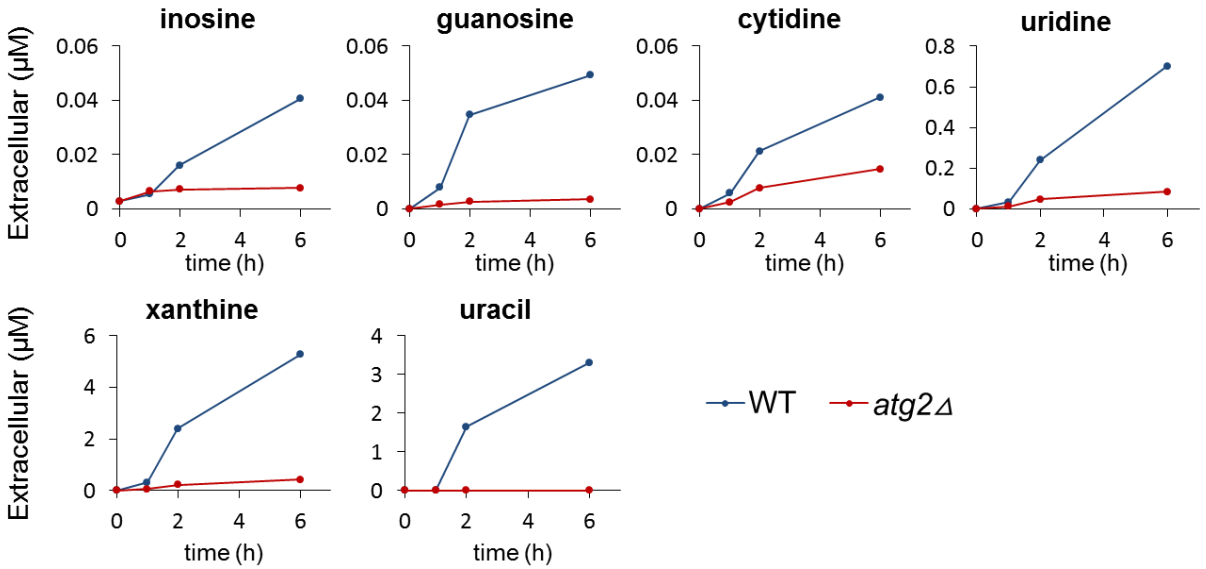

Fig. 3-15. Absolute concentrations of extracellular nucleosides and bases for the WT and *atg2*Δ under nitrogen starvation

To compare the amounts of intra- and extra- cellular products, I integrated these two data sets to see the ratio of the degradation products that were retained inside the cell (**Fig. 3-16**). After 2 h of starvation, nucleosides were mainly retained within the cells; by contrast, bases were mostly transferred to the medium. In addition, from the integration result, it is clear that most of the degradation compounds were converted into xanthine and uracil before being excreted out of the cell. Therefore, xanthine and uracil are considered to be the main final products of purine and pyrimidine, respectively, for autophagy-mediated RNA degradation. Taken together, the data indicated that cells excrete a majority of autophagy-degraded RNA as xanthine and uracil.

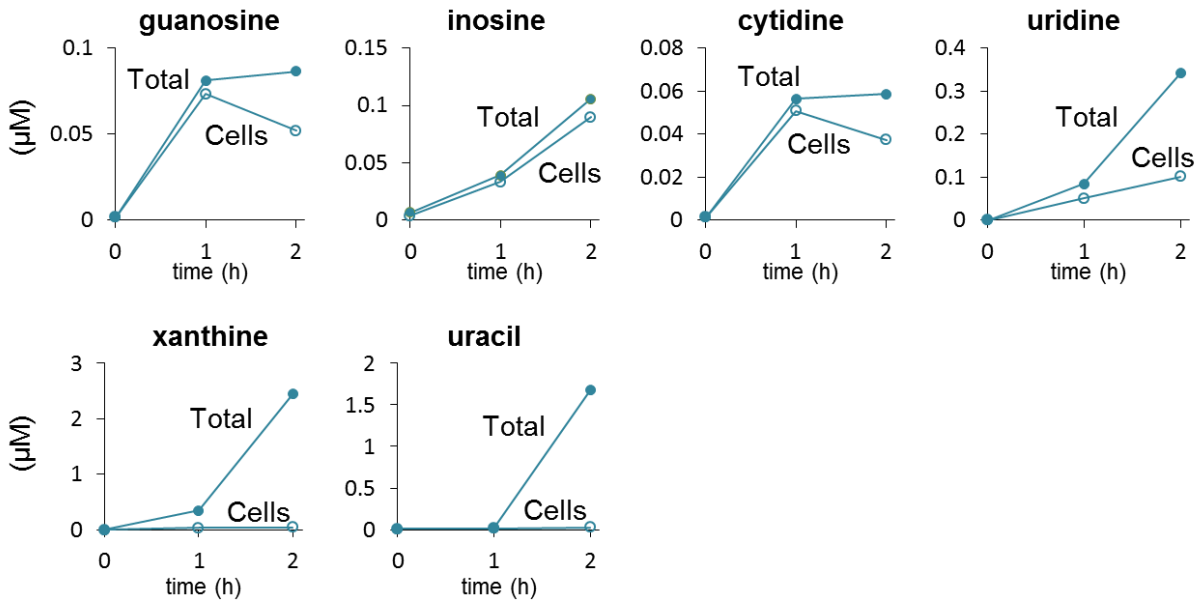

Fig. 3-16. Destinations of nucleosides and bases. Based on the intracellular and extracellular data (**Fig. 3-10** and **3-15**), the levels of nucleosides and bases in cells (open circle) and in cells and medium (closed circle) of the wild-type strain were estimated. See the detail in 3.2.5 (Flowchart of the calculation procedure).

From the bases excreted into the medium, it was estimated that a 3-4 % of RNAs were catabolized per hour under nitrogen starvation. About 80-85 % of the total cellular RNA are rRNA and 10-15 % are tRNA, whereas mRNA and other non-coding RNAs only comprise a very small portion. Therefore, most RNA degraded under starvation conditions observed in this study must be rRNA that was sequestered into autophagosomes, which is supported by the electron micrograph shown in **Fig. 2-1**. To obtain more objective evidence, autophagy-induced RNA degradation was evaluated by directly analyzing the changes in RNA species (**Fig. 3-17**). The same amount of RNA from the wild-type, *atg2*Δ and *rny1*Δ cells before and after nitrogen starvation was examined by northern blot and qRT-PCR. As contents of the nucleus, amounts of small nuclear non-coding RNA species such as small nuclear RNAs (snRNAs) and small nucleolar RNAs (snoRNAs) are presumed not be significantly affected by autophagy. Therefore, U4 (snRNA) and SnR50/SnR189 (snoRNA), were employed as internal controls for the quantitation experiments. As a result, decreases in both 25S and 18S rRNAs as well as several tRNAs in the wild-type cells under starvation conditions were observed by northern blot (**Fig. 3-17B**). qRT-PCR analysis also revealed

relative lower levels of 25S and 18S rRNAs in the wild-type cells compared with those in the *atg2*Δ and *rny1*Δ cells (**Fig. 3-17C**). However, it should be noted that due to the low quantitability of these conventional analytical methods and the small portion of each degraded RNA species relative to its original pool size, it is difficult to quantitate the accurate change in each RNA species and the kinetics of its decrease. By contrast, using metabolome analysis to quantitate the increase of degradation products such as nucleosides is a far more sensitive and accurate means to define bulk RNA degradation via autophagy.

A

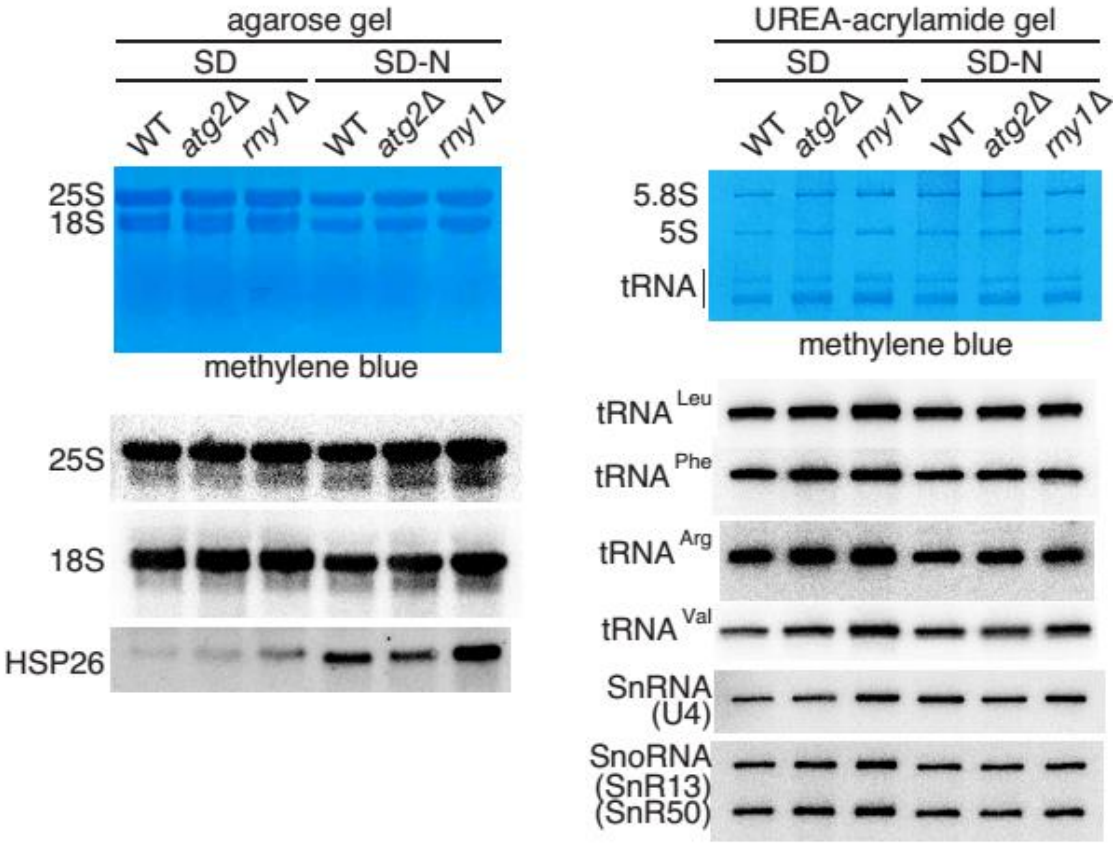

B. Northern blot (normalized to snRNA (U4) levels)

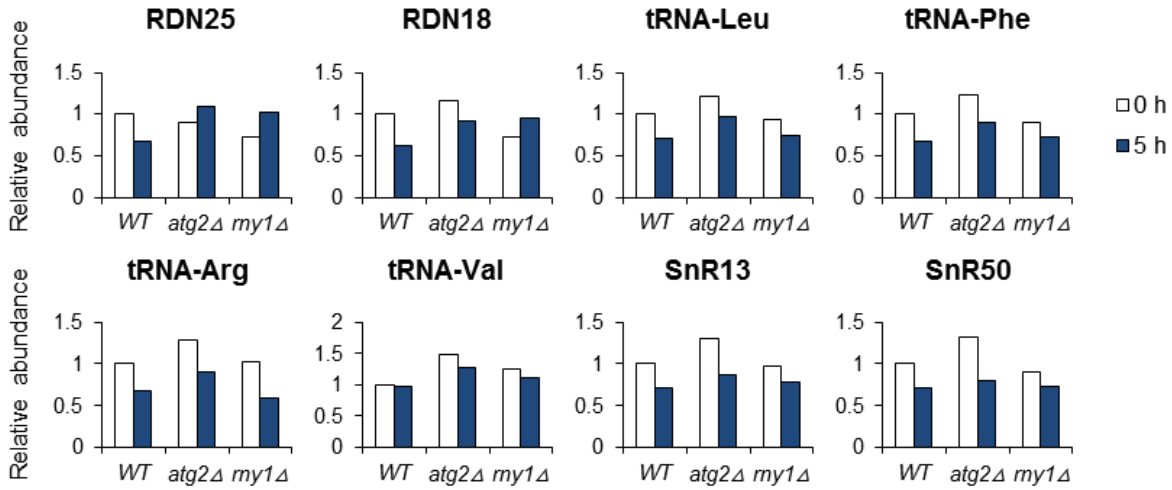

Northern blot (normalized to snoRNA (SnR50) levels)

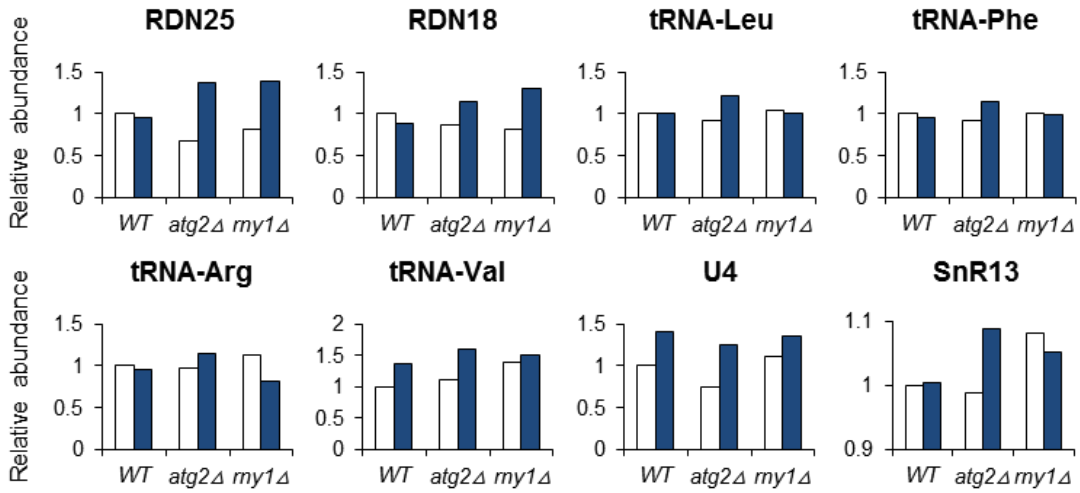

C. RT-PCR (normalized to snRNA (U4) levels)

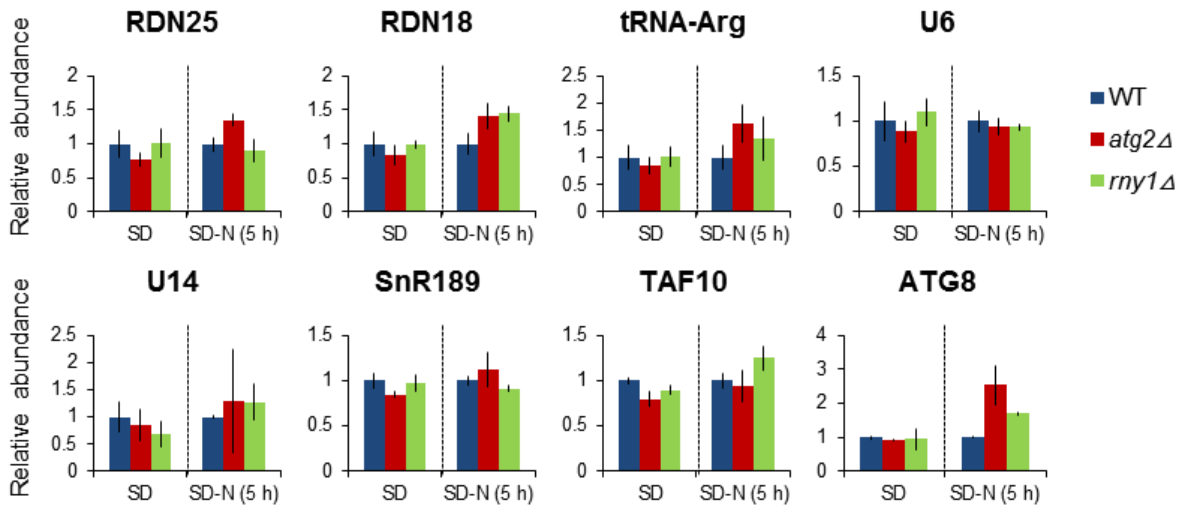

RT-PCR (normalized to snoRNA (SnR189) levels)

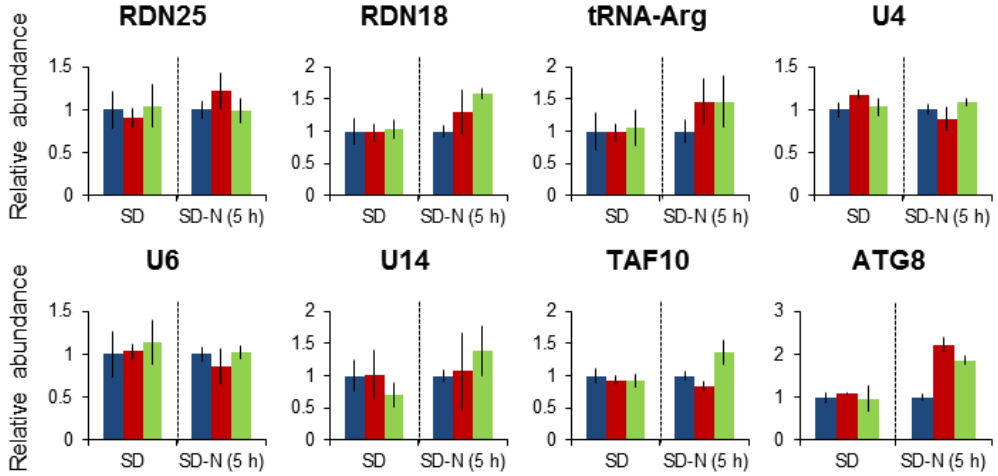

Fig. 3-17. Changes in intracellular RNA species before and after nitrogen starvation (5 h) in the wild-type, *atg2*Δ and *rny1*Δ cells. (A) Northern blot analysis. The wild-type, *atg2*Δ and *rny1*Δ cells were grown in SD, transferred to SD-N and cultured for 5 h. Five micrograms of the extracted RNAs were separated on either denaturing formaldehyde agarose gel (1%) (left) or 10 % polyacrylamide gel containing 8 M Urea (right). Blots were probed with specific oligonucleotides and RNAs were stained by methylene blue. *HSP26* (mRNA) was known to be upregulated by nitrogen starvation (Onodera and Ohsumi, 2005) (B) Quantification of (A). The fold changes were calculated relative to the respective values in SD (wild-type). Data were normalized to U4 (snRNA) or SnR50 (snoRNA). (C) qRT-PCR analysis. The amount of RNAs was measured by qRT-PCR. The mean fold changes were

calculated relative to the respective values of the wild-type in SD (left) or SD-N (right). *TAF10* (mRNA) has been shown as a good reference gene (Teste *et al.*, 2009). Date were means of triplicates and normalized to U4 (snRNA) or SnR189 (snoRNA).

3.3.9 Starvation-induced RNA degradation is conserved in the fission yeast

The fission yeast, *Schizosaccharomyces pombe*, is biologically very different from the budding yeast, *S. cerevisiae*. To determine whether a similar mechanism operates in other organisms, I performed the time-course metabolome analysis of the fission yeast (wild-type) and the autophagy-defective mutant *atg1*Δ under nitrogen starvation. As described in section 1.2, same with Atg2, Atg1 is also an essential component for autophagosome formation. Similar transient accumulations of 3'-NMPs and nucleosides were observed in the wild-type cells whereas in the *atg1*Δ cells, their levels did not increase as dramatically, indicating that autophagy-dependent RNA catabolism is well conserved between two phylogenetically distant yeast species (**Fig. 3-18**). Thus, the principal scheme of RNA degradation may be widely preserved in higher eukaryotes.

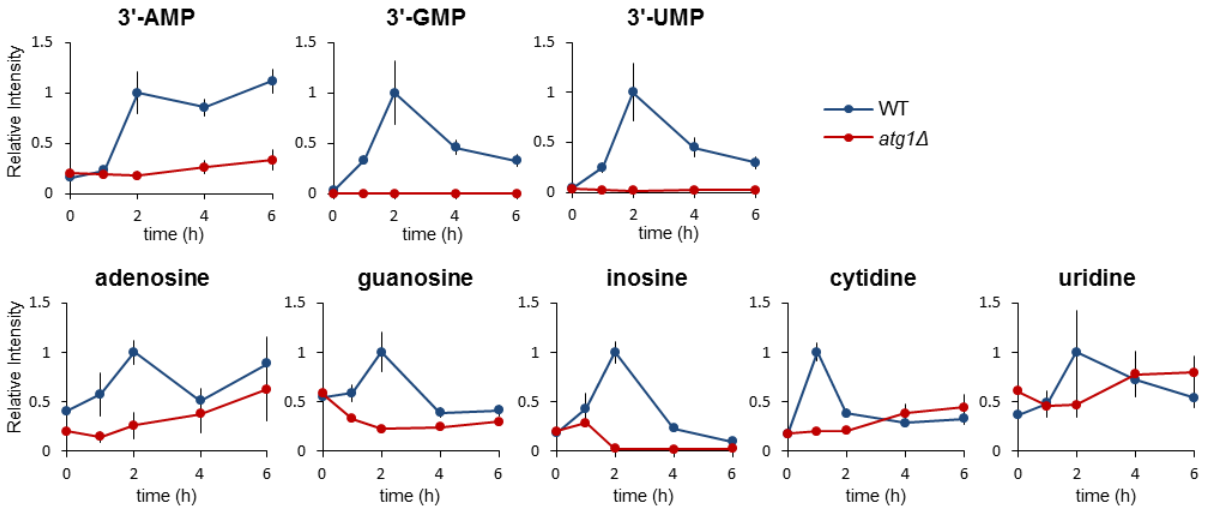

Fig. 3-18. Time-dependent changes in nucleotide and nucleoside levels in the wild-type and *atg1*Δ of *Schizosaccharomyces pombe* under nitrogen starvation. The results are presented as normalized intensities on the basis of peak height of each metabolite in the wild-type cells. All data are means of triplicates. The error bars represent the standard deviation.

3.4 Discussion

Chapter 3 characterized the molecular details of the mechanism of autophagy-mediated RNA degradation under nitrogen starvation, a process involving the T2 RNase family member Rny1, the alkali phosphatase Pho8, the purine phosphorylase Pnp1, the pyrimidine hydrolase Urh1 and one or several transporters including a vacuole-cytoplasm nucleoside transporter Fun26.

T2-type RNase is highly conserved in almost all organisms and generally has a preference for acidic pH (Irie, 1999; Luhtala and Parker, 2010). Most of these RNases are vacuolar/lysosomal enzymes, consistent with the low pH optimum of these proteins. Therefore, they are likely to function in the vacuole/lysosome to cleave RNA, and loss of their function may result in lysosomal dysfunction. Previous studies have suggested that homologues of Rny1 in plants and animals play critical roles in RNA turnover (Hillwig *et al.*, 2011). Haud *et al*. reported that loss of *RNASET2* in zebrafish resulted in accumulation of undigested rRNA within the lysosome in brain cells, as revealed by microscopy (Haud *et al.*, 2011). Henneke *et al*. also showed that in human, mutation in the *RNASET2* gene is associated with a neurological lesion, leukoencephalopathy (Henneke *et al.*, 2009). Therefore, the homologues of Rny1 broadly participate in RNA catabolism in the vacuole/lysosome, and defects in these enzymes would cause serious lysosomal storage disorders. In this study, I showed that the yeast T2-type RNase Rny1 plays a major role in autophagy-dependent RNA degradation under nitrogen starvation. Consequently, 3'-NMPs are the intermediates of RNA degradation in the vacuole. During the steady state of autophagy in the wild-type cells, 3'-NMPs remain at very low levels, suggesting that the nuclease reaction is the rate limiting step of the whole process, and that the resultant nucleotides are rapidly degraded. At current stage, it is difficult to tell whether Rny1 itself produces the mononucleotides, or instead triggers RNA degradation by cleaving large RNAs into fragments. Because rRNAs possess tight secondary structure, it remains possible that some RNA helicase/unwindase might also function in this process. Further characterization of Rny1 and/or identification of additional protein(s) that support RNA degradation are necessary in order to understand the mechanistic basis of the first step of RNA hydrolysis in the vacuole.

3’-NMPs in the vacuole are immediately converted to nucleosides by Pho8. In *pho8*Δ cells, 3’-NMPs accumulated to very high levels (**Fig. 3-4C** and **3-19A**). Furthermore, significant levels of nucleotides, nucleosides, and bases were detectable in the medium of *pho8*Δ cells after 6 h of starvation, indicating that vacuolar and plasma membranes possess transport systems for these compounds (**Fig. 3-19B**). Notably, the large quantities of nucleotides generated during the process of bulk RNA degradation are not 5’-NMPs but 3’-NMPs, possibly to prevent serious perturbation of energy metabolism and signaling as well as nucleic acid synthesis, processes in which 5’-NMPs participate.

Pho8 was initially identified as a non-specific phosphatase, and its physiological substrates have been controversial for a long time (Kaneko *et al.*, 1982; Donella-Deana *et al.*, 1993). Pho8 is classified as alkaline phosphatase because it has a pH optimum above 9.0 for the artificial substrate p-nitrophenyl phosphate (Plankert *et al.*, 1991). On the other hand, Pho8 activity for fructose 2,6-bisphosphate (FBP), one of the physiological substrates of Pho8, has an acidic pH optimum (Plankert *et al.*, 1991). A recent study showed that Pho8 plays a role in nicotinamide adenine dinucleotide metabolism, functioning as a nicotinamide mononucleotide (NMN) phosphatase in the vacuole (Lu and Lin, 2011). In this study, a new physiological function of Pho8 as a nucleotidase with a possible acidic pH optimum similar to FBPase was proposed. In addition, it is shown that Pho8 is highly induced under nitrogen starvation conditions, and it can efficiently act on 3’ nucleotides as substrates (**Fig. 3-8B and Fig. 3-4C**).

The nucleosides generated by autophagic degradation of RNA need to be transported to the cytoplasm efficiently for further breakdown. In this study, I identified a responsible transporter Fun26, which is localized on the vacuolar membrane. However, Fun26 only exhibited partial contribution to this process, which suggested the existence of other cooperating transporters that need further study.

The nucleosides transferred to the cytoplasm are rapidly further catabolized by two nucleosidases, Pnp1 and Urh1 (**Fig. 3-13A**; (Xu *et al.*, 2013)). Deamination of nucleotides, nucleosides and bases occurs, and the resultant final products, xanthine and uracil, are

excreted out of the cell. Under nitrogen starvation, the translation rate is significantly reduced due to the low abundance of amino acids, although the transcription rate is not affected much (Onodera and Ohsumi, 2005; Suzuki *et al.*, 2011). When extracellular nitrogen sources are depleted, recycling of amino acids derived from protein degradation via autophagy is essential for cell survival (Kuma *et al.*, 2004; Onodera and Ohsumi, 2005). In addition to amino acids, which are reutilized for protein synthesis as well as energy sources, ammonia liberated during RNA degradation process may also be reused as a nitrogen source. As the last step of the degradation, superfluous bases must be excreted out of the cell, probably due to the osmotic demand as a result of elevated concentrations of degradation products from bulk protein and RNA, because nitrogen atoms in purine and pyrimidine rings cannot be utilized as nitrogen sources by *S. cerevisiae* (Pantazopoulou and Diallinas, 2007). In all cases, under starvation conditions, nucleosides and bases are hardly salvaged, but instead mostly excreted to the environment, suggesting that proper disposal of nucleotides in appropriate forms may be important for the maintenance of cellular metabolic balance. Therefore, the amount of ultimate metabolites in the medium may serve as an appropriate indicator for autophagy. The fundamental mechanism of autophagy-dependent RNA degradation is likely to be conserved from yeast to human. However, the final outputs and their fates are no doubt depending on the presence and activity of metabolic enzymes, which may differ among species, organs, and cell types.

For RNA degradation, it is of great interest to know if there are any specific RNA species of tRNA, mRNA, or other cytoplasmic RNAs that are selectively degraded by autophagy. Although in this study, no selectivity in autophagy-mediated RNA degradation was observed (**Fig. 3-17B** and **3-17C**), I believe, global analysis such as RNA-seq technique might reveal a more comprehensive assessment of changes in RNA species that are regulated by autophagy, if any.

Autophagy-dependent increases in 3’-NMPs and nucleosides have also been observed in the fission yeast, suggesting the mechanism of autophagy-mediated RNA degradation is conserved in this organism. It is said that the fission yeast is phylogenetically distant from the budding yeast as much as human being is. Therefore, if these two species share the same

mechanism of autophagy-mediated RNA degradation, since autophagy is highly conserved among all eukaryotes, possibly, other eukaryote organisms, including human beings may share a similar mechanism of RNA degradation for starvation adaptation.

Autophagy is a mechanism to decompose macromolecules including proteins and RNAs. However, due to the large pool sizes of these molecules, direct monitor of the degraded amounts proved to be difficult and lacking of accuracy (**Fig. 3-17**). By contrast, approach from the other side, namely to monitor the generated degradation products, was found to be highly efficient and precise. In this study, metabolomics presented its advantages over the conventional methods to monitor autophagic RNA degradation and can be thus anticipated to be as useful for other autophagic degradation studies as well.

A

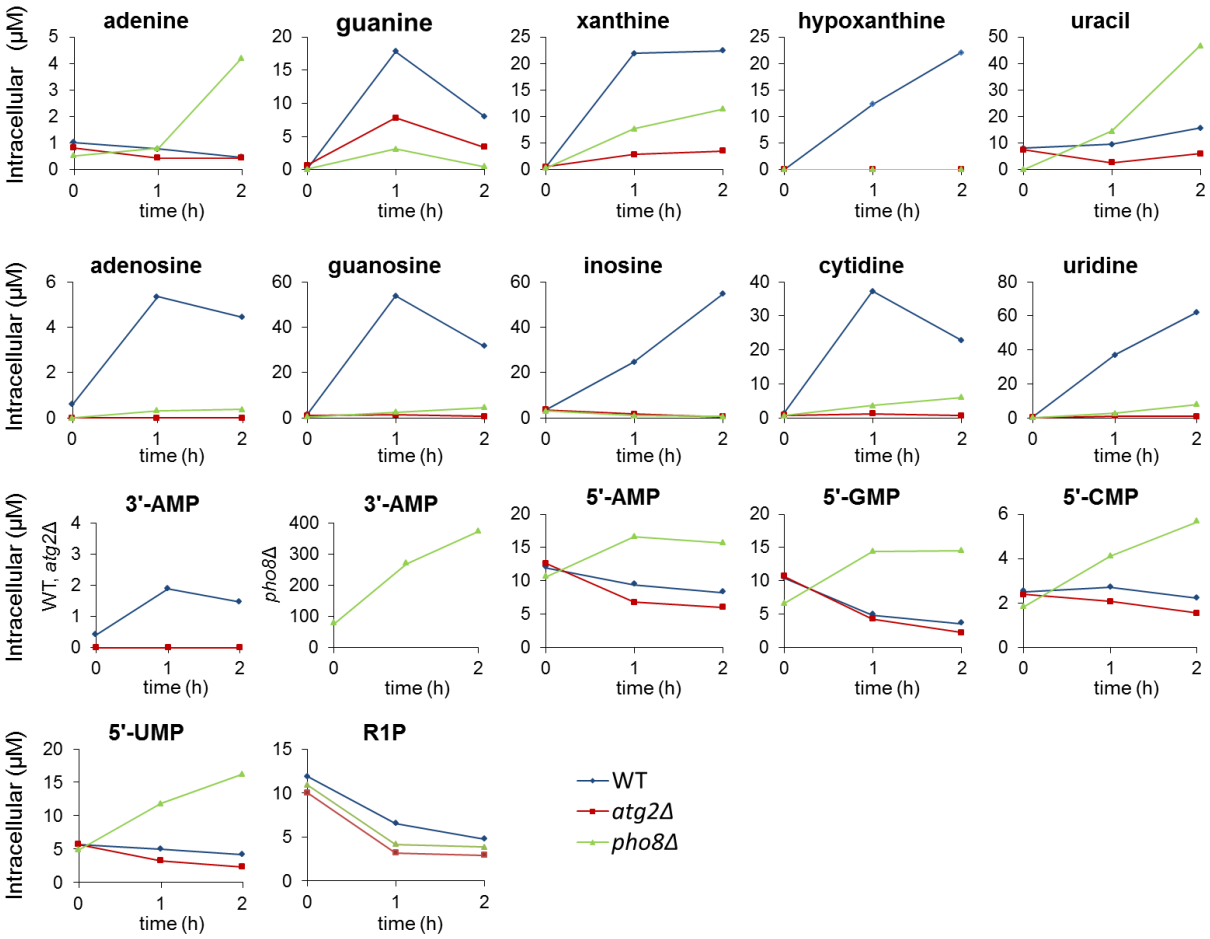

B

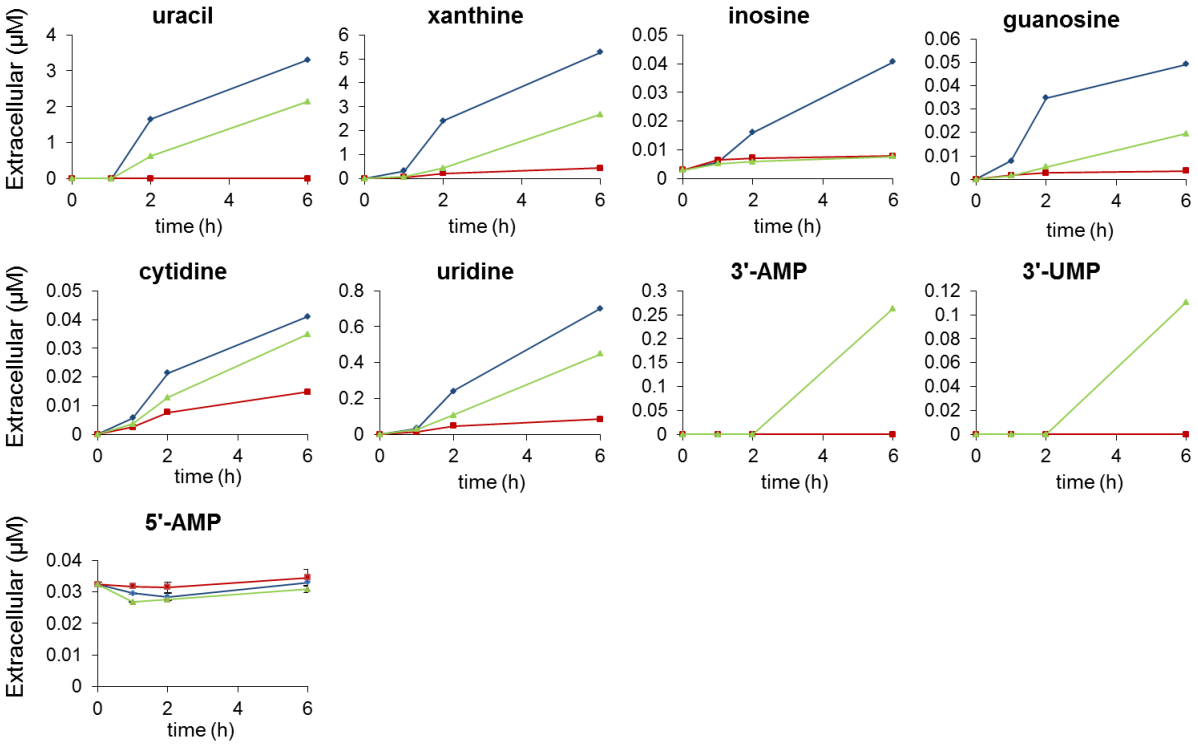

Fig. 3-19. Dynamics of nucleotides, nucleosides and bases under nitrogen starvation. (A and B) Time-dependent changes in nucleotide, nucleoside and base levels under nitrogen starvation, presented in absolute concentrations. Intracellular (A) and extracellular (B) nucleotides, nucleosides and bases. Data of nucleosides and bases were the same with in Fig. 3-11 and 3-15, except for the inclusion of *pho8*Δ. Note that 3'-AMP in *pho8*Δ is separately presented.

Chapter 4 Conclusions

4.1 Summary

This study represents the first comprehensive characterization of autophagy-dependent bulk RNA catabolism from long RNAs to the final de-aminated bases in yeast. Upon induction of autophagy, cytoplasmic constituents including large numbers of ribosomes are delivered to the vacuole via autophagosomes for degradation. The RNA sequestered to the vacuole is first cleaved by the vacuolar ribonuclease Rny1, generating 3' nucleotides. Then, the vacuolar non-specific phosphatase Pho8 acts as a nucleotidase by cleaving the phosphate group from the nucleotides, resulting in accumulation of nucleosides in the vacuole. Following the transport out of the vacuole into the cytoplasm mediated partially by Fun26, the nucleosides are further broken down into purine and pyrimidine bases by two nucleosidases, Pnp1 and Urh1. These bases are immediately converted to the final de-aminated forms, uracil and xanthine through several enzymatic steps, and excreted out of the cell. These dynamic changes in metabolites were not observed in cells defective in non-selective autophagy, but occurred normally in those defective in different types of selective autophagy.

Autophagy-dependent increases in 3'-NMPs and nucleosides have been observed in different nutrient starvations (nitrogen and carbon) and starvation-like (rapamycin treatment) conditions (**Fig. 2-4** and **2-7**; **Appendix V** and **VI**), suggesting that autophagy-mediated RNA degradation mechanism generally holds true for possibly all different types of starvation and starvation-like conditions. In addition, its universality has also been demonstrated in other species.

Through the course of this study, metabolome analysis played a key role in leading the direction of this study and was also presented as a killer technology for elucidating the pathway of RNA degradation under starvation conditions in yeast, thus fulfilling the objective of this study as laid out in Section 1.5, namely, to prove metabolomics as a useful and powerful tool for discovering and solving physiological problems, especially in characterizing metabolic pathways and verifying enzyme functions.

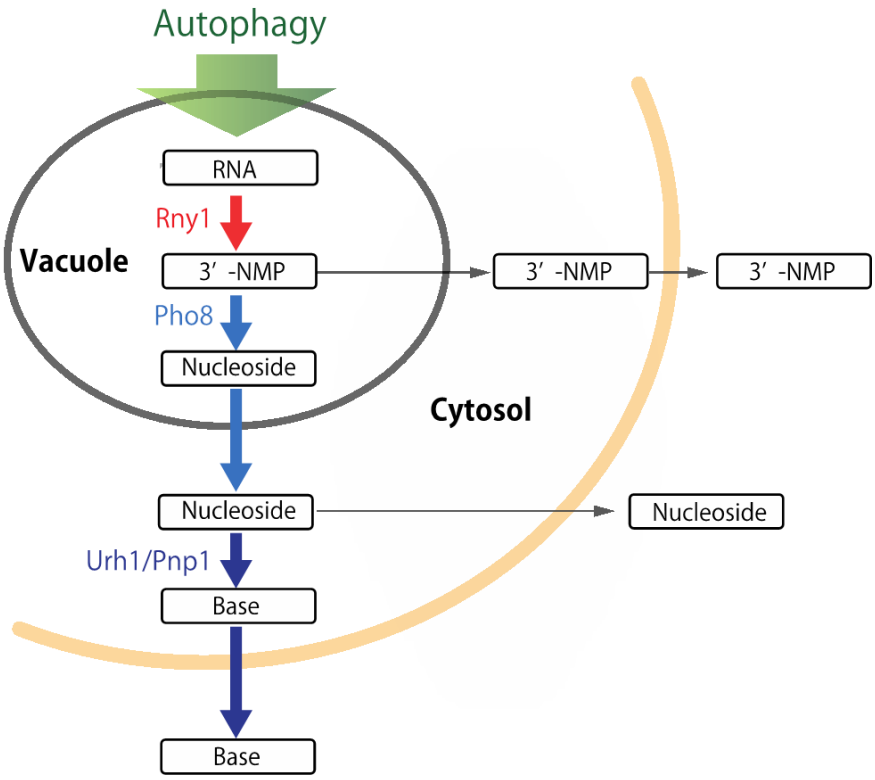

Fig. 4-1. Autophagy-mediated RNA degradation pathway in *S. cerevisiae*. Thick arrows depict the primary process in the wild-type strain. Thin arrows indicate subordinate pathways that are considered less important for this process.

4.2 Future perspectives

There are still several tasks need to be completed for a better understanding of autophagy-mediated RNA degradation: 1. Further exploration of related enzymes such as the possible RNA helicase, deaminases and transporters; 2. Investigation of the selectivity in RNA species; 3. Examination of higher organisms such as mammalian cells for further validation of its universality.

In this study, autophagy was shown to induce drastic changes in the concentrations of cellular metabolites. Autophagy inevitably causes metabolic perturbations that must be overcome; failure to do so may cause various diseases including cancer. Understanding the relationship between the entire flow of cellular metabolism and autophagy will not only provide crucial insights into cell physiology, but also open new opportunities for intervention in metabolic disorders.

Decades of researchers' efforts have finally started to reveal the mysteries of autophagy, although it might still be just the tip of the iceberg. A more and more complex face of autophagy has been presented from various aspects. This study approached from a novel view --- the metabolic changes induced by autophagy. It represents a successful example of metabolomics in autophagy study from discovering the problem to solving it. Therefore, metabolomics can be highly anticipated as one of the most powerful strategies for investigating mechanisms of physiological phenomena in future.

Acknowledgment

I would like to express my deepest gratitude to my supervisor Professor Eiichiro Fukusaki for offering me the opportunity to conduct the research at his lab as well as the invaluable instructions regarding my research direction.

My sincerest appreciation also goes to Professor Takeshi Bamba at Kyushu University, who was an associated professor in Fukusaki-lab until March 2015, Associated Professor Shuichi Shimma and Assistant Professor Hisayo Ono for their precious comments and discussions, especially Assistant Professor Hisayo Ono, who has been a kind consultant on every aspect of my life and research, and gave me so much courage to keep on whenever I felt depressed.

I would also like to thank Professor Yoshinori Ohsumi from Frontier Research Center, Tokyo Institute of Technology for the precious opportunity of collaboration and kind guidance on my research. This research would not have been possible without his support, and his rigorous scientific attitude towards research taught me how a real researcher should be.

During the process of this study, my collaborator Dr. Tomoko Kawamata unreservedly shared her ideas and information on research strategy, and helped perform large numbers of experiments. Her professional knowledge and expertise on RNA and autophagy have greatly contributed to this whole study and her passion and enthusiasm for research have been a constant source of inspiration. I have benefited from every discussion and email exchange with her that I really appreciate.

I also want to say thank you to Ms. Miou Matsunami, who kindly constructed most of the strains used in this thesis, and Dr. Tetsuro Horie for his constructive discussion and technical assistance on this study.

I am also very thankful to Professor Hajime Watanabe and Professor Toshiya Muranaka for spending their precious time on checking the manuscript. Their professional opinions have helped improve this thesis in all aspects.

Many thanks also go to Dr. Yasumune Nakayama, Dr. Hiroshi Tsugawa, Ms. Ayako Tomio, Mr. Yudai Dempo, Dr. Zanariah Binti Hashim, Mr. Shao Thing Teoh and Mr. Hitoshi Mitsunaga for sharing their valuable opinions, offering many helpful suggestions regarding cell cultivation and analytical methods as well as giving me much inspiration and encouragement.

I am also sincerely grateful for the financial support by the Japan Ministry of Education, Culture, Sports, Science & Technology (MEXT), which allowed me to concentrate on my study.

Finally, I would like to thank all the other members of Fukusaki Lab, especially our lab secretaries Ms. Yuriko Okuda and Ms. Beni Okuno for taking care of all the official documents, and Ms. Yukako Yamanaka, Ms. Yumiko Nagasawa, Ms. Erika Ohta, Dr. Shouji Kakuta, Ms. Miki Kitamura, Ms. Nastuki Mimura, Mr. Hirofumi Fujimoto, Mr. Toshiyuki Ohtake, Mr. Hiroki Fukami, Ms. Manako Ueno, Mr. Takayuki Yamada, Mr. Naoki Kawase, Mr. Shingo Noguchi, Mr. Udi Jumuhawan and Ms. Phan Nguyen Thuy An for their moral support, warm friendship and life assistance throughout the whole doctoral course. Thank you all so much for making my life wonderful and memorable.

December, 2015

References

Ashford TP, Porter KR (1962) Cytoplasmic components in hepatic cell lysosomes. *J Cell Biol*, **12:** 198–202

Bligh EG, Dyer WJ (1959) A rapid method of total lipid extraction and purification. *Can J Biochem Physiol*, **37:** 911-917

Brauer MJ, Yuan J, Bennett BD, Lu W, Kimball E, Botstein D, and Rabinowitz JD (2006) Conservation of the metabolomic response to starvation across two divergent microbes. *PNAS*, **103(51):** 19302–19307

Breker M, Gymrek M, Schuldiner M (2013) A novel single-cell screening platform reveals proteome plasticity during yeast stress responses. *J Cell Biol*, **200:** 839-850

Campomenosi P, Salis S, Lindqvist C, Mariani D, Nordstrom T, Acquati F, Taramelli R (2006) Characterization of RNASET2, the first human member of the Rh/T2/S family of glycoproteins. *Arch Biochem Biophys*, **449:** 17-26

Clark SL (1957) Cellular differentiation in the kidneys of newborn mice studied with the electron microscope. *J Biophysic And Biochem Cytol*, **3:** 349–362

Cohen M, Stutz F, Belgareh N, Haguenauer-Tsapis R, Dargemont C (2003) Ubp3 requires a cofactor, Bre5, to specifically de-ubiquitinate the COPII protein, Sec23. *Nat Cell Biol*, **5:** 661-667

Cuervo AM, Bergamini E, Brunk UT, Dröge W, French M, Terman A (2005) Autophagy and Aging: The Importance of Maintaining "Clean" Cells. *Autophagy* **1(3):** 131-140

Dawaliby R, Mayer A (2010) Microautophagy of the Nucleus Coincides with a Vacuolar Diffusion Barrier at Nuclear–Vacuolar Junctions. *Mol Biol Cell*, **21:** 4173-4183

Debnath J, Baehrecke EH, Kroemer G (2005) Does autophagy contribute to cell death? *Autophagy* 1:2, 66-74

Dice JF (2007) Chaperone-Mediated Autophagy, *Autophagy* **3(4):** 295-299

Donella-Deana A, Ostojic S, Pinna LA, Barbaric S (1993) Specific dephosphorylation of phosphopeptides by the yeast alkaline phosphatase encoded by *PHO8* gene. *Biochim Biophys Acta*, **1177:** 221-228

Farré JC, Burkenroad A, Burnett SF, Subramani S (2013) Phosphorylation of mitophagy and pexophagy receptors coordinates their interaction with Atg8 and Atg11. *EMBO Reports,* **14:** 441–449

Fiehn O (2002) Metabolomics-the link between genotypes and phenotypes. *Plant Mol. Biol,* **48:** 155–171

Hashim Z, Teoh ST, Bamba T, Fukusaki E (2014) Construction of a metabolome library for transcription factor-related single gene mutants of *Saccharomyces cerevisiae*. *J Chromatogr B*, **966:** 83–92

Hara T, Nakamura K, Matsui M, Yamamoto A, Nakahara Y, Suzuki-Migishima R, Yokoyama M, Mishima K, Saito I, Okano H, Mizushima N (2006) Suppression of basal autophagy in neural cells causes neurodegenerative disease in mice. *Nature*, **441:** 885-889

Harding TM, Morano KA, Scott SV, Klionsky DJ (1995) Isolation and characterization of yeast mutants in the cytoplasm to vacuole protein targeting pathway. *J Cell Biol*, **131:** 591-602

Haud N, Kara F, Diekmann S, Henneke M, Willer JR, Hillwig MS, Gregg RG, Macintosh GC, Gartner J, Alia A, Hurlstone AF (2011) *rnaset2* mutant zebrafish model familial cystic

leukoencephalopathy and reveal a role for RNase T2 in degrading ribosomal RNA. *Proc Natl Acad Sci USA*, **108:** 1099-1103

Henneke M, Diekmann S, Ohlenbusch A, Kaiser J, Engelbrecht V, Kohlschutter A, Kratzner R, Madruga-Garrido M, Mayer M, Opitz L, Rodriguez D, Ruschendorf F, Schumacher J, Thiele H, Thoms S, Steinfeld R, Nurnberg P, Gartner J (2009) RNASET2-deficient cystic leukoencephalopathy resembles congenital cytomegalovirus brain infection. *Nat Genet*, **41:** 773-775

Hillwig MS, Contento AL, Meyer A, Ebany D, Bassham DC, Macintosh GC (2011) RNS2, a conserved member of the RNase T2 family, is necessary for ribosomal RNA decay in plants. *Proc Natl Acad Sci USA*, **108:** 1093-1098

Huang H, Kawamata T, Horie T, Tsugawa H, Nakayama Y, Ohsumi Y, Fukusaki E (2014) Bulk RNA degradation by nitrogen starvation-induced autophagy in yeast. *EMBO J*, **34:** 154-168

Igarashi H, Mogi S, Wakamatsu A, Minamide Y, Kudoh S (2011) Characteristic Features of an Analytical Column with a Pentafluorophenylpropyl Stationary Phase Applied To a Determination of a Fluorinated Phenyl Alanyl Derivative Compound, Gw823093, In Human Urine Using an Lc-Esi-Ms/Ms Method. *J Anal Bioanal Techniques*, **S5:** 001

Irie M (1999) Structure-function relationships of acid ribonucleases: lysosomal, vacuolar, and periplasmic enzymes. *Pharmacol Ther*, **81:** 77-89

Jumhawa U, Putri SP, Yusianto, Marwani E, Bamba T, Fukusaki E (2013) Selection of Discriminant Markers for Authentication of Asian Palm Civet Coffee (Kopi Luwak): A Metabolomics Approach. *J Agric Food Chem*, **61:** 7994-8001

Kabeya Y, Kamada Y, Baba M, Takikawa H, Sasaki M, Ohsumi Y (2005) Atg17 Functions in Cooperation with Atg1 and Atg13 in Yeast Autophagy. *Mol Biol Cell*, **16:** 2544-2553

Kaneko Y, Tamai Y, Toh-e A, Oshima Y (1985) Transcriptional and post-transcriptional control of *PHO8* expression by PHO regulatory genes in *Saccharomyces cerevisiae*. *Mol Cell Biol*, **5:** 248-252

Kaneko Y, Toh-e A, Oshima Y (1982) Identification of the genetic locus for the structural gene and a new regulatory gene for the synthesis of repressible alkaline phosphatase in *Saccharomyces cerevisiae*. *Mol Cell Biol*, **2:** 127-137

Kanki T, Wang K, Cao Y, Baba M, Klionsky DJ (2009) Atg32 is a mitochondrial protein that confers selectivity during mitophagy. *Dev Cell*, **17:** 98-109

Kaushik S, Bandyopadhyay U, Sridhar S, Kiffin R, Martinez-Vicente M, Kon M, Orenstein SJ, Wong E, Cuervo AM (2011) Chaperone-mediated autophagy at a glance. *Cell Science at a Glance*, **124(4):** 495-499

Kawamata T, Kamada Y, Kabeya Y, Sekito T, Ohsumi Y (2008) Organization of the pre-autophagosomal structure responsible for autophagosome formation. *Mol Biol Cell*, **19:** 2039-2050

Kim Y, Aronov P, Zakharkin SO, Anderson D, Perroud B, Thompson IM, Weiss RH (2007) Urine Metabolomics Analysis for Kidney Cancer Detection and Biomarker Discovery. *Molecular & Cellular Proteomics*, **8:** 558-570

Kleemann R, Verschuren L, Erk MJ, Nikolsky U, Cnubben NHP, Verheij ER, Smilde AK, Hendriks HFJ, Zadelaar S, Smith GJ, Kaznacheev V, Nikolskaya T, Melnikov A, HurtCamejo E, Greef J, Ommen B, Kooistra T (2007) Atherosclerosis and liver inflammation induced by increased dietary cholesterol intake: a combined transcriptomics and metabolomics analysis. *Genome Biology*, **8:** R200

Klionsky DJ (2007) Autophagy: from phenomenology to molecular understanding in less than a decade. *Nat Rev Mol Cell Biol*, **8:** 931-937

Klionsky DJ, Cuervo AM, Seglen PO (2007) Methods for Monitoring Autophagy from Yeast to Human. *Autophagy* **3(3):** 181-206

Klionsky DJ, Emr SD (1989) Membrane protein sorting: biosynthesis, transport and processing of yeast vacuolar alkaline phosphatase. *EMBO J*, **8:** 2241-2250

Kohda TA, Tanaka K, Konomi M, Sato M, Osumi M, Yamamoto M (2007) Fission yeast autophagy induced by nitrogen starvation generates a nitrogen source that drives adaptation processes. *Genes Cells*, **12:** 155-170

Kohrer K, Domdey H (1991) Preparation of high molecular weight RNA. *Methods Enzymol*, **194:** 398–405

Komatsu M, Waguri S, Ueno T, Iwata J, Murata S, Tanida I, Ezaki J, Mizushima N, Ohsumi Y, Uchiyama Y, Kominami E, Tanaka K, Chiba T (2005) Impairment of starvation-induced and constitutive autophagy in Atg7-deficient mice. *J. Cell Biol*, **169:** 425-434

Kraft C, Deplazes A, Sohrmann M, Peter M (2008) Mature ribosomes are selectively degraded upon starvation by an autophagy pathway requiring the Ubp3p/Bre5p ubiquitin protease. *Nat Cell Biol*, **10:** 602-610

Kuma A, Hatano M, Matsui M, Yamamoto A, Nakaya H, Yoshimori T, Ohsumi Y, Tokuhisa T, Mizushima N (2004) The role of autophagy during the early neonatal starvation period. *Nature*, **432:** 1032-1036

Kunz JB, Schwarz H, Mayer A (2003) Determination of Four Sequential Stages during Microautophagy *in Vitro*. *J Bio. Chem*, **279:** 9987-9996.

Kurtz JE, Exinger F, Erbs P, Jund R (1999) New insights into the pyrimidine salvage pathway of *Saccharomyces cerevisiae*: requirement of six genes for cytidine metabolism. *Curr Genet*, **36:** 130-136

Kushnirov VV (2000) Rapid and reliable protein extraction from yeast. *Yeast*, **16:** 857-860

Lardeux BR, Heydrick SJ, Mortimore GE (1987) RNA degradation in perfused rat liver as determined from the release of [14C]cytidine. *J Biol Chem*, **262:** 14507-14513

Lardeux BR, Mortimore GE (1987) Amino acid and Hormonal Control of Macromolecular Turnover in Perfused Rat Liver. *J Biol Chem*, **262:** 14514-14519

Lardeux BR, Heydrick SJ, Mortimore GE (1988) Rates of rat liver RNA degradation *in vivo* as determined from cytidine release during brief cyclic perfusion *in situ*. *Biochem J,* **252:** 363-367

Lecoq K, Belloc I, Desgranges C, Konrad M, Daignan-Fornier B (2001) YLR209c encodes *Saccharomyces cerevisiae* purine nucleoside phosphorylase. *J Bacteriol,* **183:** 4910-4913

Lemasters JJ (2005) Selective Mitochondrial Autophagy, or Mitophagy, as a Targeted Defense Against Oxidative Stress, Mitochondrial Dysfunction, and Aging. *Rejuvenation Res*, **8:** 3-5

Levine B (2006) Unraveling the Role of Autophagy in Cancer. *Autophagy*, **2(2):** 65-66

Liang XH, Jackson S, Seaman M, Brown K, Kempkes B, Hibshoosh H, Levine B (1999) Induction of autophagy and inhibition of tumorigenesis by beclin 1. *Nature*, **402:** 672-676

Lin NY, Beyer C, Giessl A, Kireva T, Scholtysek C, Uderhardt S, Munoz LE, Dees C, Distler A, Wirtz S, Krönke G, Spencer B, Distler O, Schett G, Distler JH (2012) Autophagy regulates TNFα-mediated joint destruction in experimental arthritis. *Ann Rheum Dis* **72:**761-768

Lu SP, Lin SJ (2011) Phosphate-responsive signaling pathway is a novel component of NAD+ metabolism in *Saccharomyces cerevisiae*. *J Biol Chem*, **286:** 14271-14281

Luhtala N, Parker R (2010) T2 Family ribonucleases: ancient enzymes with diverse roles. *Trends Biochem Sci*, **35:** 253-259

MacIntosh GC, Bariola PA, Newbigin E, Green PJ (2001) Characterization of Rny1, the *Saccharomyces cerevisiae* member of the T2 RNase family of RNases: unexpected functions for ancient enzymes? *Proc Natl Acad Sci USA*, **98:** 1018-1023

Mao K, Chew LH, Inoue-Aono Y, Cheong H, Nair U, Popelka H, Yip CK, Klionsky DJ (2013) Atg29 phosphorylation regulates coordination of the Atg17-Atg31-Atg29 complex with the Atg11 scaffold during autophagy initiation. *Proc Natl Acad Sci USA*, **110:** E2875-E2884

Mathew R, Karp CM, Beaudoin B, Vuong N, Chen G, Chen HY, Bray K, Reddy A, Bhanot G, Gelinas C, Dipaola RS, Karantza-Wadsworth V, White E (2009) Autophagy suppresses tumorigenesis through elimination of p62. *Cell,* **137:** 1062–1075

Mehrpour M, Esclatine A, Beau I, Codogno1 P (2010) Overview of macroautophagy regulation in mammalian cells. *Cell Research,* **20:** 748–762

Merkler DJ, Wali AS, Taylor J, Schramm VL (1989) AMP Deaminase from Yeast. *J Biol Chem*, **264:** 21422-21430

Mitra S, Tsvetkov AS, Finkbeiner S (2009) Protein turnover and inclusion body formation. *Autophagy,* **5(7):**, 1037-1038

Mizushima N, Noda T, Yoshimori T, Tanaka Y, Ishii T, George MD, Klionsky DJ, Ohsumi M, Ohsumi Y (1998) A protein conjugation system essential for autophagy. *Nature* **395:** 395–398

Mochida K, Oikawa Y, Kimura Y, Kirisako H, Hirano H, Ohsumi Y, Nakatogawa H (2015) Receptor-mediated selective autophagy degrades the endoplasmic reticulum and the nucleus. *Nature*, **522:** 359–362

Mortimore GE, Lardeux BR, Heydrick SJ (1989) Mechanism and control of protein and RNA degradation in the rat hepatocyte: two modes of autophagic sequestration. *Revis Biol Celular*, **20:** 79-96

Münz C (2006) Autophagy and antigen presentation. *Cellular Microbiology*, **8(6):** 891–898

Nakatogawa H, Suzuki K, Kamada Y, Ohsumi Y (2009) Dynamics and diversity in autophagy mechanisms: lessons from yeast. *Nature Rev Mol Cell Biol*, **10:** 458-467

Noda T, Matsuura A, Wada Y, Ohsumi Y (1995) Novel system for monitoring autophagy in the yeast *Saccharomyces cerevisiae*. *Biochem Biophys Res Commun*, **210:** 126-132

Noda T, Ohsumi Y (1998) Tor, a phosphatidylinositol kinase homologue, controls autophagy in yeast. *J Biol Chem*, **273:** 3963-3966

Obara K, Sekito T, Niimi K, Ohsumi Y (2008) The Atg18–Atg2 complex is recruited to autophagic membranes via phosphatidylinositol 3-phosphate and exerts an essential function. *J Biol Chem*, **283:** 23972–23980

Ohsumi Y (2014) Historical landmarks of autophagy research. *Cell Res*, **24:** 9-23

Okamoto K, Kondo-Okamoto N, Ohsumi Y (2009) Mitochondria-anchored receptor Atg32 mediates degradation of mitochondria via selective autophagy. *Dev Cell*, **17:** 87-97

Onodera J, Ohsumi Y (2005) Autophagy is required for maintenance of amino acid levels and protein synthesis under nitrogen starvation. *J Biol Chem*, **280:** 31582-31586

Pantazopoulou A, Diallinas G (2007) Fungal nucleobase transporters. *FEMS Microbiol Rev*, **31:** 657-675

Pestov DG, Shcherbik N (2012) Rapid cytoplasmic turnover of yeast ribosomes in response to rapamycin inhibition of TOR. *Mol Cell Biol*, **32:** 2135–2144

Plankert U, Purwin C, Holzer H (1991) Yeast fructose-2,6-bisphosphate 6-phosphatase is encoded by PHO8, the gene for nonspecific repressible alkaline phosphatase. *Eur J Biochem*, **196:** 191-196

Qiao W, Ellis C, Steffen J, Wu CY, Eide DJ (2009) Zinc status and vacuolar zinc transporters control alkaline phosphatase accumulation and activity in *Saccharomyces cerevisiae*. *Mol Microbiol*, **72:** 320-334

Randow F (2011) How cells deploy ubiquitin and autophagy to defend their cytosol from bacterial invasion. *Autophagy*, **7(3):** 304-309

Raught B, Gingras AC, Sonenberg N (2001) The target of rapamycin (TOR) proteins. *PNAS*, **98:** 7034-7044

Reggiori F, Komatsu M, Finley K, Simonsen A (2012) Autophagy: more than a nonselective pathway. *Int J Cell Biol*, **2012:** 219625

Roberts P, Moshitch-Moshkovitz S, Kvam E, O'Toole E, Winey M, Goldfarb DS (2003) Piecemeal microautophagy of nucleus in *Saccharomyces cerevisiae*. *Mol Biol Cell*, **14:** 129-141

Saint-Marc C, Pinson B, Coulpier F, Jourdren L, Lisova O, Daignan-Fornier B (2009) Phenotypic Consequences of Purine Nucleotide Imbalance in *Saccharomyces cerevisiae*. *Genetics*, **183:** 529-538

Schauer N, Semel Y, Roessner U, Gur A, Balbo I, Carrari F, Pleban T, Perez-Melis A, Bruedigam C, Kopka J, Willmitzer L, Zamir D, Fernie AR (2006) Comprehensive metabolic profiling and phenotyping of interspecific introgression lines for tomato improvement. *Nature Biotechnology* **24:** 447 - 454

Scott SV, Baba M, Ohsumi Y, Klionsky DJ (1997) Aminopeptidase I is targeted to the vacuole by a nonclassical vesicular mechanism. *J Cell Biol*, **138:** 37-44

Scott SV, Guan J, Hutchins MU, Kim J, Klionsky DJ (2001) Cvt19 is a receptor for the cytoplasm-to-vacuole targeting pathway. *Mol Cell*, **7:** 1131-1141

Shcherbik N (2013) Golgi-mediated glycosylation determines residency of the T2 RNase Rny1p in *Saccharomyces cerevisiae*. *Traffic*, **14:** 1209-1227

Suzuki K (2013) Selective autophagy in budding yeast. *Cell Death Differ*, **20:** 43-48

Suzuki K, Kondo C, Morimoto M, Ohsumi Y (2010) Selective transport of alpha-mannosidase by autophagic pathways: identification of a novel receptor, Atg34p. *J Biol Chem*, **285:** 30019-30025

Suzuki SW, Onodera J, Ohsumi Y (2011) Starvation induced cell death in autophagy-defective yeast mutants is caused by mitochondria dysfunction. *PLoS One*, **6:** e17412

Takeshige K, Baba M, Tsuboi S, Noda T, Ohsumi Y (1992) Autophagy in yeast demonstrated with proteinase-deficient mutants and conditions for its induction. *J Cell Biol*, **119:** 301-311

Teste MA, Duquenne M, Francois JM, Parrou JL (2009) Validation of reference genes for quantitative expression analysis by real-time RT-PCR in *Saccharomyces cerevisiae*. *BMC Mol Biol*, **10:** 99

Thompson DM, Parker R (2009) The RNase Rny1p cleaves tRNAs and promotes cell death during oxidative stress in *Saccharomyces cerevisiae*. *J Cell Biol*, **185:** 43-50

Till A, Lakhani R, Burnett SF, Subramani S (2012) Pexophagy: the selective degradation of peroxisomes. *Int J Cell Biol*, **2012:** 512721–512738

Torriani A (1960) Influence of inorganic phosphate in the formation of phosphatases by *Escherichia coli*. *Biochimica et Biophysica Acta*, **38:** 460–469

Tsukada M, Ohsumi Y (1993) Isolation and characterization of autophagy-defective mutants of *Saccharomyces cerevisiae*. *FEBS letters*, **333:** 169-74.

Tyson CB, Lord PG, Wheals AE (1979) Dependency of size of *Saccharomyces cerevisiae* cells on growth rate. *J Bacteriol*, **138:** 92–98

Vickers MF, Yao SYM, Baldwin SA, Young JD, Cass CE (2000) Nucleoside Transporter Proteins of *Saccharomyces cerevisiae*. *J Biol Chem*, **275:** 25931–25938

Vida TA, Emr SD (1995) A new vital stain for visualizing vacuolar membrane dynamics and endocytosis in yeast. *J Cell Biol*, **128:** 779–792

Walseth TF, Graff G, Moos MC Jr., Goldberg ND (1980) Separation of 5′-ribonucleoside monophosphates by ion-pair reverse-phase high-performance liquid chromatography. *Anal Biochem*, **107:** 240-245

Warner JR (1999) The economics of ribosome biosynthesis in yeast. *Trends Biochem Sci*, **24:** 437-440

Xu YF, Letisse F, Absalan F, Lu W, Kuznetsova E, Brown G, Caudy AA, Yakunin AF, Broach JR, Rabinowitz JD (2013) Nucleotide degradation and ribose salvage in yeast. *Mol Syst Biol*, **9:** 665

Yorimitsu T, Klionsky DJ (2005) Atg11 Links Cargo to the Vesicle-forming Machinery in the Cytoplasm to Vacuole Targeting Pathway. *Molecular Biol Cell*, **16:** 1593–1605

List of Publications

Original paper

Hanghang Huang, Tomoko Kawamata, Tetsuro Horie, Hiroshi Tsugawa, Yasumune Nakayama, Yoshinori Ohsumi, Eiichiro Fukusaki (2014) Bulk RNA degradation by nitrogen starvation-induced autophagy in yeast. *EMBO J*, 34,154-168 (DOI 10.15252/embj.201489083)

Conferences

Hanghang Huang, Tomoko Kawamata, Hiroshi Tsugawa, Yasumune Nakayama, Takeshi Bamba, Yoshinori Ohsumi, Eiichiro Fukusaki. "Metabolic and molecular dissection of bulk RNA degradation via autophagy in yeast". 10th International Conference of the Metabolomics Society, Tsuruoka, Japan. June 23rd-26th, 2014.

Hanghang Huang, Tomoko Kawamata, Hiroshi Tsugawa, Yasumune Nakayama, Takeshi Bamba, Yoshinori Ohsumi, Eiichiro Fukusaki. "Bulk RNA degradation by nitrogen starvation-induced autophagy in yeast". 11th KAIST-OSAKA University Symposium, Suita, Japan. September 22nd-24th, 2014.

Appendix

I. Optimization of experimental conditions and methods

1) pH

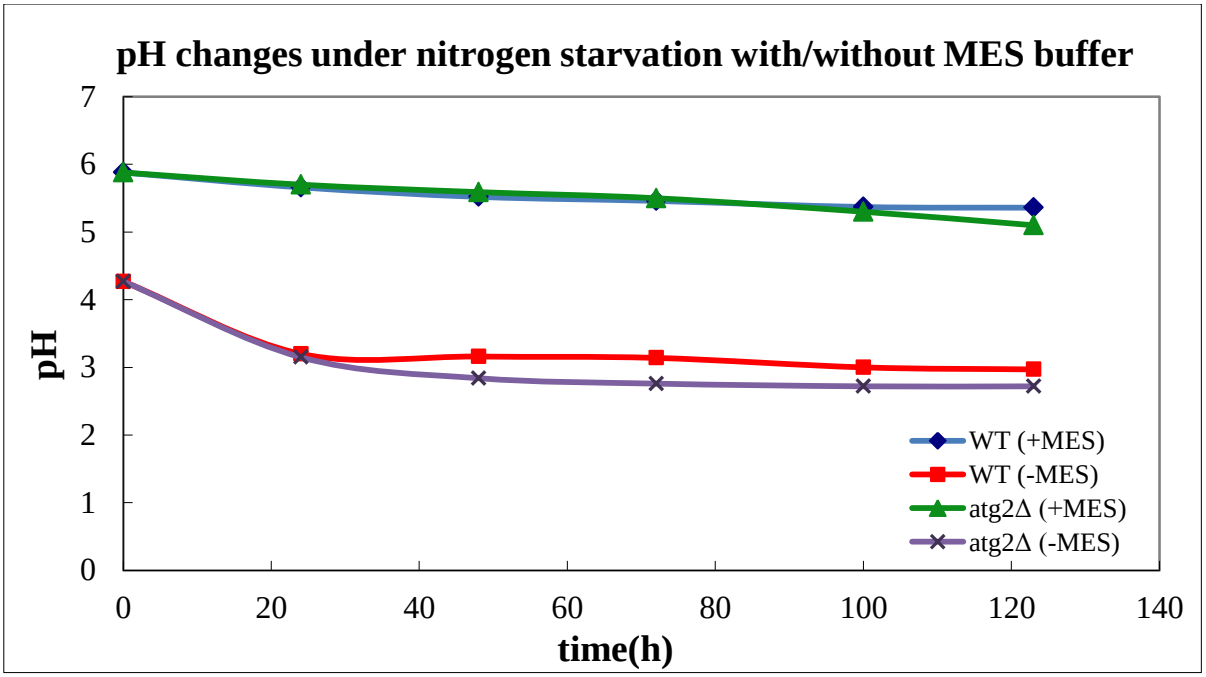

+MES/-MES – Medium with/without 50mM MES/KOH

2) Aeration efficiency

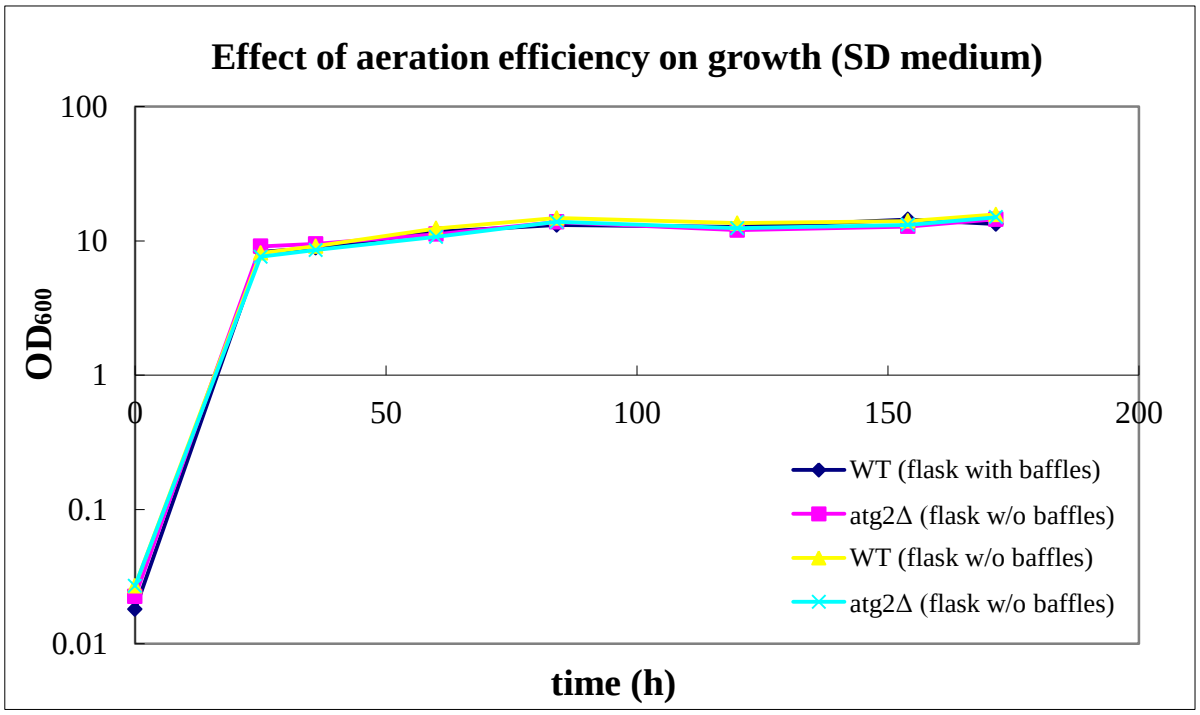

3) Washing methods

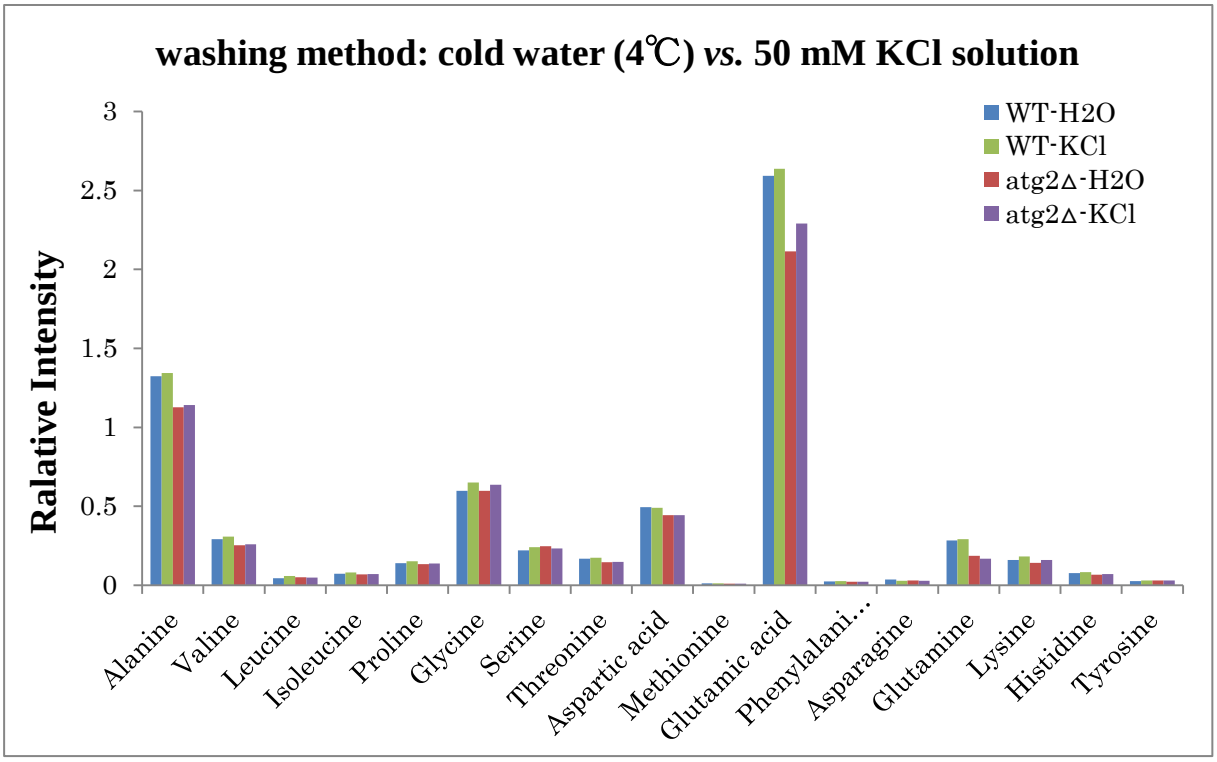

4) Extraction methods

Boiling water (BW) *vs.* Extraction mixture (EM)*

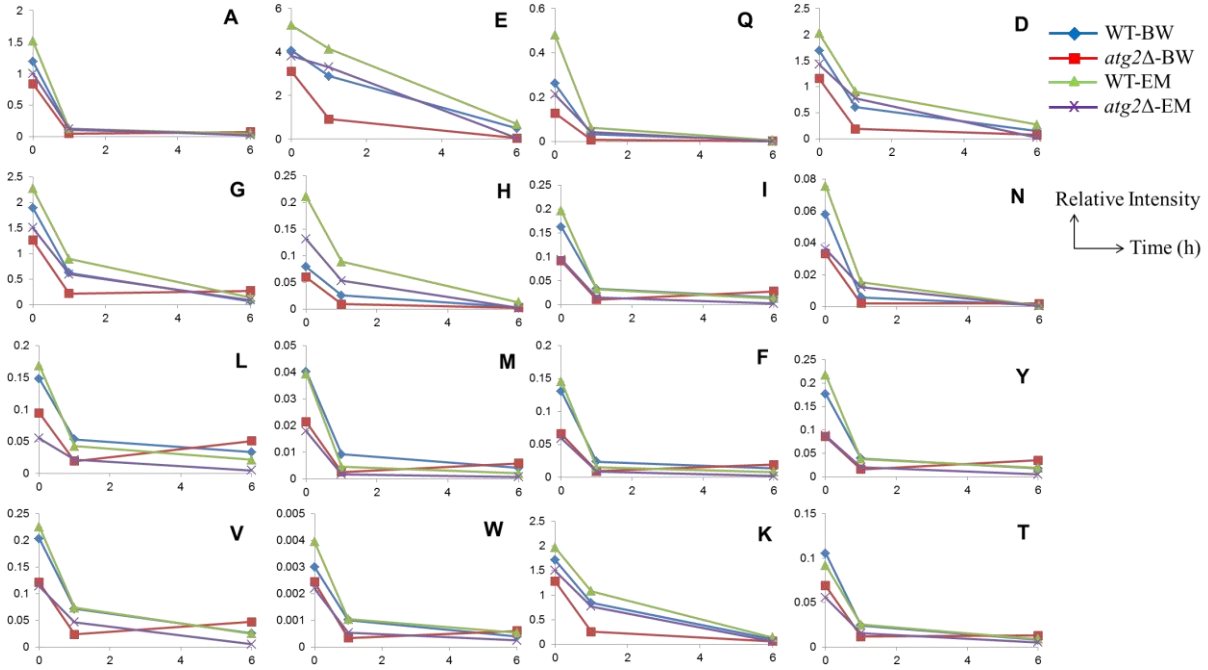

*Data (amino acids) were shown in abbreviation.

II. Growth curves

Nutrient-rich medium (SD medium)

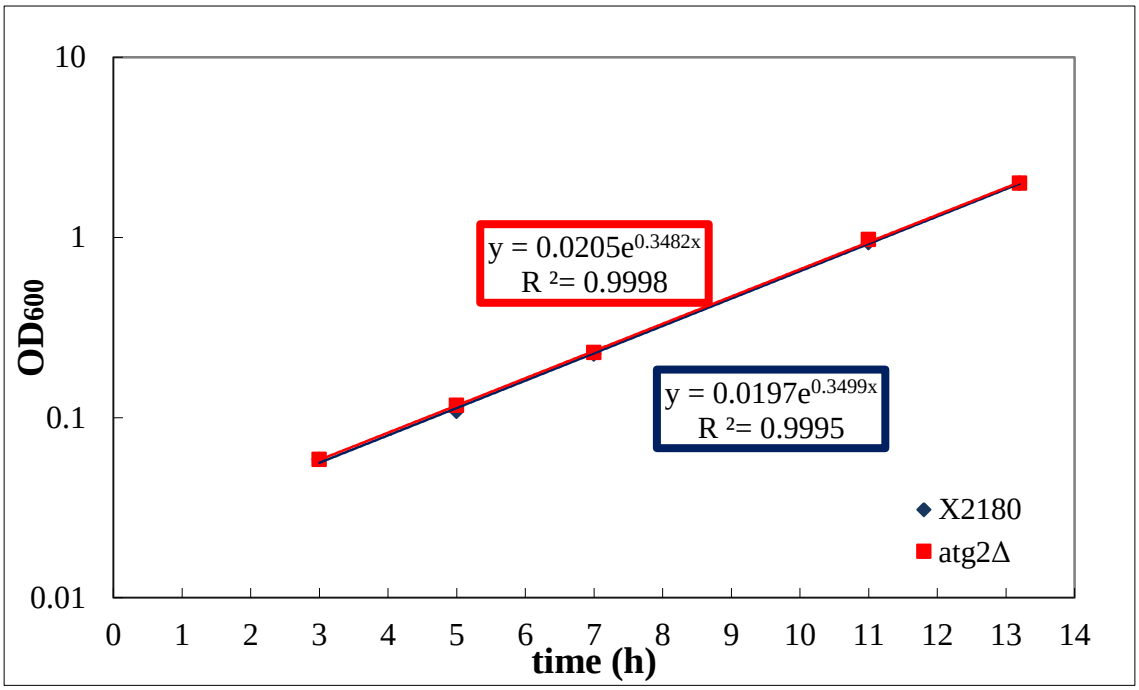

Nitrogen-deprivation medium (SD-N medium)

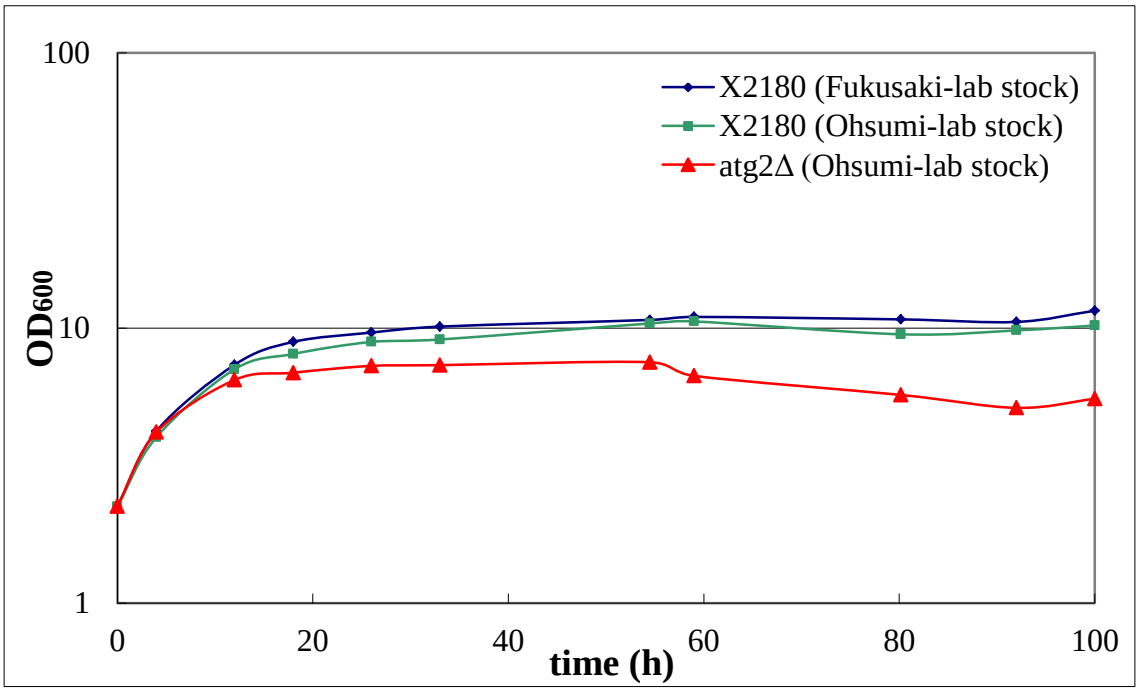

III. Principal Component Analysis (PCA)

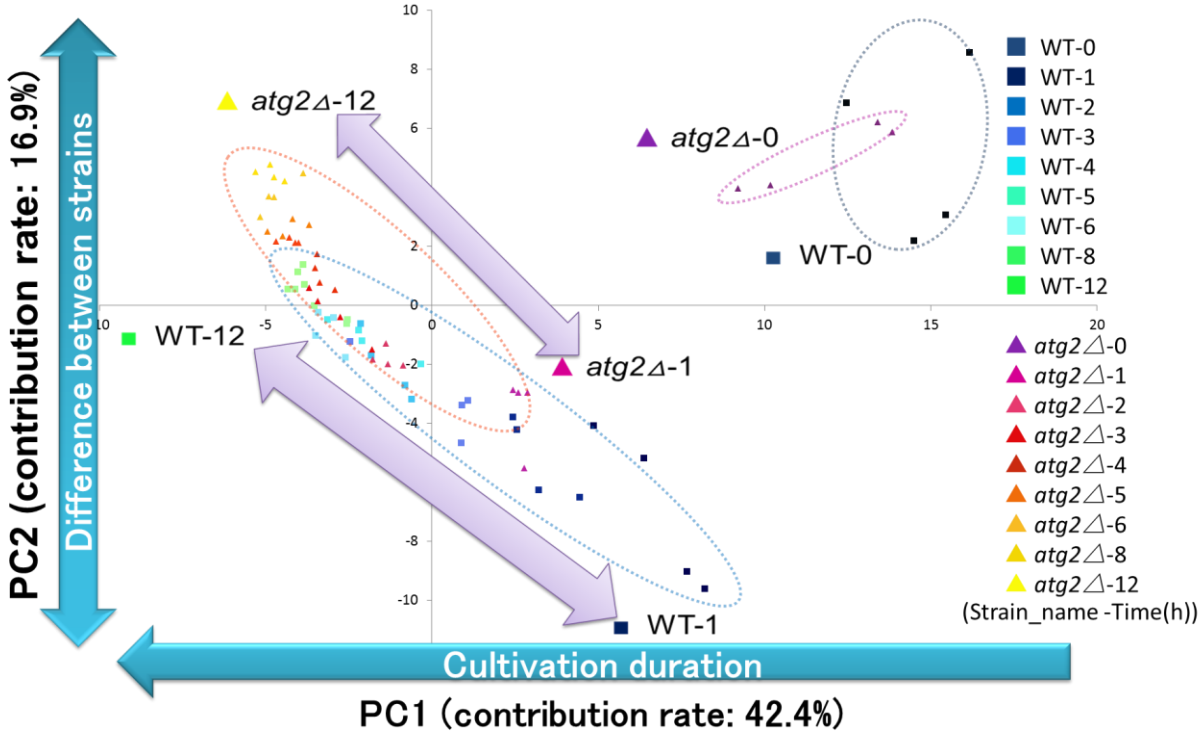

The wild-type and *atg2*Δ cells were grown in SD and transferred to SD-N at time 0. Cells were collected at 0, 1, 2, 3, 4, 5, 6, 8 and 12 h after starvation, extracted and analyzed by LC/MS as described in section 2.2.4~2.2.5.

IV. MRM transition information

Table S-1. MRM for PFPP stationary-phase liquid chromatography

Compounds	Transition*	Retention time (min)	Target Q1 Pre Bias (V)	Target Collision Energy (V)	Target Q3 Pre Bias (V)	Electrode Mode
adenine	136.05>119.05	6.25	-23	-20	-23	positive
xanthine	153.05>110.05	4.134	-29	-20	-10	positive
hypoxanthine	137.05>119.05	6.619	-21	-20	-28	positive
cytosine	112.05>52	3.64	-20	-40	-15	positive
uracil	113.05>40	3.246	-19	-43	-29	positive
thymine	127.05>54.05	5.958	-12	-40	-17	positive
adenosine	268.1>136.05	7.824	-29	-20	-24	positive
guanosine	284.1>152.05	6.805	-30	-10	-17	positive
cytidine	244.1>112.05	5.25	-16	-20	-16	positive
uridine	245.1>113.05	4.35	-27	-10	-15	positive
deoxyadenosine	252.1>136.05	7.695	-17	-20	-27	positive
deoxyguanosine	268.1>152.05	7.12	-18	-10	-15	positive
deoxycytidine	228.1>112.05	6.8	-25	-10	-24	positive
Thymidine	243.1>127.05	7.209	-27	-20	-29	positive
alanine	90.05>44.05	2.3	-16	-20	-19	positive
beta-alanine	89.9>30.15	3	-14	-15	-30	positive
asparagine	133.05>74	2.04	-14	-20	-16	positive
aspartic acid	134.05>74	2.04	-14	-20	-14	positive
arginine	175.1>70.05	2.9	-25	-40	-13	positive
cysteine	122>59	2.2	-29	-40	-13	positive
cystine	241.05>152	1.96	-25	-10	-14	positive
glutamate	148.05>84.05	2.22	-15	-20	-24	positive
glycine	76.05>30.05	3.9	-17	-20	-13	positive
histidine	156.1>110.05	2.6	-16	-20	-13	positive

isoleucine	132.1>86.1	7.6	-16	-10	-13	positive
leucine	132.1>86.1	7.3	-16	-10	-13	positive
lysine	147.1>84.1	2.1	-24	-20	-15	positive
methionine	150.05>56.05	4.2	-20	-20	-29	positive
phenylalanine	166.1>120.1	9.05	-19	-10	-29	positive
proline	116.05>70.05	2.5	-20	-20	-29	positive
serine	106.05>60.05	2.05	-19	-10	-29	positive
threonine	120.05>74.05	2.15	-19	-10	-29	positive
tryptophan	205.1>188.05	11.8	-19	-10	-29	positive
tyrosine	182.1>91.05	7.2	-19	-40	-29	positive
valine	118.1>72.1	3.9	-19	-10	-29	positive
PIPES	301>193.25	1.81	10	28	10	negative
(+)-10-Camphorsulfonic acid	231.15>80.1	9	10	28	10	negative

Table S-2. MRM for ion-pairing liquid chromatography

Compounds	Transition*	Retention time (min)	Target Q1 Pre Bias (V)	Target Collision Energy (V)	Target Q3 Pre Bias (V)	Electrode Mode
PIPES	301>193.05	6.479	12	28	21	negative
(+)-10-Camphorsulfonic acid	231.1>80	11	10	32	30	negative
Alanine	148>88	1.2	20	10	15	negative
Arginine	173.1>131.1	0.905	13	15	25	negative
Asparagine	131>113.1	1.151	10	15	21	negative
Aspartate	132>88.05	3.416	10	14	15	negative
Cysteine	239>120.1	1.25	11	13	21	negative
Glutamate	146>102.05	3.202	11	15	18	negative
Glutamine	145>127.05	1.16	12	18	18	negative
Histidine	154>93	0.907	12	21	16	negative
Leucine	190.05>130.05	2.496	13	10	23	negative

Isoleucine	190.05>130.05	1.201	13	10	23	negative
Lysine	145>73.1	0.8	12	13	26	negative
Methionine	148>47.05	1.987	11	14	16	negative
Phenylalanine	164>147.05	4.785	13	18	27	negative
Proline	174>114	1.331	11	10	20	negative
Serine	104>74.1	1.138	12	16	13	negative
Threonine	118>74.05	1.186	21	16	26	negative
Tryptophan	203.1>116.05	6.571	13	18	19	negative
Tyrosine	180>163.05	2.569	12	18	18	negative
Valine	176.1>116.05	1.554	12	10	20	negative
Glutathione	306.05>143.05	7.133	16	20	26	negative
Pyroglutamate	188>128	6.331	22	12	20	negative
4-Hydroxy-L-proline	190.05>130.05	1.179	13	10	23	negative
Guanine	150>133.05	2.281	11	21	23	negative
Xanthine	151.05>108	3	16	20	19	negative
Hypoxanthine	135.05>92.05	2.647	14	18	16	negative
Uracil	111>42	1.968	20	18	14	negative
Thymine	125.05>42	3.849	10	18	14	negative
Guanosine	282.1>150.05	4.528	23	21	29	negative
Inosine	267>135.05	4.402	21	23	25	negative
Cytidine	302>242	1.657	24	10	19	negative
Uridine	243>110.05	3.319	19	17	20	negative
Deoxyguanosine	266.1>150.05	4.813	18	19	28	negative
Thymidine	301.1>241	5.229	23	10	18	negative
AMP	346.1>79	9.683	14	38	13	negative
GMP	362.1>79	8.81	27	26	13	negative
XMP	363.1>211.05	9.7	27	20	21	negative
IMP	347.05>79	8.77	25	40	28	negative
CMP	322.1>79	7.729	25	28	14	negative
UMP	323.1>79	8.503	26	36	13	negative

TMP	321.1>195.05	9.596	25	20	22	negative
cAMP	328.1>134.05	10.366	26	27	25	negative
3`-AMP	346.2>211.05	10.425	12	18	21	negative
3`-GMP	362>79.1	10.138	29	28	13	negative
3`-UMP	323.1>211.15	10.104	23	17	21	negative
3`-TMP	321.2>195.15	10.163	15	16	19	negative
ADP	426.1>79.05	10.866	17	46	13	negative
GDP	442.1>79	10.759	18	45	13	negative
CDP	402.1>79	10.708	16	42	14	negative
UDP	403.1>159	10.766	16	28	29	negative
ADP-Glu	588.05>346.05	10.743	24	23	24	negative
ADP-Rib	558.05>346.05	10.767	22	27	16	negative
UDP-Glu	565.05>323.05	10.645	22	27	15	negative
ATP	506.1>159	11.254	20	40	29	negative
GTP	522.1>159	11.186	20	33	29	negative
CTP	482.1>159	11.185	19	36	29	negative
UTP	483.1>159	11.207	19	36	29	negative
PRPP	389.1>177.05	11.212	28	21	30	negative
Orotate	155.05>111.05	7.529	12	14	20	negative
4-Aminobutyrate	162>102	1.037	11	8	18	negative
2-Aminobutyrate	162>102	1.258	11	8	18	negative
G6P	259.05>97	6.176	20	17	17	negative
F6P	259.05>97	6.703	20	17	17	negative
G1P	259.05>79	6.941	20	28	27	negative
F1P	259.05>97	7.737	20	17	17	negative
F1,6P	339.05>97	10.795	26	18	17	negative
GAP	169>97	7.019	13	12	17	negative
DHAP	169.05>97	8.327	13	12	17	negative
E4P	199.05>97	7.335	13	12	17	negative
BPG	265.05>167.05	10.894	20	18	29	negative

3PGA	185.05>97	10.772	14	16	17	negative
Phosphoenolpyruvate	167.05>79	10.928	17	15	27	negative
KDPG	257.05>97	10.781	10	18	17	negative
R1P	229.05>79	7.75	16	25	27	negative
R5P	229.05>97	6.535	18	13	18	negative
Ru5P	229.05>97	7.482	18	13	18	negative
RuBP	309.05>79	10.5	24	47	13	negative
S7P	289.1>97	6.637	20	21	16	negative
S1,7P	369.1>97	10.8	14	27	17	negative
6-Phospho-D-gluconate	275.05>97	10.709	19	17	16	negative
NAD	662.1>540.1	7.91	26	18	26	negative
NADH	664.1>79	10.83	24	57	13	negative
NADP	742.1>620.1	10.758	26	18	30	negative
NADPH	744.1>159.05	11.491	26	49	30	negative
FMN	455.1>97	10.934	18	27	17	negative
FAD	784.1>346.1	11.145	20	37	23	negative
Nicotinate	122>78	9.85	13	16	13	negative
Pyridoxamine 5-phosphate	247.05>230	1.9	17	11	23	negative
Thiamine pyrophosphate	424.1>302.05	6.95	30	16	20	negative
Pantothenate	218.05>88	9.905	17	17	15	negative
Ascorbate	175>115.05	5.448	19	12	20	negative
Oxaloacetate	131>87	9.014	25	10	27	negative
Pyruvate	87.05>43	7.98	10	11	14	negative
Citrate	191.05>87	10.86	13	18	14	negative
Isocitrate	191.05>73	10.868	13	22	26	negative
2-Oxoglutarate	145.1>101.05	10.686	15	10	17	negative
Succinate	117>73	10.102	13	15	12	negative
Fumarate	115.05>71	10.153	13	10	12	negative
Malate	133.05>115	10.511	10	17	21	negative
Oxalacetate	131>87	9.31	25	11	27	negative

Amino adipic acid	160>116	3.057	12	17	21	negative
Shikimate	173.1>93	4.555	11	17	16	negative
Glycerate	105>75.05	4.768	12	13	26	negative
Glycolate	75>47.05	4.903	16	13	16	negative
Glyoxylate	73>73	5.9	15	5	15	negative
Lactate	89>43	6.258	20	14	15	negative
α-Glycerophosphate	171.1>79	6.863	13	18	13	negative
β-Glycerophosphate	171.1>79	7.616	13	18	13	negative
2-Isopropylmalate	175.1>113.05	10.966	13	18	20	negative
Acetyl phosphate	139>79	10	27	14	30	negative
Trehalose	341>89	1.302	15	23	16	negative
CoA	766.1>79	11.374	20	54	13	negative
Acetyl CoA	808.1>408.1	11.386	20	37	28	negative
Succinyl CoA	866.1>408.1	11.38	20	41	27	negative

* Precursor ion > Product ion

V. Supplementary data for Fig. 2-4

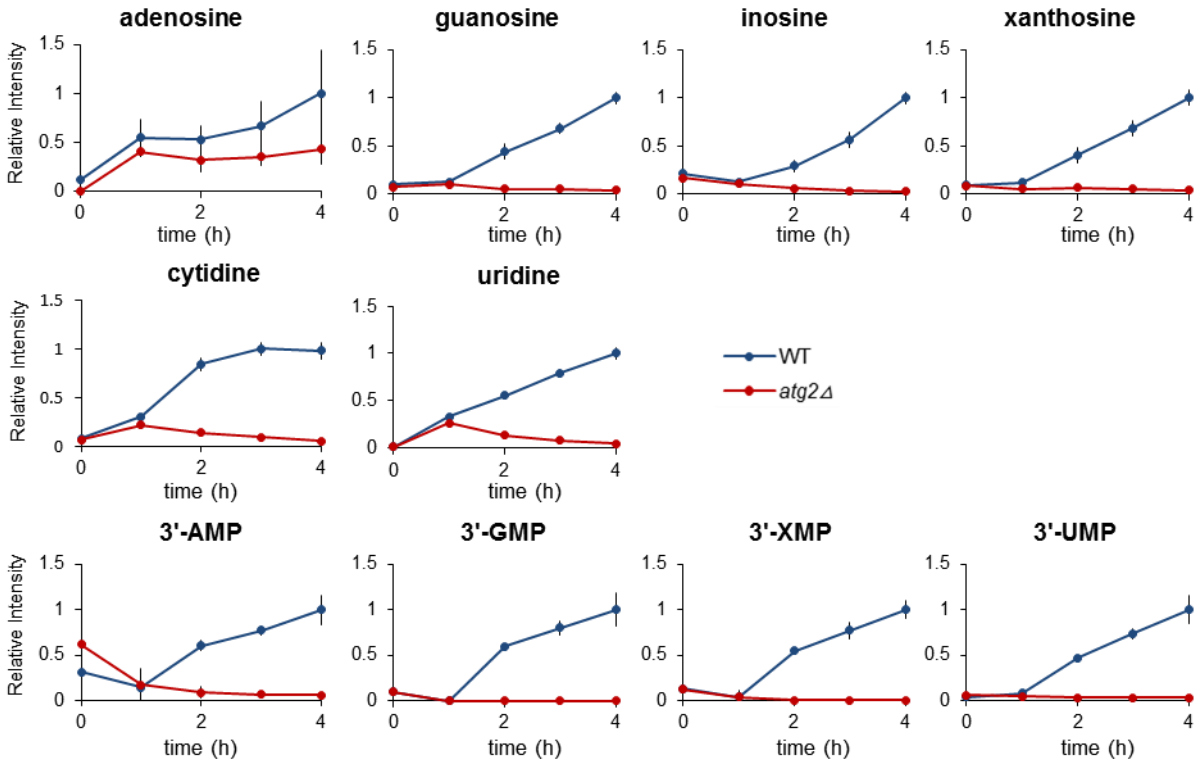

VI. Supplementary data for Fig. 2-7

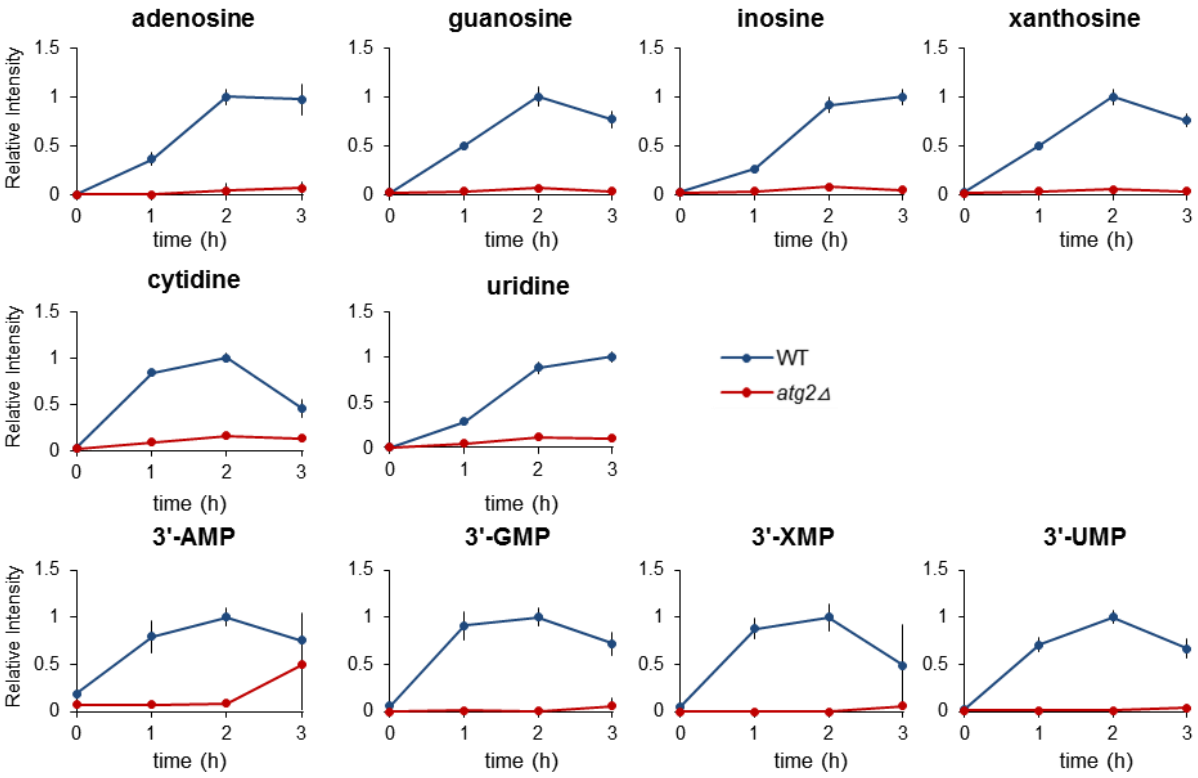

VII. Supplementary data for Fig. 3-2A

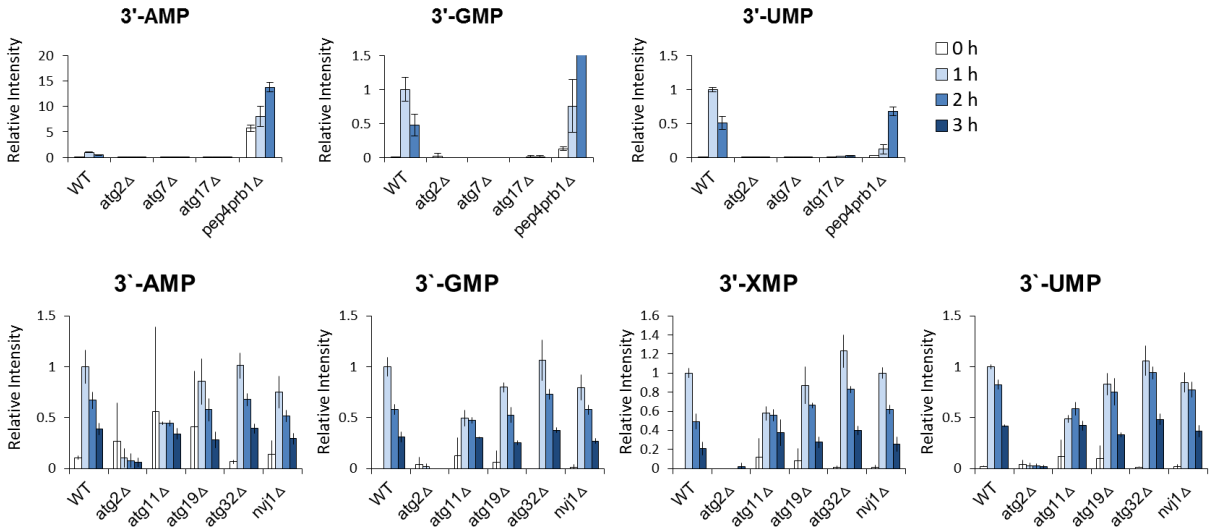

VIII. Supplementary data for Fig. 3-4

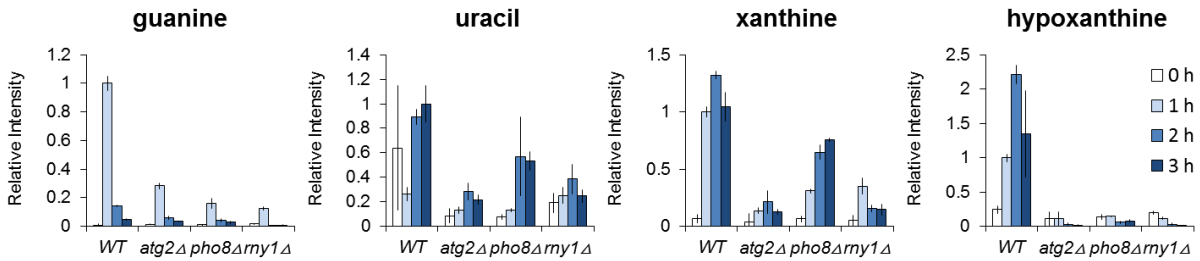

IX. Supplementary data for section 3.3.8

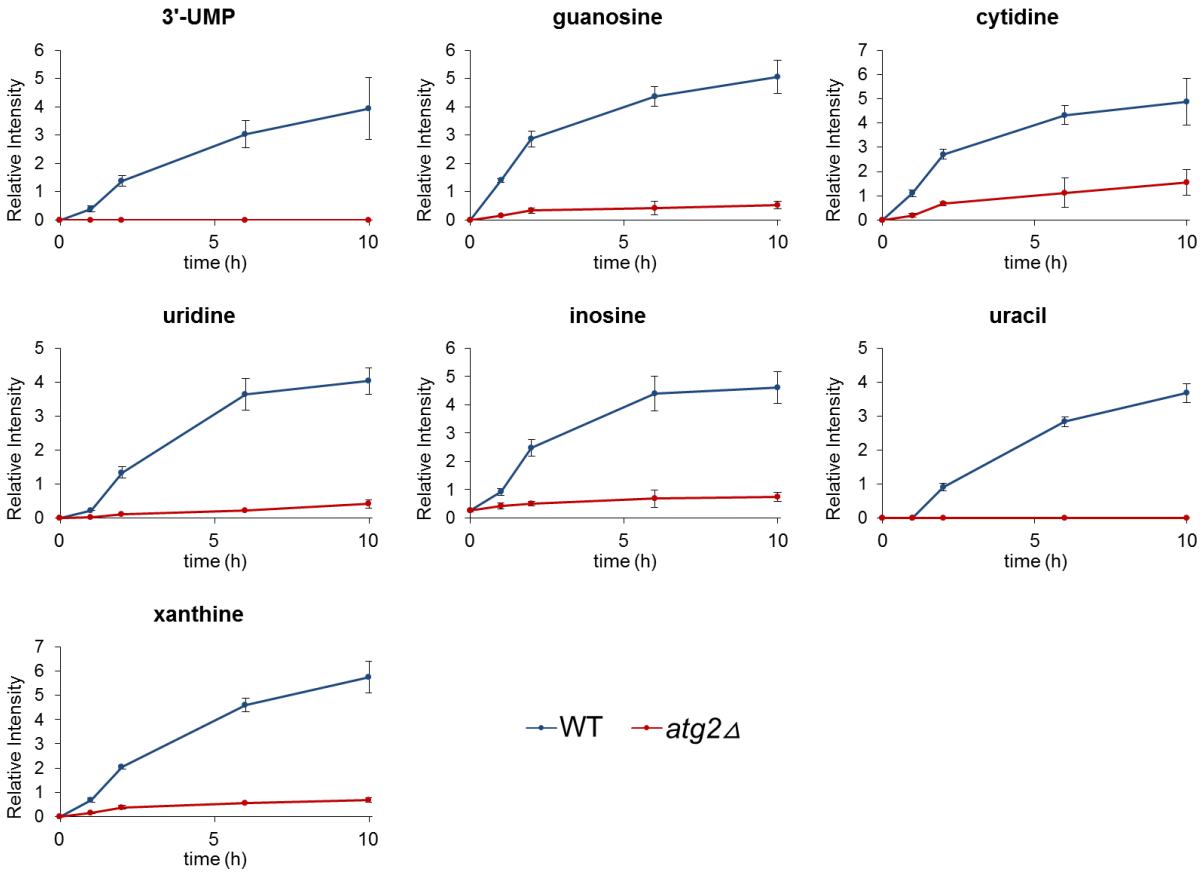

Time-dependent changes in nucleotide, nucleoside and base levels in the medium for WT and *atg2*Δ under nitrogen starvation

X. Changes in intracellular ribose levels in WT and *atg2*Δ under nitrogen starvation

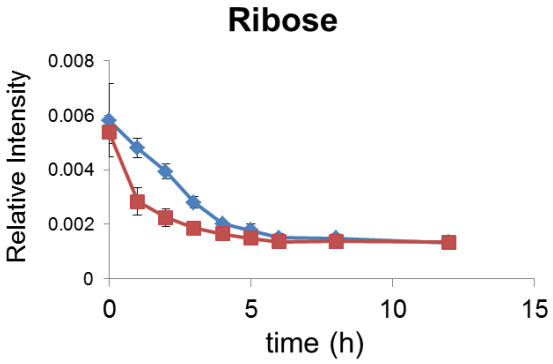

*Ribose is a degradation product of pyrimidine nucleoside.

*Data were obtained from gas chromatography-mass spectrometer (GC/MS).